DEVELOPMENT OF NON-AMORPHOUS SOLID DISPERSIONS FOR POORLY-SOLUBLE DRUGS USING A NOVEL EXCIPIENT AND HOT MELT EXTRUSION

by

Hwee Jing Ong

A Dissertation

Submitted to the Faculty of Purdue University

In Partial Fulfillment of the Requirements for the degree of

Doctor of Philosophy

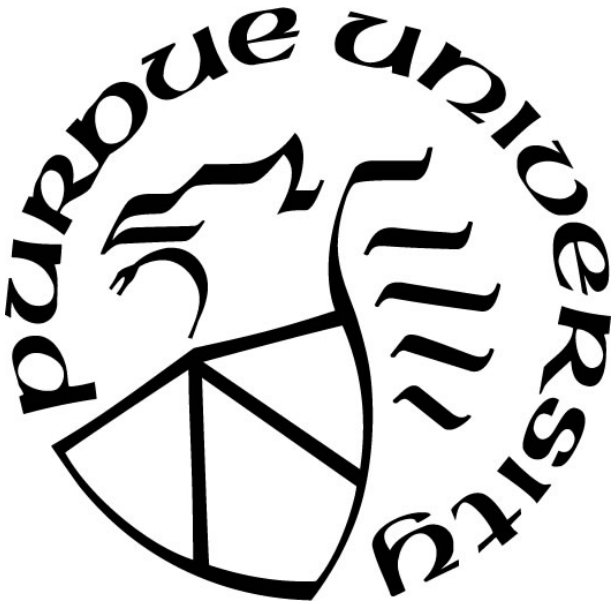

Department of Industrial & Physical Pharmacy

West Lafayette, Indiana

December 2018

THE PURDUE UNIVERSITY GRADUATE SCHOOL
STATEMENT OF COMMITTEE APPROVAL

Dr. Rodolfo Pinal, Chair
Department of Industrial and Physical Pharmacy
Dr. Gregory Knipp
Department of Industrial and Physical Pharmacy
Dr. Kinam Park
Weldon School of Biomedical Engineering
Department of Industrial and Physical Pharmacy
Dr. Osvaldo Campanella
School of Agricultural & Biological Engineering

Approved by:
Dr. Rodolfo Pinal
Head of the Graduate Program

To My Family,

who has made this journey possible

ACKNOWLEDGMENTS

First, I would like to express my sincere gratitude to Dr. Rodolfo Pinal for his guidance and enthusiasm in my advancement as a scientist and as a person. I am grateful to him for being a constant source of inspiration and being endlessly patient with me.

I would also like to thank Mr. Mario Alberto Cano-Vega, Dr. Juan Manuel Martinez Alejo, Dr. Yihua Pei, and Dr. Monika Lavan for their invaluable friendship throughout these years.

Last but not least, many thanks to Dr. Robert Carlton for introducing me to the fascinating world of pharmaceutics and his encouragement to pursue my dreams.

TABLE OF CONTENTS

LIST OF TABLES

LIST OF FIGURES

ABSTRACT

Author: Ong, Hwee Jing. PhD
Institution: Purdue University
Degree Received: December 2018
Title: Development of Non-Amorphous Solid Dispersions for Poorly-Soluble Drugs Using a Novel Excipient and Hot Melt Extrusion
Committee Chair: Rodolfo Pinal

Drug solubility is a persistent challenge in pharmaceutical product development. The objective of this research is to develop a formulation/processing strategy by means of a biodendrimeric solid dispersion (BDSD) platform, for increasing the solubility and dissolution rate of poorly water-soluble drugs. The BSDS platform combines a novel type of excipient, referred to as DLB, with a new application of the hot melt extrusion (HME) process.

Four model compounds – phenytoin (PHT), griseofulvin (GSF), ibuprofen (IBU), and loratadine (LOR) – were used to evaluate the solubilization effect of an octenylsuccinate-modified dendrimer-like biopolymer (OS-DLB). Shake-flask solubility measurements show that OS-DLB exerts significant solubilizing effect when present at less than 0.2% in water. The presence of hydrophobic C_8 chains on OS-DLB creates the type of favorable nonpolar microenvironment necessary for producing a parallel liquid phase equilibrium responsible for the increase in the total amount of drug dissolved in aqueous media. The higher the hydrophobicity of the drug, the higher the observed solubilization effect. Isothermal titration calorimetry studies show that drug solubilization by OS-DLB occurs by means of entropy-driven interactions. These studies also show that the intermolecular interaction between IBU and OS-DLB in solution exhibits very small energy change upon mixing but a stronger effect on entropy. In comparison, the intermolecular interaction between the less hydrophobic GSF and OS-DLB have significant effects on both enthalpy and entropy. Consequently, in terms of solubilization enhancement, it was found that the interaction between IBU and OS-DLB is entropy-driven (more favorable), while in the case of GSF, the interacting molecules are arranged to maximize enthalpic interaction.

Based on the solubility studies, a formulation/processing approach for enhancing the dissolution rate of the model drugs was developed. The biopolymer serving as both carrier and solubilizing agent, was coprocessed with poloxamer, functioning as a processing aid, using hot melt extrusion (HME) as an enabling technology. The result is a non-amorphous solid dispersion, exhibiting high and long-lasting supersaturation upon dissolution. A 3-factor, 3-level Box-Behnken design was implemented to define the optimal design space for the formulation/extrusion process. The results obtained from multivariate data analysis (partial least squares and principal components analysis) and response surface modeling suggest that drug release performance of IBU BDSDs is strongly influenced by the processing variables, while maximum release of GSF from the BDSDs can be attained through selective combination of functional excipients.

CHAPTER 1. INTRODUCTION

Solubility is a persistent challenge in pharmaceutical product development. It has been estimated that at least 40% of currently marketed drugs and up to 70% of new chemical entities (NCEs) are poorly water-soluble.[1] The general strategy for solubilizing an organic compound in aqueous solutions consists of several stages, summarized as follows[2]:

1. *Preliminary evaluation*. The magnitude of the solubility and/or stability problem is assessed from available literature data, calculated values such as octanol-water partition coefficient, ionization constant and aqueous solubility, and basic reasoning based on the structure of the drug and from known properties of structurally-related compounds. No drug is used and no actual measurements are involved.
2. *Characterization of the drug in aqueous solutions*. This involves the evaluation of the accelerated stability, ionization constant and aqueous solubility of the drug in water and in aqueous solutions of pharmaceutically acceptable vehicles. The evaluation of the octanol-water partition coefficient of the solute is also useful in evaluating the polarity of the solute and in estimating the effectiveness of various solubilizing agents.
3. *Selection of acceptable excipients*. The limits of acceptability of various types of solubilizing agents are determined:
    1. Acceptable pH range, buffer components and concentrations
    2. Acceptable cosolvents and concentrations
    3. Acceptable surfactants and concentrations
    4. Acceptable complexing ligands and concentrations.

    The determination of these limits helps eliminate certain approaches from further consideration, hence save time and effort required for subsequent solubilization studies.
4. *Development of a strategy for solubilization*. Solubilization approaches can be broadly divided into solute and solvent modification. Solute modification involves either the alteration of the physical properties of the crystal or the incorporation of a second component in the solute phase. These approaches are effective in

enhancing the apparent solubility and dissolution rate of organic compounds. However, this increase in apparent solubility is thermodynamically unstable. Solvent modification is more effective in producing thermodynamically stable enhancement in solubility. Common solvent modification approaches are pH adjustment, cosolvency, micellization, and complexation.

5. *Chemical, physical and biological evaluation of the solubilized drug*. A major problem associated with solubilization is the effect of excipients on the chemical stability of the drug. The understanding of the degradation mechanism of the drug is useful in improving its chemical stability. On the other hand, a physical stability problem is the precipitation of solubilized solutes upon dilution of the solubilization vehicle. The likelihood of precipitation can be reduced by using a more efficient solubilization system, by increasing the buffer capacity, by using excess cosolvent or surfactant, or by reducing the dose. Biological effects may be attributed to the properties of the drug or the formulation. The toxicity of high concentrations of excipients must be considered.

In general, each drug must be approached as a separate problem. The general strategy for solubilization has to be modified according to the structure and properties of the drug, as well as the desired route of administration, dosage form, and dose. Solid dosage forms, taken with plain water, is the most common way drugs are taken by patients. Therefore, the objective of this research is to develop a strategy for increasing the solubility of poorly water-soluble active pharmaceutical ingredients (APIs) from solid formulations reconstituted with plain water. The formulation part of this research entails the application of a novel type of excipient, referred to as phytoglycogen. Phytoglycogen is a naturally-occurring, nano-dendrimeric polysaccharide extracted from sweet corn. In the phytoglycogen excipient, the natural nanoparticles are chemically modified with octenylsuccinate (OS) groups, and the result is a biopolymeric carrier matrix with solubility-enhancing functionality. Accordingly, this material is referred to as octenylsuccinate-modified dendrimer-like biopolymer (OS-DLB) throughout this report. The solubilization mechanism of OS-DLB does not quite fall into one of the established categories of solubilizing agents. On the one hand, OS-DLB resembles micelles. However,

unlike micelles, the particles exhibit a nonpolar exterior and a polar interior, and are fixed in size and rigid in shape. On the other hand, OS-DLB behaves similarly to complexing agents, but the "complexes" do not possess definite stoichiometry nor exhibit well-defined geometry. Chapters 3 and 4 are devoted to elucidating the solubilization mechanisms of OS-DLB. The processing part of this research focuses on the development of biodendrimeric solid dispersions (BDSDs) using hot melt extrusion (HME). The result is a nonamorphous solid dispersion system, capable of enhancing the drug release rate of poorly soluble drugs, while maintaining the physical stability of the API. Chapter 5 is devoted to understanding the effect of extrusion processing parameters on the performance of BDSDs using Quality by Design (QbD) principles.

The first part of this chapter is devoted to the understanding of the thermodynamics of ideal and real solutions. Ideal solutions are not commonly encountered, but they serve as a reference point for discussing real solutions. In the area of real mixtures, the focus is on the solubilization of a crystalline organic solute. The second part centers on solid formulation design, with emphasis on the use of surfactants, complexing ligands, as well as synthetic and natural polymers. The role of these excipients in modulating the solubility and release of drugs will be discussed. The third part focuses on HME – an emerging solubility enabling technology. It addresses some of the fundamental processing principles, as well as the pharmaceutical applications of HME.

1.1 Thermodynamics of Solubility

1.1.1 Ideal solution

The solubility of one substance in another is a quantitation of the extent of mixing when the substances are placed in intimate contact and allowed to reach equilibrium. If both substances are gases, they mix in all proportions and have infinite mutual solubility. If both substances, ***1*** and ***2***, are liquid, the degree of mixing depends on the relative magnitude of the adhesive (***1-2***) and cohesive forces (***1-1*** and ***2-2***). An example of a nearly ideal solution is a mixture of water H_2O and heavy water D_2O. In practice, truly ideal solutions are not

common. Some examples of (nearly) ideal mixtures are benzene and toluene, hexane and heptane, and methylene chloride and methylene bromide. In an ideal mixture of solute ***1*** and solvent ***2***, the adhesive forces are exactly equal the cohesive forces, therefore the enthalpy of mixing ΔH_{mix}^{ideal} is equal to zero:

$$\Delta H_{mix}^{ideal} = H_{11} + H_{22} - H_{12} = 0 \qquad 1.1$$

By definition, the total volume of an ideal solution is equal to the sum of the volumes of its components, therefore the volume of mixing ΔV_{mix}^{ideal} is equal to zero:

$$\Delta V_{mix}^{ideal} = V_1 + V_2 - V_{12} = 0 \qquad 1.2$$

The configurational entropy *S* of solute ***1*** and solvent ***2*** is given by

$$S_1 = k_B \ln \Omega_1 \qquad 1.3$$

$$S_2 = k_B \ln \Omega_2 \qquad 1.4$$

respectively, where k_B is the Boltzmann's constant, and Ω is a measure of the randomness of the system. The value of Ω is the number of distinguishable arrangements in which the molecules can exist in the pure phase, thus

$$\Omega_1 = \frac{N_1!}{N_1!} = 1 \qquad 1.5$$

$$\Omega_2 = \frac{N_2!}{N_2!} = 1 \qquad 1.6$$

where N_1 and N_2 denote the number of solute and solvent molecules, respectively. There is only one arrangement in the initial state of each component since the molecules of solute ***1*** are indistinguishable amongst themselves, and likewise the molecules of solvent ***2***. Consequently,

$$S_1 = k_B \ln \Omega_1 = 0 \qquad 1.7$$

$$S_2 = k_B \ln \Omega_2 = 0 \qquad 1.8$$

In an ideal mixture of solute ***1*** and solvent ***2***, the entropy of the mixture S_{mixt} is given by

$$S_{mixt} = k_B \ln \Omega_{mixt} \qquad 1.9$$

where Ω_{mixt} is the total number of distinguishable arrangements in which the solute and solvent molecules can be arranged in the mixture. Similarly, Ω_{mixt} can be expressed as

$$\Omega_{mixt} = \frac{(N_1 + N_2)!}{N_1!\,N_2!} = \frac{N!}{N_1!\,N_2!} \qquad 1.10$$

where $N = N_1 + N_2$. Applying Stirling's approximation $\ln N! \approx N \ln N - N$ which is valid when N is a very large number, Equation 1.10 becomes

$$\ln \Omega_{mixt} = N_1 \ln \frac{N}{N_1} + N_2 \ln \frac{N}{N_2} \qquad 1.11$$

Consequently, the entropy of the mixture S_{mixt} can be written as

$$S_{mixt} = k_B \left(N_1 \ln \frac{N}{N_1} + N_2 \ln \frac{N}{N_2} \right) \qquad 1.12$$

The entropy of mixing is then given by

$$\Delta S_{mix}^{ideal} = S_{mixt} - (S_1 + S_2) = k_B \left(N_1 \ln \frac{N}{N_1} + N_2 \ln \frac{N}{N_2} \right) \qquad 1.13$$

A mixture of two components in a single phase is more random than when the components are in separate phases, therefore the entropy of mixing is almost always positive. The entropy of mixing is maximum when the overall randomness of the system is at its maximum. For an ideal mixture, ΔV_{mix}^{ideal} is equal to zero. This implies that the volume occupied by solute ***1***, solvent ***2***, and the mixture is proportional to N_1, N_2, and N, respectively. Therefore, Equation 1.13 can be written as

$$\Delta S_{mix}^{ideal} = k_B \left(N_1 \ln \frac{V}{V_1} + N_2 \ln \frac{V}{V_2} \right) \qquad 1.14$$

Equation 1.14 can be expressed in terms of number of moles instead of number of molecules using the following relation

$$k_B = \frac{R}{N_A} \qquad 1.15$$

where R is the ideal gas constant and N_A is the Avogadro's constant. Therefore,

$$\Delta S_{mix}^{ideal} = R \left(n_1 \ln \frac{V}{V_1} + n_2 \ln \frac{V}{V_2} \right) \qquad 1.16$$

where n_1 and n_2 denote the number of moles of solute and solvent, respectively.

The Gibbs free energy of mixing ΔG_{mix} determines whether and to what extent the substances mix to form a homogeneous phase. The free energy of mixing is defined as

$$\Delta G_{mix} = \Delta H_{mix} - T\Delta S_{mix} \tag{1.17}$$

where T is the temperature in kelvins. If the free energy of mixing is negative, mixing occurs spontaneously. If the free energy of mixing is greater than zero, phase separation occurs. Since in an ideal solution the enthalpy of mixing is equal to zero,

$$\Delta G_{mix}^{ideal} = -T\Delta S_{mix}^{ideal} \tag{1.18}$$

Combining the preceding equation with Equation 1.16 gives

$$\Delta G_{mix}^{ideal} = -RT\left(n_1 \ln\frac{V}{V_1} + n_2 \ln\frac{V}{V_2}\right) \tag{1.19}$$

Expressing Equation 1.19 in terms of mole fraction, which upon rearrangement becomes

$$\Delta G_{mix}^{ideal} = RT\left(n_1 \ln X_1 + n_2 \ln X_2\right) \tag{1.20}$$

where n_1 and n_2 denote the mole fraction of solute and solvent, respectively.

The total Gibbs free energy of an ideal solution G is

$$G = G_1 + G_2 + \Delta G_{mix}^{ideal} \tag{1.21}$$

where G_1 and G_2 denote the free energy of solute ***1*** and solvent ***2***, respectively, before mixing. At constant temperature and pressure, the partial molar free energy of solute ***1*** in the ideal solution is given by

$$\left(\frac{\partial G}{\partial n_1}\right)_{T,P,n_2} = \left(\frac{\partial G_1}{\partial n_1}\right)_{T,P,n_2} + \left(\frac{\partial G_2}{\partial n_1}\right)_{T,P,n_2} + \left[\frac{\partial\left(\Delta G_{mix}^{ideal}\right)}{\partial n_1}\right]_{T,P,n_2} \tag{1.22}$$

Since $\left(\frac{\partial G_2}{\partial n_1}\right)_{T,P,n_2} = 0$, combining the preceding equation with Equation 1.20 gives

$$\left(\frac{\partial G}{\partial n_1}\right)_{T,P,n_2} = \left(\frac{\partial G_1}{\partial n_1}\right)_{T,P,n_2} + RT\left[\frac{\partial\left(n_1 \ln X_1 + n_2 \ln X_2\right)}{\partial n_1}\right]_{T,P,n_2} \tag{1.23}$$

By substituting the mole fraction relation for each of the component $X_1 = \frac{n_1}{n_1 + n_2}$ and $X_2 = \frac{n_2}{n_1 + n_2}$ into Equation 1.23, which upon rearrangement becomes

$$\left(\frac{\partial G}{\partial n_1}\right)_{T,P,n_2} = \left(\frac{\partial G_1}{\partial n_1}\right)_{T,P,n_2} + RT \ln X_1 \qquad 1.24$$

Let μ_1 and μ_1^o be the chemical potentials of solute ***1*** in the mixture and in the pure phase, respectively. From the definition of μ,

$$\mu_1 = \left(\frac{\partial G}{\partial n_1}\right)_{T,P,n_2} \qquad 1.25$$

$$\mu_1^o = \left(\frac{\partial G_1}{\partial n_1}\right)_{T,P,n_2} \qquad 1.26$$

and therefore, Equation 1.24 can be written as

$$\mu_1 = \mu_1^o + RT \ln X_1 \qquad 1.27$$

1.1.2 Nonideal solutions

Aqueous solutions of organic compounds are highly nonideal. This is so because water-water-interactions are very much stronger than organic solute-solute interactions and organic solute-water interactions. In fact, the tendency of nonpolar groups to aggregate in aqueous media, also known as the "hydrophobic effect", arises primarily from the strong attractive forces between water molecules and not the attractive forces between nonpolar solutes. The strong attractive forces in water arise from the strength of O-H…O hydrogen bonds, and to the fact that each water molecule can form up to four hydrogen bonds with four neighboring water molecules. The precise arrangement of water molecules in the liquid state is unclear, but the tetrahedral symmetry of the oxygen bond orbitals and the tetrahedral structure of ice suggest a local tetrahedral arrangement of water molecules in the liquid state as well.[3] Therefore, in order to solubilize a solute in water, the tetrahedral network of hydrogen bonds must be disrupted or distorted. If the solute is ionic or polar, it can form strong ion-dipole or dipole-dipole interactions with water molecule, respectively. These attractive forces more than compensate for the disruption or distortion of the hydrogen bonds in water, thus ionic and polar solutes are easier to solubilize in water. However, if the solute is nonpolar, the weak organic solute-water interactions are not sufficient to compensate for the disruption or distortion of the hydrogen bond network in

water. The strong attractive forces in water are said to “squeeze out” the nonpolar solutes, therefore organic compounds are difficult to solubilize in water.

A solution is ideal if all the solutes obey Henry’s law. A solute of a solution is said to obey Henry’s law if the vapor pressure of the solute P_i is proportional to its mole fraction in solution:

$$P_i = kX_i \tag{1.28}$$

where k is a constant. In a nonideal solution where there is some deviation from Henry’s law, the activity coefficient γ is introduced to reflect both the enthalpic and entropic contributions to the free energy of mixing of an organic solute in water. Therefore,

$$\mu_i = \mu_i^o + RT \ln \gamma_i X_i \tag{1.29}$$

At infinite dilution $(X_i \to 0)$, the activity coefficient approaches unity $(\gamma_i \to 1)$, therefore μ_i is equal to the chemical potential of the pure solute in a hypothetical liquid state corresponding to extrapolation from infinite dilution along the Henry law gradient. Simply put, the solution approaches ideal behavior. The extent to which the activity coefficient of the solute differs from unity is a measure of its deviation from ideal behavior.

1.1.3 Ideal solubility of a crystalline solute

The above discussion assumes that substance u is a liquid. If substance u is a solid, the energetics of converting the solid to a supercooled liquid has to be first considered. A supercooled liquid is a hypothetical state in which the naturally occurring solid solute is assumed to exist in the liquid state at a temperature below its true melting temperature. Figure 1-1 is a schematic representation of converting a solid to a supercooled liquid. The first step is the heating of the solid to its melting temperature T_m, followed by the melting of the solid at T_m, and finally cooling of the liquid to T. Therefore, the enthalpy of converting a solid to a supercooled liquid ΔH is the sum of the enthalpies for the three processes:

$$\Delta H = \int_T^{T_m} C_P^S dT + \Delta H_f + \int_{T_m}^{T} C_P^L dT = C_P^S \left(T_m - T\right) + \Delta H_f - C_P^L \left(T_m - T\right) \tag{1.30}$$

where C_p is the heat capacity, the superscripts S and L refer to the solid and liquid states, respectively, and ΔH_f is the enthalpy of fusion. Analogously, the entropy of converting a solid to a supercooled liquid ΔS can be written as:

$$\Delta S = \int_{T}^{T_m} \frac{C_P^S}{T} dT + \Delta S_f + \int_{T_m}^{T} \frac{C_P^L}{T} dT = C_P^S \ln \frac{T_m}{T} + \Delta S_f - C_P^L \ln \frac{T_m}{T} \qquad 1.31$$

where ΔS_f is the entropy of fusion. Assuming that both C_P^L and C_P^S are independent of temperature, substitution of $\Delta C_P = C_P^L - C_P^S$ into Equations 1.30 and 1.31 gives

$$\Delta H = \Delta H_f - \Delta C_P \left(T_m - T \right) \qquad 1.32$$

$$\Delta S = \Delta S_f - \Delta C_P \ln \frac{T_m}{T} \qquad 1.33$$

The free energy of converting a solid to a supercooled liquid ΔG is defined as

$$\Delta G = \Delta H - T \Delta S \qquad 1.34$$

Substitution of Equations 1.32 and 1.33 into Equation 1.34, and upon rearrangement, gives

$$\Delta G = \Delta H_f - T \Delta S_f - \Delta C_P \left(T_m - T \right) + T \Delta C_P \ln \frac{T_m}{T} \qquad 1.35$$

Since $\Delta H_f = T_m \Delta S_f$,

$$\Delta G = \Delta S_f \left(T_m - T \right) - \Delta C_P \left(T_m - T \right) + T \Delta C_P \ln \frac{T_m}{T} \qquad 1.36$$

The relationship between the free energy change and the equilibrium constant is given by

$$\Delta G = -RT \ln \frac{X^S}{X^L} = -RT \ln X_{ideal} \qquad 1.37$$

where X_{ideal} is the ideal solubility of a crystalline solid. Substitution of Equation 1.36 into Equation 1.37, and upon rearrangement, gives

$$\ln X_{ideal} = -\frac{\Delta S_f \left(T_m - T \right)}{RT} + \frac{\Delta C_P}{R} \left(\frac{T_m - T}{T} - \ln \frac{T_m}{T} \right) \qquad 1.38$$

Equation 1.38 can be further simplified based on one or both of the following assumptions. The first assumption is that $\Delta C_P \approx 0$, thus $\ln X_{ideal} \approx -\frac{\Delta S_f \left(T_m - T \right)}{RT}$. The second

assumption is that $\Delta C_P \approx \Delta S_f$, therefore $\ln X_{ideal} \approx \frac{\Delta S_f}{R} \ln \frac{T_m}{T}$. Mishra and Yalkowsky[4, 5] found that the first approximation gives a better prediction for most solids that melt below 600°C. Therefore, after converting to the common logarithm, Equation 1.38 can be written as

$$\log X_{ideal} \approx -\frac{\Delta S_f \left(T_m - T\right)}{2.303RT} \qquad 1.39$$

Equation 1.39 is the general equation for estimating the ideal solubility of organic compounds. It is an intrinsic property of the solid and it is the same regardless of the solvent. It is solely dependent on the crystal lattice energy of the solid. A good indicator of the crystal lattice energy of a solid is its melting temperature, as demonstrated by McLaughlin and Zainal.[6] The authors observed that the solubilities of nearly ideal solutions of polycyclic aromatic hydrocarbons in benzene is directly proportional to their melting temperatures (Figure 1-2).

The observed aqueous solubility of a crystalline organic compound X_{obs} deviates from its ideal solubility in the same manner as described for liquids (see Section 1.1.2). Therefore, combining Equations 1.29 and 1.39 gives

$$\log X_{obs} \approx -\frac{\Delta S_f \left(T_m - T\right)}{2.303RT} - \log \gamma \qquad 1.40$$

The activity coefficient reflects the deviation from ideality. As a solute and solvent approach ideal mixing, $\gamma \to 1$ and $\log \gamma \to 0$, therefore the observed solubility of the solute approaches the maximum solubility achievable $\left(\log X_{ideal}\right)$ as if it were dissolved in an ideal solvent. However, aqueous solutions of organic compounds are highly nonideal, such that $\gamma \gg 1$, thus imposing an additional and large limitation on Equation 1.40.

1.2 Solid Formulation Design

Historically, excipients in pharmaceutical formulations were viewed merely as inert "supports" that facilitate the preparation, administration and preservation of APIs.[7] The principal classifications of these inert ingredients include binders, disintegrants, fillers, lubricants, coloring agents, sweeteners, preservatives, and suspending agents, among others. They make up almost 90% of the total weight of each drug product.[8] These traditional pharmaceutical excipients rarely, if ever, exert any direct therapeutic effects. In fact, they should not, but it is now recognized that excipients can affect the therapeutic effect of APIs. Today, excipients are "more than just the sugar in the pill".[9] These rationally-designed "functional excipients" are now endowed with sophisticated properties intended to improve the physicochemical and biopharmaceutical characteristics of drugs.[10] Drug-excipient interactions can be a double-edged sword in pharmaceutical development. On the positive edge, these functional excipients can enhance the solubility, release, stability and absorption of drugs. As discussed earlier, solubilizing agents such as buffers, cosolvents, surfactants and complexing ligands can increase the apparent solubility and dissolution rate of poorly water-soluble drugs. Drug absorption can be improved by means of mucoadhesive biodegradable polymers, such as sodium alginate and hydroxypropyl cellulose, that allow the solid dosage form to maintain intimate contact with the absorption site for a longer period of time.[8, 11] Ammar et al.[12] demonstrated that the stability of chlorpromazine hydrochloride improved significantly when delivered as a 1:1 complex with β-cyclodextrin. On the negative edge, these novel excipients may possess functional groups or residues that can participate in chemical or physical interactions with the active ingredients, leading to degradation, and/or retardation of dissolution rate and bioavailability.[13] Dubost et al.[14] reported that trace levels of reducing sugar impurities in mannitol can cause oxidative degradation of a lyophilized formulation of a cyclic heptapeptide drug. The relative impact of mannitol and sucrose on the oral bioavailability of cimetidine, a hydrophilic drug, was investigated by Adkin et al..[15] The authors found that the bioavailability of mannitol formulations were significantly lower than that of sucrose formulations due to the lowered small intestinal transit times of mannitol formulations. The implication of these examples is that excipients can no longer be regarded as inert substances. In fact, the U.S. Food and Drug Administration (FDA) has

recognized that some excipients are “potential toxicants” and has since issued a guidance on nonclinical safety studies to support the use of novel excipients in pharmaceuticals.[16] This guidance recommends testing strategies for pharmaceutical proposed for short-term, intermediate, and long-term use, toxicity studies for pulmonary, injectable, and topical pharmaceutical, as well as safety evaluations for excipients proposed for use in over-the-counter and generic drug products. Evidently, the need for more extensive understanding of their roles in drug delivery systems is greater than ever.

1.2.1 Surfactants

Surfactants (a contraction for “***surf***ace ***act***ive ***a***ge***nts***”) are amphiphiles that possess both polar (hydrophilic) and nonpolar (hydrophobic) moieties. When a surfactant is dissolved in water, the surfactant molecules are oriented such that the polar regions (head groups) interacts strongly with the more polar side of the interface (water) and the nonpolar regions (tails) are in contact with the less polar side of the interface (air or organic compound). The relative proportion of the hydrophilic and hydrophobic moieties of the surfactant is known as the hydrophilic lipophilic balance (HLB).[17] The HLB scale ranges from 0 (hydrophobic end) to 20 (hydrophilic end), and it is indicative of the emulsification behavior, rather than the efficiency or effectiveness of the surfactant as an emulsifier. Surfactants with a HLB range of 4-6 are recommended for water-in-oil (W/O) emulsification, while surfactants with a HLB range of 8-18 are suitable for oil-in-water (O/W) emulsification. The HLB values for other purposes of surfactants are listed in Table 1-1.

The nonpolar moiety of surfactants is typically composed of one or more hydrocarbon chains, usually linear and saturated. Surfactants with less than 10 carbons in the nonpolar regions are not sufficiently amphiphilic to be effective solubilizing agents, while those of more than 18 carbons are too insoluble to be useful.[2] Surfactants are classified according to the nature of the polar group: nonionic, anionic, cationic or zwitterionic. Nonionic surfactants contain either hydroxy groups, ether groups, or a combination of the two as polar moieties. The polarity of the head group can be adjusted by altering the number of hydroxy and/or ether groups.[18] Some of the common classes of nonionic surfactants are

Brij, Myrj, poloxamer, polysorbate, Span, Tween, and Triton. Anionic surfactants consists of negatively charged polar groups such as carboxylates, sulfates, sulfonates, and phosphates. The common anionic surfactants are sodium laurate, potassium myristate, sodium lauryl sulfonate, sodium lauryl sulfate, and sodium diamyl sulfosuccinate. Cationic surfactants consists of positively charged polar groups such as ammonium, quaternary ammonium, and pyridinium. Examples of cationic surfactants are lauryl ammonium chloride, lauryl trimethylammonium bromide, and cetyl pyridinium chloride. Zwitterionic surfactants consists of both anionic and cationic groups. They include amino acids, betaines, carnitines, and phosphatidyl cholines. The characteristic of zwitterionic surfactants is dependent on the pH of the solution in which they are dissolved. In solutions at low pH, they behave like a cationic surfactant, whereas in solutions at high pH, they behave like an anionic surfactant. The solubility of zwitterionic surfactants is at the minimum at the isoelectric point due to "tail-biting" between their ionic groups.[19]

Surfactants, by their very nature, have an affinity for biological membranes. Among the local effects of surfactant, the irritant action on tissues, mucous membranes, and skin is of considerable importance.[20] Florence and Gillan[21] demonstrated that certain nonionic surfactants, by virtue of their structure, can penetrate between the lipid chains of the absorbing membrane, which in turn reduce the flux of drug molecules. Likewise, Grasso and Lansdown[22] reported that repeated applications of sodium lauryl sulfate and cetrimide can lead to an impairment in the barrier function of the skin and ultimately, severe tissue damage. A comprehensive review of the toxicology properties of surfactants is provided by Gloxhuber[23].

1.2.1.1 Solubilization by micellization

A micelle is an aggregation of surfactant monomers to form a single structure. In aqueous solutions, the surfactant monomers in a micelle are oriented such that the nonpolar moieties are in maximum contact with one another while the polar moieties are in maximum contact with water. The critical micelle concentration (CMC) is effectively the solubility of the surfactant monomer, above which, surfactant monomers aggregate to form micelles

(Figure 1-3a). The relationship between the total surfactant concentration C_t, the micellar surfactant concentration C_{mic}, and CMC is given by

$$C_{mic} = C_t - CMC \qquad 1.41$$

Like most organic compounds, the solubility of the surfactant monomer increases with temperature. At the critical micelle temperature also known as the Krafft point, the solubility of the surfactant monomer exceeds the CMC and micellization occurs. Above the Krafft point, the solubility of the surfactant increases rapidly with increasing temperature. The total solubility of the surfactant is equivalent to the sum of the solubilities of the monomeric and micellar surfactant. In general, for *ionic* surfactants, an increase in temperature increases the CMC of the surfactant, but reduces the micelle size slightly due to the reduction in entropy as a result of aggregation.[2] The opposite is observed for *nonionic* surfactants. An increase in temperature results in a large increase in micelle size due to the dehydration of the polar chains, which in turn reduces the solubility of monomeric nonionic surfactant and consequently the CMC.[2, 24] The dependence of surfactant solubility on temperature is graphically represented in Figure 1-3b. Other nonstructural factors that affect the size of a micelle are pH, concentration of the surfactant, as well as the nature and concentration of solutes in the solution.[2]

Figure 1-3c shows the general curve of solubilization by surfactants. At surfactant concentrations below the CMC, the solubility of a solute is equivalent to its aqueous solubility, S_w, and the surfactant acts solely as a wetting agent. Wetting agents promotes the penetration of water into the solid phase by reducing the interfacial tension of the aqueous medium in the microenvironment of the solid.[20] The dissolution process begins once water comes into contact with the solute. At surfactant concentrations above the CMC, the solubility of the solute increases linearly with surfactant concentration. Drug solubilization by micellar surfactants occurs by means of incorporation of solutes in the micelle. The more hydrophobic the solute, the more likely it is to be incorporated in the core of the micelle. Conversely, the less hydrophobic the solute, the more likely it is to be incorporated near the surface of the micelle.[2]

The solubilization capacity of a surfactant κ is the ability of the surfactant to solubilize a solute. The most important structural feature of a surfactant that is related to its solubilization capacity is the alkyl chain length. Klevens[25] showed that the longer the aliphatic chain of the surfactant, the larger the nonpolar (hydrocarbon) region of the micelle to accommodate more hydrophobic solute molecules. The solubilization capacity of a surfactant is defined as the number of moles of solute that can be solubilized by one mole of micellar surfactant

$$\kappa = \frac{S_m}{C_{mic}} = \frac{S_t - S_w}{C_t - CMC} \tag{1.42}$$

where S_m and S_t denote the solubility of the solute in the micelle and the total solubility of the solute, respectively. The general equation for micellar solubilization, represented by the line in Figure 1-3b is

$$S_t = S_w + \kappa\left(C_t - CMC\right) = S_w + \kappa C_{mic} \tag{1.43}$$

The micellar partition coefficient K_M is another measure of the affinity of the solute for a micelle. Unlike the solubilization capacity, the micellar partition coefficient can be used to compare the ability of different surfactants to solubilize the same solute. Similar to the octanol-water partition coefficient, the micellar partition coefficient can be approximated by the concentration ratio of the solute at saturation:

$$K_M = \frac{S_m}{S_w} \tag{1.44}$$

Substituting Equations 1.41 through 1.43 into Equation 1.44, the micellar partition coefficient can be represented as follows:

$$K_M = \frac{\kappa\left(C_t - CMC\right)}{S_w} = \frac{\kappa C_{mic}}{S_w} \tag{1.45}$$

For any given concentration of micellar surfactant, the general equation for micellar solubilization (Equation 1.43) can be written in terms of the micellar partition coefficient

$$S_t = S_w + K_M S_w \tag{1.46}$$

1.2.2 Complexing ligands

Complexation is defined as the "reversible, (noncovalent) stoichiometric association of two or more molecules into a distinct, well-defined structural entity".[2] Complexes can be classified into three categories: ionically-bonded, hydrogen-bonded or nonbonded. Ionically-bonded and hydrogen-bonded complexes are stabilized by interactions between specific atoms of the solute and the ligand to form noncovalent bonds. These bonded complexes have definite stoichiometry and well-defined geometry. Examples of ionically-bonded complexes are metal-ion complexes, coordination complexes, chelates, metal-olefin complexes, and charge-charge complexes. Nonbonded complexes can be further categorized as inclusion complexes and stacking complexes. In comparison to ionically-bonded and hydrogen-bonded complexes, nonbonded complexes are more efficient in solubilizing nonpolar molecules in water.[2] This is so because in the case of bonded complexes, water, which is a strong binding agent, competes with the ligand for ionic or hydrogen bonds, thus reduces the tendency for solute-ligand bonding. The remaining of this section is devoted to the discussion of nonbonded complexation.

Inclusion compound hosts represent one of the most important nonbonded complexing agents. In aqueous media, solubilization of nonpolar molecules occurs by means of incorporating the nonpolar moiety of a solute molecule (in part or as a whole) into the nonpolar cavity of a molecule (or molecules) of the complexing agent. The driving force for inclusion complexation is similar to the driving force for micellar solubilization; the solute is oriented in a way that reduces the interfacial contact area between the nonpolar moiety and water. Both micelles and inclusion compound hosts provide a favorable nonpolar microenvironment (a secondary equilibrium) that is well-suited to accommodate nonpolar molecules that are "squeezed out" of water. The most common single molecule host is the cyclodextrins.[2] Cyclodextrins are cyclic oligosaccharides containing 6, 7, or 8 (α-1,4)-linked D-glucopyranoside units (giving rise to α-, β-, and γ-cyclodextrin, respectively). These "parent" cyclodextrins (especially β-cyclodextrin), as well as their complexes, have limited solubility in water due to their compactness and rigidity as compared to the linear dextrins.[26] As a result, a number of cyclodextrins derivatives of pharmaceutical interest, such as 2-hydroxypropyl-β-cyclodextrin, sulfobutylether β-

cyclodextrin sodium salt, methylated β-cyclodextrin, and 2-hydroxypropyl-γ-cyclodextrin, have been synthesized to enhance their aqueous solubility. Studies have shown that some of the ionizable and hydrophilic cyclodextrin derivatives are potent absorption enhancers for transmucosal absorption of peptide drugs[27] and effective carriers for oligonucleotide delivery[28]. More importantly, toxicology studies have shown that orally administered cyclodextrins (natural and derivatives) are well-tolerated due to lack of absorption from the gastrointestinal tract.[29]

Unlike the interior of a micelle which is fluid and is able to conform to the shape and size of the solute molecules, the interior of a cyclodextrin molecule is fixed in size and rigid in shape. Matsui and Mochida[30] demonstrated the importance of solute size and shape on the formation of inclusion complexes, as shown in Table 1-2. Most of the linear alcohols complex preferentially with α-cyclodextrin. Since the top and bottom diameters of the cavity of α-cyclodextrin are 4.7 and 5.3 Å, respectively[31], and the average length of an aliphatic C-C bond is approximately 1.537 Å, a molecule of 1-pentanol is able to fit snugly into the cavity of α-cyclodextrin. Cyclic and tertiary alcohols complex more strongly with β-cyclodextrin (top and bottom diameters 6.0 and 6.5 Å, respectively) because they do not fit into the cavity of α-cyclodextrin. The polarity of the solute is also an important driving force for inclusion complexation. It has been estimated that the polarity of the cavity of a cyclodextrin closely matches the polarity of ethanol.[32] Frömming et al.[33] observed that nitrosomefenorex, but not mefenorex, was able to form inclusion complexes with β- and γ-cyclodextrin, due to the lower polarity of nitrosomefenorex compared to mefenorex.

Stacking complexes are formed from the interaction between aromatic molecules that have a large contact area. A 1:1 stacked complex is composed of two planar molecules whose aromatic moieties are arranged to maximize overlapping and to minimize the interfacial contact area with water. Sandwich complexes are 2:1 or 1:2 complexes, in which a molecule is sandwiched on both sides by its cocomplexant. Stacked complexes are well-defined structures of definite stoichiometry and equilibrium constants, as clearly demonstrated by Sanghvi et al..[34] Aside from having a planar aromatic region, there are no specific structural requirements for stacking complexation.[2]

1.2.2.1 Solubilization by complexation

The formation of a complex from *m* molecules of solute *S* and *n* molecules of complexing ligands *L* can be represented as follows:

$$mS + nL \underset{}{\overset{K_{m:n}}{\rightleftharpoons}} S_m L_n \qquad \text{Equilibrium 1}$$

where the complexation constant $K_{m:n}$ is defined as

$$K_{m:n} = \frac{[S_m L_n]}{[S]^m [L]^n} \qquad 1.47$$

$[S_mL_n]$, $[S]$, and $[L]$ denote the concentrations of complex, free solute, and free ligand, respectively. For a 1:1 complex, Equation 1.47 becomes

$$K_{1:1} = \frac{[SL]}{[S][L]} \qquad 1.48$$

For simplicity, $[S]$ and $[L]$ are represented by *S* and *L*, respectively. The total solubility of the solute S_t and the ligand L_t can be represented by Equations 1.49 and 1.50, respectively

$$S_t = S_w + [SL] \qquad 1.49$$

$$L_t = L + [SL] \qquad 1.50$$

Combining Equations 1.48 through 1.50, the general equation for the solubilization by a complexing ligand is

$$S_t = S_W + \frac{K_{1:1} S_w L_t}{1 + K_{1:1} S_w} \qquad 1.51$$

Phase solubility diagrams provide a graphical representation of the apparent solubility of a compound as a function of ligand concentration, and a means for (partial) understanding of the nature of the molecular interactions in solution. Figure 1-4a shows the phase solubility diagram of Type A systems, characterized by the formation of soluble complexes between *S* and *L*. According to Higuchi and Connors[35], Type A_L represents a system in which all the complexes formed are of the first order in *L*, i.e. *SL*, S_2L, S_3L, …, S_mL. Type A_P represents a system in which the complexes formed are of a higher order than one in *L*, i.e. SL_2, SL_3, …, SL_n. The origin of Type A_N is unclear, but it is often attributed to one of the following two possibilities. First, the effective nature of the solvent changes at high concentrations of the ligand, thus leading to a change in the complex formation constant.

Second, the ligand self-associates at high concentrations, therefore affecting the degree of complexation. Figure 1-4b shows the phase solubility diagram of Type B systems, characterized by the formation of insoluble complexes between *S* and *L*. The portion between S_w and **a** of Type B_S resembles Type A diagrams where soluble complexes between *S* and *L* are formed. At point **a**, the solubility of the complex is reached. Further addition of *L* results in the formation of more complexes, which in turn must precipitate. At point **b**, all of the solid *S* is consumed, and further addition of *L* results in the depletion of *S* in solution and concomitant precipitation of the insoluble complex. The interpretation of Type B_I is similar, except that the solubility of the complex is so low that the solubility enhancement of *S* is not detected.

1.2.3 Polymers

Since the last quarter of the 20th century, the development of rationally-designed polymer-based therapeutics, which include protein-polymer conjugates, drug-polymer conjugates, polymer drugs, polymer-DNA complexes, polymeric micelles, and supramolecular drug-delivery systems, has become one of the most rapidly evolving and active areas of research in the pharmaceutical field.[36-38] Synthetic polymers are now an integral part of drug development, with many exhibiting intricate architectures, such as star polymers, multivalent polymers, dendrimers, dendronized polymers, and block copolymers (Figure 1-5).[37] Some of the potential advantages of these architectures include a well-defined polymer chemistry, tailored surface multivalency, and significantly lower melt viscosities than their linear counterparts of the same molecular weight.[37, 39]

The downside, however, is that many synthetic polymers can elicit a defense reaction *in vivo*, which may lead to a host of cellular and humoral responses.[40] Studies have shown that poly(ethylene glycol) (PEG), a polymer of choice for stealth drug delivery systems, can cause side effects and complications such as hypersensitivity reactions, undesirable changes in pharmacokinetics, and accumulation in tissues.[41] Christensen et al.[42] reported that long-term parenteral administration of pharmaceutical preparations of high molecular weight PVP led to the accumulation of PVP in tissues, causing complications ranging from

tuberculosis to cancer. While most of these synthetic polymers and other functional excipients can either be found in the FDA List of Inactive Ingredients for Approved Drug Products or are generally recognized as safe (GRAS), some of these materials are still subject to ingestion limits and present some safety concerns, especially in the pediatric population, where intake limits can be easily reached.[43]

In recent years, there has been an increasing interest in the use of low cost, naturally-sourced, low-toxicity, biodegradable, and/or biocompatible polymers. Most of the naturally-based polymers are derived from polysaccharides, proteins, and lipid compounds.[44] In particular, polysaccharide-based polymers have emerged as an important class of drug delivery vehicle.[45] Polysaccharides are inexpensive and abundantly available in nature. From a pharmaceutical perspective, polysaccharides possess many advantageous physicochemical characteristics, such as hydrophilic nature, innocuous or even beneficial biological activities (e.g. anti-inflammatory, anti-oxidant and anti-microbial), and availability of free carboxyl and hydroxyl groups distributed along the backbone for chemical modification.[46, 47] Polysaccharides can be classified according to their origin, such as plant polysaccharides (e.g. cellulose, pectins, and starches), seaweed polysaccharides (e.g. alginates, carrageenans, and gum agar), microbial polysaccharides (e.g. xanthan gum, gellan gum, and pullulan) and animal polysaccharides (e.g. chitin and chitosan).

Conceptually, polysaccharides, like synthetic polymers, exhibit many similar and advantageous features but with far less toxicity. Highly branched, three-dimensional, dendrimer-like polysaccharides, such as amylopectin and phytoglycogen, are particularly advantageous because they offer a multiplicity of reactive chain-ends.[48] Several studies have demonstrated the potential of amylopectin as a multivalent host.[49-51] However, owing to the difficulty of identifying and characterizing the binding sites on this polydispersed hyperbranched polysaccharide, it has not been widely used as a drug carrier in the pharmaceutical industry.[49] In comparison, phytoglycogen, a “regular” dendrimer, has been successfully demonstrated as a drug carrier[52, 53], largely because it offers precise end-group multiplicity and functionality.[48] Phytoglycogen is a glycogen-like α-D-glucan found in

plants with *sugary-1* mutations, such as those of maize, sorghum, and rice.[54] Phytoglycogen particles are highly water-soluble, roughly spherical, and monodisperse with typical size range of 30-100 nm.[55] Furthermore, phytoglycogen has a number of unique and advantageous properties, such as high levels of water retention, low viscosity in water, and excellent stability in aqueous dispersions, which make it a promising biopolymer for pharmaceutical applications.[56, 57]

Chemical functionalization of the free carboxyl and hydroxyl groups on the polysaccharides offers the opportunity for tuning the physicochemical characteristics of the polysaccharides, which in turn allows the conjugation or complexation of hydrophobic drugs for subsequent *in vivo* delivery.[46] Among the various polysaccharide derivatives, there has been a growing interest in octenylsuccinate (OS)-derivatized starches in recent years.[58] OS starches have been widely used by the food industry for several decades[58] and are generally recognized as safe. The incorporation of hydrophobic OS groups into normally hydrophilic starch molecules renders the starch amphiphilic properties. Kuentz et al.[59] demonstrated that OS starches were able to adequately wet hydrophobic drugs in water without additional aid from a surfactant. OS starches are also excellent emulsifiers and stabilizers, as demonstrated by Charoen et al..[60] The authors observed that O/W emulsions stabilized by OS starch were more stable to external conditions (pH, salt, and temperature) than those stabilized by whey protein. As a result of their excellent emulsifying and stabilizing properties, OS starches have also been used extensively as an encapsulating agent. Paramita et al.[61] successfully encapsulated oil mixtures of medium-chain triglycerides and *d*-limonene in OS-starch by means of spray drying to produce powder particles with high oil load.

1.2.3.1 Solubilization by polymers

The effect of polymers on the solubility (and dissolution rate) of an organic compound depends on how they are combined and how they interact with one another. They can either be physically mixed to form two separate solid phases, or combined in a way that alters the

crystal structure of the organic compound. The latter approach frequently leads to the formation of solid solutions.[2]

In a true physical mixture, the components are simply mixed. There is no interaction between the components in the solid state, and therefore the original crystal structure of the components is maintained. Assuming that the components do not interact in solution, the solubility and/or dissolution rate of each component in a physical mixture should be identical to that of the pure component in the absence of any additional components. This is evident in the data of Goldberg et al.[62], in which the authors found minimal difference in the dissolution rate of griseofulvin between the pure drug and a physical mixture containing 80% (w/w) of succinic acid. However, in a separate study, Thommes et al.[63] observed that the dissolution rate of griseofulvin from a physical mixture containing 90% (w/w) of mannitol was significantly faster than that of the pure drug. The authors suggested that mannitol facilitated the wetting of the hydrophobic drug particles. These observations reflect that a judicious choice of excipients can either limit or improve the release performance of a drug, even when the drug is simply mixed with the excipients as in a physical mixture.

A simple eutectic mixture consists of two solid components that significantly reduce the melting temperature of each other. The minimum temperature at which the components are maximally miscible in the liquid state is the eutectic temperature. When the solution at eutectic composition is rapidly cooled below the eutectic temperature, a very finely divided physical mixture of the two crystalline compounds is produced. The technique of preparing eutectic mixtures was first described by Sekiguchi and Obi[64] in 1961. Later, Goldberg et al.[62, 65, 66] demonstrated that a fraction of the drug was in fact molecularly dispersed in the soluble carrier, forming a “solid solution” instead of a eutectic mixture.

In a solid solution, the solute of interest (drug) is molecularly dispersed in a carrier (usually a polymer). Any organic compound has some miscibility in the other in the solid state, however, the extent of solubility is usually too low to be of any practical value.[2] The partial miscibility of one substance with another substance is due to the entropy of mixing.

Entropy is primarily responsible for partial miscibility of all organic compounds with one another. The rendering of the drug to the molecular level reduced or eliminated the limitation imposed by the crystal lattice energy of the solid (ideal solubility), thereby contributed to the enhancement in dissolution and bioavailability of the drug.

Through careful selection of a carrier, the dissolution rate of a poorly soluble drug can be enhanced by up to several orders of magnitude.[67] Hydrophilic (e.g. polyvinylpyrrolidone, hydroxypropyl cellulose and polyethylene oxide) and pH-responsive (e.g. Eudragit® E grades, chitosan, and hydroxypropylmethylcellulose phthalate) polymers are some of the most commonly used water-soluble carrier matrices. Drug release from hydrophilic polymers is mostly diffusion- and erosion-controlled.[68] Hence, the rate of release from such preparations is typically not constant and exhibits a time-dependent profile. pH-responsive polymers may achieve zero-order drug release, but are limited by the pH of the dissolution medium.[69] Release-modifying agents such as pore formers, superdisintegrants, and surfactants, are frequently incorporated into the formulation to modulate the drug release kinetics from polymer matrices. Bodmeier and Paeratakul[70] prepared potassium chloride tablets coated with aqueous latexes dispersed with dibasic calcium phosphate. Dibasic calcium phosphate acted as a pore-former and upon contact with simulated gastric fluids, it leached out rapidly to form a rate-controlling, microporous membrane. Constant drug release was achieved and could be controlled by varying the amount of dibasic calcium phosphate and thickness of the film coat.

A major limitation of solid solutions is the physical stability limitations of such systems. Depending on the solubility of the drug in the carrier as well as the physical stability of the system (i.e., the natural tendency of the drug to regenerate the crystal), the drug may either remain molecularly dispersed in the solid solution or crystallize as a whole or in part on aging.[71] When exposed to a volume of aqueous medium insufficient to dissolve all the drug, the drug in a solid solution presents as a supersaturated solution and precipitates, thereby losing the advantages of a solid solution. A variety of crystallization inhibition techniques have been proposed. For example, poly(vinylpyrrolidone) (PVP) is the polymer of choice for the study of amorphous solid dispersions because it is amorphous and does not

transform to its crystalline state over time.[71] Furthermore, PVP has a high glass transition temperature (177°C), hence it will increase the glass transition temperature of the dispersion system, relative to that of the pure amorphous drug, thus reducing the mobility of the drug molecules and tendency of the drug to crystallize.[72]

1.3 Hot Melt Extrusion

Hot melt extrusion (HME) is one of the most widely used processing technologies in the plastics industry. Over the last four decades, the science and technology of HME has been successfully exploited by the pharmaceutical industry as an alternative "platform technology" for preparing pharmaceutical solid dosage forms.[73] A wide array of pharmaceutical dosage forms, such as pellets[74], granules[75], immediate release tablets[76], modified release tablets[77], orally disintegrating tablets[78], transdermal delivery systems[79], transmucosal delivery systems[80], transungual delivery systems[81], and implants[82], have been successfully developed.

The successful production of pharmaceutical products by means of HME involves a strong interplay between the formulation and the process, as described by Schenck et al..[83] As shown in Figure 1-6, the characteristics of a hot melt extruded product are governed by three interrelated groups of variables: (1) design variables, (2) process variables, and (3) material variables.[84] The impact of these three groups of variables on the final product properties will be summarized in the subsequent sections.

1.3.1 Design variables

HME is a highly complex processing technology. It involves simultaneous process functions, such as transport, mixing and compression of particulate components, melting of polymeric materials, mechanochemical reactions, and shaping of a molten / dough-like material through a die.[85] Hot melt extruders can be classified according to the characteristics of the equipment, including the number of screws, the direction of rotation of the screws (co-rotating or counter-rotating), the degree of element intermeshing, and the

screw size as a function of diameter.[86] The primary differences between single-screw and twin-screw extruders are in their transport mechanism and in their mixing abilities.[87] In single-screw extruders, the transport mechanism is the frictional forces in the solids conveying zone and the viscous forces in the melt conveying zone. Material transport is more dependent on the frictional forces between the polymer and the screw than on the frictional forces between the polymer and the barrel wall. A potential implication is that a stagnant layer may remain on the screw surface, hence impacting the degree of mixing in the extruder. In twin-screw extruders, the two screws, arranged side by side, can either rotate in the same direction (co-rotating) or in the opposite directions (counter-rotating). Twin-screw extruders perform both distributive and dispersive mixing.[73] Distributive mixing can be viewed as homogenization, wherein the material is divided and recombined to achieve compositional and thermal uniformity without the disruption of the morphological structure of the components. Distributive mixing is useful for mixing heat and shear-sensitive materials. In dispersive mixing, intense shear forces are imparted to the material and the material is reduced significantly in size, which ultimately leads to the molecular dispersion of the components. Twin-screw extruders can be further classified into non-intermeshing and intermeshing, though co-rotating twin-screw extruders are generally of the intermeshing design. Non-intermeshing extruders cannot form closed or semi-closed compartments because the screws are positioned apart from each other, therefore non-intermeshing extruders have a lower degree of positive conveying. However, given the large vent opening, they are useful for removing large amounts of volatiles from the material or for processing highly viscous materials.[87] Intermeshing extruders are “self-wiping” or “self-cleaning”, i.e. the material does not rotate with the screw. The self-wiping characteristic is advantageous as it minimizes material stagnation, thus prevents localized overheating of the material being processed. Since they operate by a “first in, first out” principle, the residence time distribution of the material is very narrow. In comparison to single-screw extruders, intermeshing co-rotating twin-screw extruders provide more efficient mixing, smaller residence time distributions, and minimal material stagnation, therefore they are of greater pharmaceutical interest.[84]

1.3.2 Process variables

The HME process variables can be divided into two groups. Examples of independent variables include temperature profile of the barrel, rotating speed of the screw, and feeding rate. Examples of dependent variables include product temperature, residence time distribution, die and barrel pressure, and torque.

The processing temperature is often the first parameter to be considered in the extrusion process. Typically, the barrel temperature profile is set at least 30°C above the glass transition or melting temperature of the polymer.[84] This is to ensure that the melt viscosity of the polymer is relatively low so that the torque generated during the extrusion process is within the toque limitation of the extruder. The processing temperature is also dependent on the degradation temperature of the polymer and the drug, as well as the desired processing regime (miscibility regime or solubilization regime) in relation of the melting of the drug. DiNunzio et al.[86, 88] defined the miscibility regime as an operating space where the processing temperature is above the melting temperature of the drug, whereas in the solubilization regime, the processing temperature is below the melting temperature of the drug. Processing in the miscibility regime is likely to result in amorphous solid dispersion (ASD) systems. While the successful preparation of ASDs is largely dependent on the miscibility of the drug with the polymer, the distribution of the drug in the polymer phase is the limiting factor. A screw configuration comprising of mixing and kneading elements is required for providing the necessary distributive and dispersive mixing in order create a homogenous dispersion. Conversely, processing in the solubilization regime is likely to result in either ASD or “bottom-up” crystalline solid dispersions. Likewise, the successful preparation of ASDs depends on the miscibility of the components. However, the successful preparation of crystalline solid dispersions is largely attributable to the immiscibility and antisolvent function of the polymer. As suggested by DiNunzio et al.[86, 88], at raised temperatures and in the presence of shear forces, the drug can dissolve in the polymer melt, and upon cooling, the drug can precipitate to form crystalline solid dispersions. The particle size and crystalline structure of the drug can be tuned according to the level of mixing and rate of cooling during the extrusion process. DiNunzio et al.[86, 88], however, failed to recognize a second probable mechanism of producing crystalline

solid dispersion. When processed with a carrier matrix that is immiscible with the drug, along with a suitable processing aid, and at temperatures lower than the melting point of the drug, the original crystal lattice structure of the drug is likely to be maintained during the extrusion process. The result is a crystalline solid dispersion with excellent thermodynamic stability, as illustrated in this research. Since the flow properties of a polymer depends on its melt viscosity, the processing temperature also affects the flow rate of a material, which in turn influences its residence time in the extruder. Nikitine et al.[89] observed that the flow rate of Eudragit® E100 increased with temperature due to a decrease in melt viscosity, which in turn promoted the flowing of the polymer.

Screw speed is also a critical parameter in controlling the melt temperature, degree of mixing, specific energy input, and sometimes the melt pressure in a twin-screw extruder.[90] While the extruder barrel is heated, much of the energy imparted to the material is provided by the rotation of screws.[84] As the solids are conveyed in the barrel, heat is generated through frictional, plastic and viscous energy dissipation in the fully filled kneading blocks. Frictional energy dissipation arises from the frictional movement of solid particles, plastic energy dissipation from the irreversible deformation of solid particles, and viscous energy dissipation from the irreversible deformation of the molten material.[73] In the same study by Nikitine et al.[89], the authors found that the effect of screw speed on the residence time of a pseudoplastic polymer is similar to the effect of temperature. The higher the screw speed (shear rate), the lower the melt viscosity of the polymer, and therefore the shorter the residence time of the material in the extrusion barrier. These conditions are ideal for processing thermally labile materials. However, in a study by Crowley et al.[91], the authors showed that at high screw speeds, polyethylene oxide degraded as a result of polymer melt fracture, a process in which the polymer chains are forced to orient themselves into a random configuration and/or undergo random chain scission, resulting in the formation of lower molecular weight chains.

There are two modes of feeding: flood feeding and starve feeding.[92] In flood feeding, the raw materials are placed in a hopper situated over the screw. As the screw rotates, the material conveyed is directly related to the screw speed. The higher the screw speed, the

greater the amount of material conveyed. Variations in the properties of the raw materials that affect the frictional forces between the raw materials and the surfaces of the extruder will result in variations in residence time and specific energy imparted to the material. Consequently, the quality of the extrudate will be likely impacted. In starve feeding, a separate metering device is used to control the rate of raw materials delivered to the extruder. This implies that the feeding rate is independent of screw speed, and that screw speed can be varied independently of throughput. Starve feeding is also more efficient in terms of mixing, as compared to flood feeding.[73] In general, changes in feed rate does not have a significant effect on the solid state properties of the drug or the critical quality attributes of the extrudate, as demonstrated by several studies.[93, 94]

As shown in Figure 1-6, the residence time of a material in the extruder is a dependent variable. It is controlled by the processing temperature, screw speed, and feed rate, as discussed earlier. However, in extruders where there is a "backflow" or recirculation channel, the operator is able to retain the material in the system for as long as desired, thus defining the residence time. As described earlier, the residence time of a material in the extruder plays a critical role in the quality of the extrudate.[95] On the one hand, a minimum residence time is required for sufficient mixing to obtain a homogenous product. On the other hand, heat and/or shear sensitive material can degrade over time.

1.3.3 Material variables

The choice of functional excipients in hot melt extruded formulations is critical in (1) improving the processability and robustness of the extrusion process, (2) tailoring the drug release kinetics, and (3) ensuring adequate physical and chemical stability of the formulation during and after HME. These functional excipients can be broadly classified as polymeric carriers, plasticizers, release-modifying agents, bulking agents, antioxidants, lubricants, can other miscellaneous additives. The role of excipients in modulating the drug release kinetics has already been discussed in Section 1.2.3. The focus of this section is on plasticizers, a crucial excipient after polymeric carriers in the extrusion process.

Plasticizers are low molecular weight compounds that are capable of forming secondary bonds with polymer chains, thus reducing polymer-polymer chain secondary bonding and providing more mobility for the polymers.[96] Consequently, plasticizers are expected to reduce the modulus, tensile strength, hardness, melt viscosity, and glass transition temperature, while at the same time, increase the flexibility, elongation at break, and toughness of the polymer.[97] In the ideal case wherein the plasticizer and polymer mix perfectly at the molecular level, only one glass transition/melting temperature will be observed. In the case wherein two glass transition/melting events occur, the components are not completely miscible with each other and segregation is expected.[98] In the context of HME, the incorporation of plasticizers allows the extrusion to be performed at lower processing temperatures, thus reduces the propensity for thermal degradation of the components in the formulation and improves the processability of the extrusion process.

Plasticizers can be divided into three categories: (1) traditional plasticizers, intentionally added to the formulation to achieve the desired properties, (2) non-traditional plasticizers present in the formulation, unintentionally providing plasticizing properties, and (3) specialty plasticizers (supercritical carbon dioxide).[96] Traditional plasticizers that have been investigated in hot melt extruded dosage forms include citric acid, diethyl phthalate, glycerol, methylparaben, low molecular weight polyethylene glycols, sugar alcohols (e.g. sorbitol, xylitol, lactitol), surfactants, triacetin and triethylcitrate. Several of these plasticizers offer multiple functionalities. Ghebremeskel et al.[99] demonstrated the potential of surfactants – incorporated as plasticizers – for increasing the apparent solubility and enhancing the dissolution rate of poorly water-soluble drugs formulated as ASDs using HME. However, it is well known that surfactants in ASDs may result in physical instability due to reduced glass transition temperature and increased water uptake by the dispersion.[100] In some cases, the incorporation of plasticizers may result in antiplasticization, a process in which the rigidity of the polymer is increased due to the presence of low concentrations of plasticizer. Chamarthy and Pinal[101] found that at low concentrations, sorbitol behaved as an antiplasticizer for soluble starch. The tensile strength of the starch extrudates increased significantly, which in turn affected the drug release kinetics of the diffusion-controlled drug delivery system.

Non-traditional plasticizers are mostly low molecular weight compounds present in the formulation for other (intended or unintended) functions, but contributing to the overall plasticization effect of the formulation during the extrusion process. Several studies have shown that drugs can act as a plasticizer in hot melt extruded dosage forms, with low melting drugs exhibiting a greater plasticization effect.[102-104] Brabander et al.[105] evaluated the plasticizing effect of ibuprofen at various drug loadings (0, 5, 10 and 20% w/w) on hot melt extruded ethylcellulose. The authors observed a single glass transition temperature for different solid solutions, indicating complete miscibility between the drug and the polymer. Residual solvents and water in the formulation are also potential plasticizers when extrusion is performed below the boiling temperature of the solvent.[96]

The use of supercritical carbon dioxide as a solvent in the processing of biocompatible/biodegradable polymers for pharmaceutical and medical applications has gained traction over the last decade.[106] Similar to the abovementioned plasticizers, the role of carbon dioxide is to reduce the melt viscosity of the polymer during the extrusion process. Supercritical carbon dioxide-assisted extrusion is used for the production of foam drug delivery systems. Such systems have low densities (high porosities), therefore they can float in the stomach for sustained drug delivery. In particular, foam drug delivery systems are advantageous for drugs with an absorption window in the upper small intestine.[107] A major drawback of this technology is its high cost relative to other plasticization techniques.

1.3.4 Applications of HME

1.3.4.1 Amorphous solid dispersions

HME has been established as a robust means of producing ASDs with improved dissolution rate. For example, the results obtained by Verreck et al.[93] showed that ASDs of itraconazole and hydroxypropylmethylcellulose (HPMC) (40:60 weight) prepared by HME exhibited a significant enhancement in dissolution rate, compared to the physical mixture. Furthermore, the ASDs were physically and chemically stable up to 6 months when stored under accelerated stability conditions. However, it should be noted that the physical stability observed in this case study is the exception, not the rule.[71] In a study by Forster et al.[104],

the dissolution rates of four poorly soluble compounds (indomethacin, lacidipine, nifedipine and tolbutamide) processed by HME with hydrophilic amorphous polymers (PVP and PVP/VA) were markedly improved, as compared to the crystalline drug. However, the authors noted that only ASDs of indomethacin with drug load of 50% remained amorphous (physically stable) after storage for 4-8 weeks at 25°C and 75% relative humidity. Water is ubiquitous. Water is also known to be a good plasticizer with a glass transition temperature of 136 K.[108] Relative to crystalline materials, amorphous materials are capable of absorbing large quantities of water vapor into the bulk solid phase in addition to surface adsorption.[109] The plasticizing effect of absorbed water can cause an increase in free volume and polymer chain mobility and a corresponding decrease in glass transition temperature.[110] Consequently, changes in the chemical and physical properties of the individual components in the ASD may occur. The magnitude of water vapor absorption is influenced by environmental factors such as temperature and partial vapor pressure, as well as formulation factors such as number and type of polar functional groups capable of forming hydrogen bonds with water.[109]

1.3.4.2 Nonamorphous solid dispersions

Relative to the number of investigations reported on ASDs, the number of successfully marketed products is small. At present, there are approximately 12 drugs marketed as ASDs, as shown in Table 1-3. The inherent physical instability of ASDs often diminishes their viability as a widespread solubilization/formulation approach. In comparison, non-amorphous solid dispersion systems that do not require the obliteration of the crystal lattice structure of the drug offer an alternative rational approach to overcome the challenges associated with drugs that exhibit poor aqueous solubility. Nonamorphous solid dispersions, by virtue of being nonamorphous, are thermodynamically more stable than their amorphous counterparts. Furthermore, this approach is useful for drugs that are not good glass formers and/or that are difficult to stabilize in the amorphous state. Thommes et al.[63] presented a coprocessing approach, in which poorly water-soluble drugs (griseofulvin, phenytoin and spironolactone) were dispersed at the particulate level in crystalline mannitol by HME, at a temperature above the melting point of mannitol but

below that of each drug. The *in vitro* drug release from the resultant "solid crystal suspensions" was over 2 orders of magnitude faster than that of the pure drug. In a related study by Reitz et al.[111], the authors formulated a solid crystal suspension of griseofulvin as tablets, and investigated the bioavailability of griseofulvin in beagle dogs. The authors reported that the solid crystal suspension formulation exhibited 27% higher bioavailability than a marketed griseofulvin product. Similarly, Hülsmann et al.[112] demonstrated that with the judicious combination of excipients (PEG 6000, PVP, and PVA 64 as polymeric carriers, and Sucroester® WE15 and Gelucire® 44/14 as additives), coupled with HME, the dissolution rate of 17β-Estradiol hemihydrate, a poorly water-soluble drug, can be improved while retaining a predominantly crystalline state of the drug. The authors reported that a 30-fold increase in dissolution rate was obtained for a formulation containing 10% API, 50% PVP and 40% Gelucire 44/14. In these case studies, the accelerated dissolution rate and enhancement of bioavailability can be largely attributed to the improved wettability of the poorly soluble drug in the suspension/dispersion as a result of embedding the drug particles in a highly hydrophilic carrier.

1.3.4.3 Pharmaceutical cocrystals and salts

HME was recently introduced as a feasible route for screening and manufacturing of pharmaceutical relevant materials, such as cocrystals and salts, by means of mechanochemistry. Mechanochemistry broadly refers to reactions, normally of solids, induced by the application of mechanical force, such as grinding and milling, with little or no solvent being required.[113] Solid-state mechanochemistry involves two distinct processes.[114] The first step involves the increase of internal and surface energy, increase of surface area, and decrease of coherent energy of solids. This step is also known as mechanochemical activation. The second step involves the spontaneous aggregation, adsorption, or recrystallization in the activated system. These processes may occur during or after the mechanical process.

Pharmaceutical cocrystals are molecular adducts of definite stoichiometry where one component is a drug and the other is a pharmaceutically acceptable crystal coformer.[115]

Pharmaceutical cocrystallization has been widely investigated in both academia and industry as it represents a promising method to modify the physicochemical properties of a drug by means of designing and constructing directional and complementary noncovalent interactions, such as hydrogen bonds and halogen bonds, with coformers.[116] Cocrystallization also provides a means of improving the mechanical properties of a drug through modification of the crystal packing arrangement of the drug.[117] Traditionally, cocrystals are prepared by solution methods (evaporation of a heteromeric solution, reaction crystallization, and cooling crystallization) and grinding methods (neat grinding and liquid-assisted grinding).[118] The highly efficient and intensive mixing associated with HME offers an alternative (grinding) method to produce cocrystals, as demonstrated by Daurio et al.[119]. Four neat cocrystals – caffeine-oxalic acid, nicotinamide-trans cinnamic acid, carbamazepine-saccharin, and theophylline-citric acid – were successfully prepared. In addition, the authors found that the incorporation of catalytic amounts of benign solvents (water or ethanol) promoted the formation of hydrates/solvates of cocrystals, thereby providing further flexibility in designing cocrystals. Boksa et al.[120] demonstrated a novel method for the simultaneous formulation and production of carbamazepine-nicotinamide cocrystal with the aid of a functional polymer matrix (Soluplus®) using HME. On the one hand, the polymer matrix functioned as a processing aid for the extrusion process. On the other hand, the functional matrix provided a means for fine-tuning the apparent solubility and dissolution rate of the cocrystal.

Similarly, HME was introduced as a viable method for the production of pharmaceutical salts. Salt formation is one of the most commonly used techniques to improve aqueous solubility, dissolution rate, and potentially bioavailability of weakly acidic or basic pharmaceutical solids.[121] Crystallization is the most common technique for the isolation and purification of pharmaceutical salts, both in the laboratory and on the manufacturing scale.[122] However, it is a complex and labor-intensive process that requires large volumes of (usually toxic) solvent. Furthermore, from the time the crystals of the drug substance are synthesized until the time when the crystals are ready for incorporation into the final product, the solid undergoes multiple operations, such as filtration and drying. In contrast, hot melt extrusion is a solvent-free process that offers significant advantages such as short

processing time and excellent process efficiency. Daurio et al.[123] successfully demonstrated the potential of HME to produce naproxen sodium salt. In this case study, naproxen sodium salt was prepared using two approaches: neat and liquid-assisted extrusion. Liquid-assisted extrusion was advantageous because it obviates the need of processing at high temperatures, thereby reduces the propensity for thermal degradation for the drug and the coformer.

1.4 Research Overview

The working hypothesis of this research is that the use of OS-DLB as a solubilizing agent offers the potential for increasing the apparent solubility of poorly water-soluble drugs. In combination with HME, OS-DLB as a carrier matrix is capable of enhancing drug release performance whilst maintaining the physicochemical properties of the API in the solid dispersion.

Chapter 2 presents a proof-of-concept study, in which it demonstrates the potential of BDSDs for enhancing the solubility and dissolution rate of four poorly water-soluble model compounds, namely phenytoin (PHT), griseofulvin (GSF), ibuprofen (IBU) and loratadine (LOR). The approach utilizes OS-DLB serving as both solubilizing agent and carrier matrix, poloxamer (PLX) as a processing aid, and HME as an enabling processing technology. The result is a nonamorphous solid dispersion capable of producing high and long-lasting supersaturation upon dissolution in aqueous medium, despite the retention of a predominantly crystalline state of the drug after HME processing.

Chapter 3 examines the solubilization effect of OS-DLB and PLX on the model compounds. By itself, the solubilizing power of OS-DLB increases with increasing hydrophobicity of the solute. In the presence of PLX, the solubilization effect of OS-DLB on the model dugs is accentuated to varying degrees. The difference in solubilization profiles is discussed in terms of the polarity match between the API and the hydrophobic microenvironment created by the synergistic effect of OS-DLB and PLX.

In Chapter 4, isothermal titration calorimetry was performed to further assess the role of drug hydrophobicity on the energetics of intermolecular interactions with OS-DLB and PLX. The results indicate that the intermolecular interaction between IBU and OS-DLB is weaker but in greater abundance than that between the less hydrophobic molecules (PHT and GSF) and OS-DLB, hence a greater solubilizing effect of OS-DLB on IBU is observed The results also suggest that solubilization of highly hydrophobic drugs by OS-DLB occurs by means of entropy-driven interactions.

Chapter 5 demonstrates an integrated approach of experimental design, multivariate methods, and response surface modeling to aid in the understanding of the controlling factors affecting dissolution and crystallinity of BDSDs prepared by HME. The processing strategy for producing a quality BDSD depends on the solubility properties (crystallinity and hydrophobicity) of the model compounds. The processing of IBU BDSDs requires a delicate balance of processing variables while optimal GSF BDSD performance can be achieved through careful combination of functional excipients.

Finally, Chapter 6 discusses some of the future studies in the development of OS-DLB and BDSDs in the context of drug solubilization, as well as the potential applications of the BDSD platform and HME in the pharmaceutical industry.

Table 1-1. Correlation between HLB values and uses of surfactants.[17]

HLB Range	Use
4-6	W/O emulsifiers
7-9	Wetting agents
8-18	O/W emulsifiers
13-15	Detergents
15-18	Solubilizing agents

Table 1-2. Apparent association constants for complexes of α- and β-cyclodextrins.[30] Reproduced with permission from The Chemical Society of Japan.

Alcohol	**α-cyclodextrin**	**β-cyclodextrin**
Methanol	-0.03	-0.49
Ethanol	0.75	-0.03
1-Propanol	1.37	0.57
2-Propanol	0.69	0.58
1-Butanol	1.95	1.22
2-Methyl-1-propanol	1.44	1.62
2-Butanol	1.42	1.19
2-Methyl-2-propanol	0.64	1.68
1-Pentanol	2.51	1.80
2-Methyl-1-butanol	2.04	2.08
3-Mthyl-1-butanol	1.87	2.25
2,2-Dimethyl-1-propanol	1.47	2.76
2-Pentanol	2.13	1.49
3-Pentanol	1.94	1.35
3-Methyl-2-butanol	1.27	1.92
2-Methyl-2-butanol	1.53	1.91
1-Hexanol	2.95	2.34
2-Hexanol	2.55	1.98
4-Methyl-2-pentanol	1.72	2.04
3,3,-Dimethyl-2-butanol	1.30	2.75
2-Methyl-2-pentanol		1.99
3-Methyl-3-pentanol		2.15
1-Heptanol	3.36	2.85
2-Methyl-2-hexanol		2.33
3-Ethyl-3-pentanol		2.28
1-Octanol	3.80	3.17
2-Octanol	3.15	3.13
Cyclobutanol	1.59	1.18
Cyclopentanol	1.66	2.08
Cyclohexanol	1.81	2.70
Cycloheptanol	1.90	3.23
Cyclooctanol	2.25	3.30
Benzyl alcohol	1.33	1.70
2-Phenylethanol		2.15

Table 1-3. List of currently marketed products utilizing HME technology.[124] Reproduced with permission from Springer Nature.

Trade Name	Drug	Carrier	Processing Technology	Company
Isoptin ER-E	Verapamil	HPC, HPMC	Melt extrusion	Abbvie
Cesamet	Nabilone	PVP	Solvent evaporation	Valeant
Sporanox	Itraconazole	HPMC	Bead coating	Janssen
Prograf	Tacrolimus	HPMC	Solvent evaporation	Fujisawa
Kaletra	Ritonavir, lopinavir	PVP/VA	Melt extrusion	Abbvie
Intelence	Etravirine	HPMC	Spray drying	Janssen
Zortress	Everolimus	HPMC	Spray drying	Novartis
Norvir	Ritonavir	PVP/VA	Melt extrusion	Abbvie
Onmel	Itraconazole	HPMC	Melt extrusion	Stiefel
Zelboraf	Vemurafenib	HPMCAS	Coprecipitation	Roche
Incevik	Telaprevir	HPMCAS	Spray drying	Vertex
Kalydeco	Ivacaftor	HPMCAS	Spray drying	Vertex

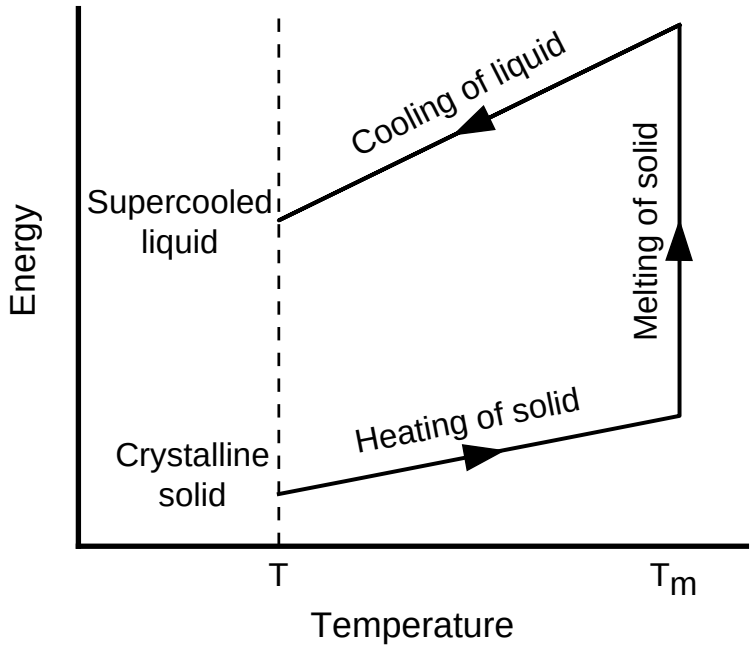

Figure 1-1. Conversion of a crystalline solid to a hypothetical supercooled liquid.

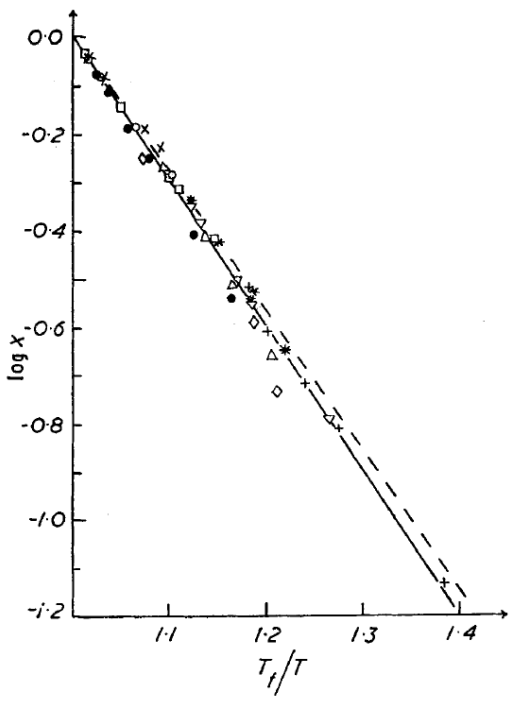

Plot of log *x against* T_f/T.

□ *Naphthalene.* ○ *Diphenyl.* ▽, Fluorene. ◇, Acenaphthene. ×, *o*-Terphenyl. +, Pyrene. △, Fluoranthene. ●, *m*-Terphenyl. ✻, Phenanthrene. *Ideal solubility curve* — — —.

Figure 1-2. Solubility of polycyclic aromatic hydrocarbons in benzene.[6] Reproduced with permission from Royal Society of Chemistry.

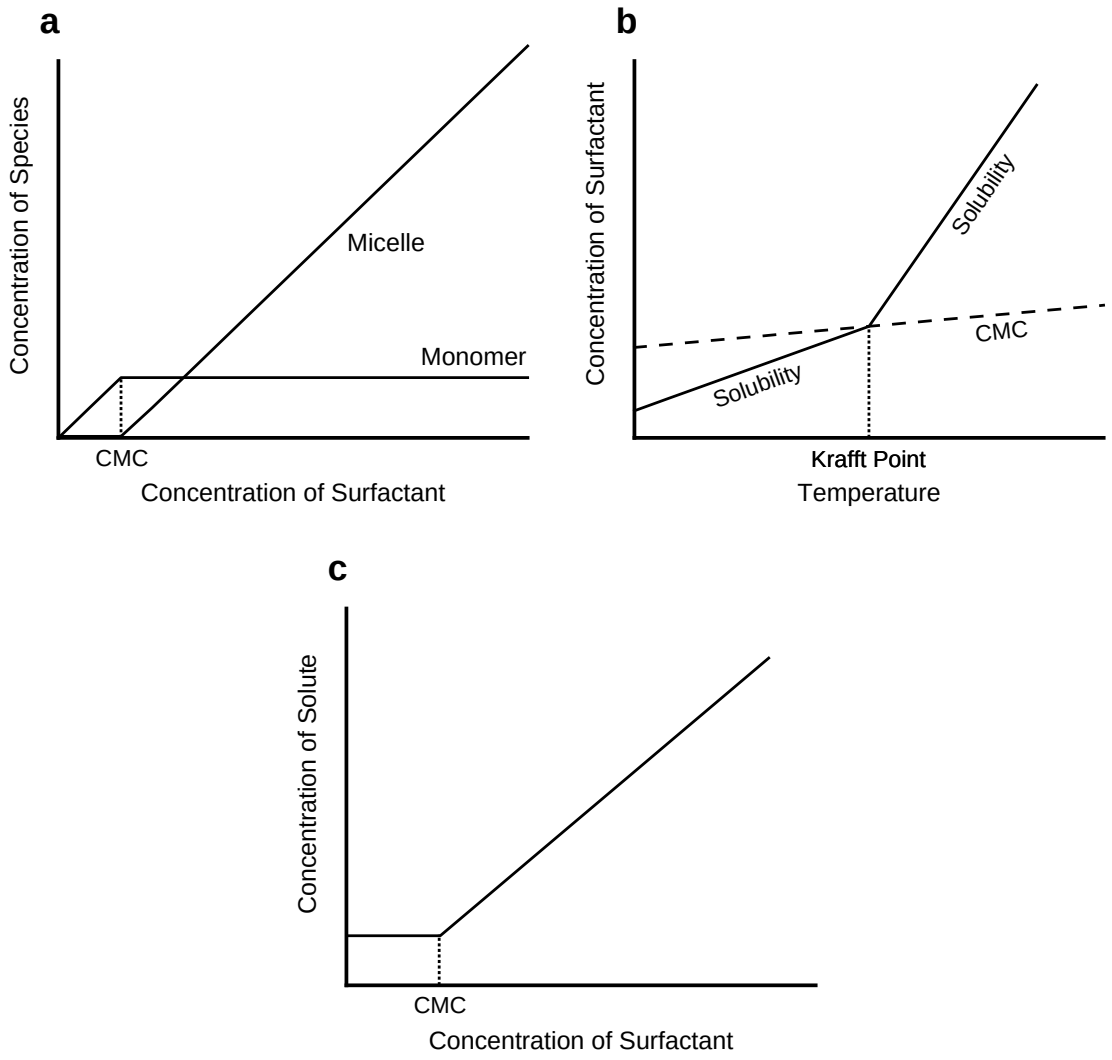

Figure 1-3. **(a)** Concentration of monomeric and micellar surfactant as a function of total surfactant concentration. **(b)** Effect of temperature on surfactant solubility and critical micelle concentration of an ionic surfactant. **(c)** General solubilization curve for surfactants.

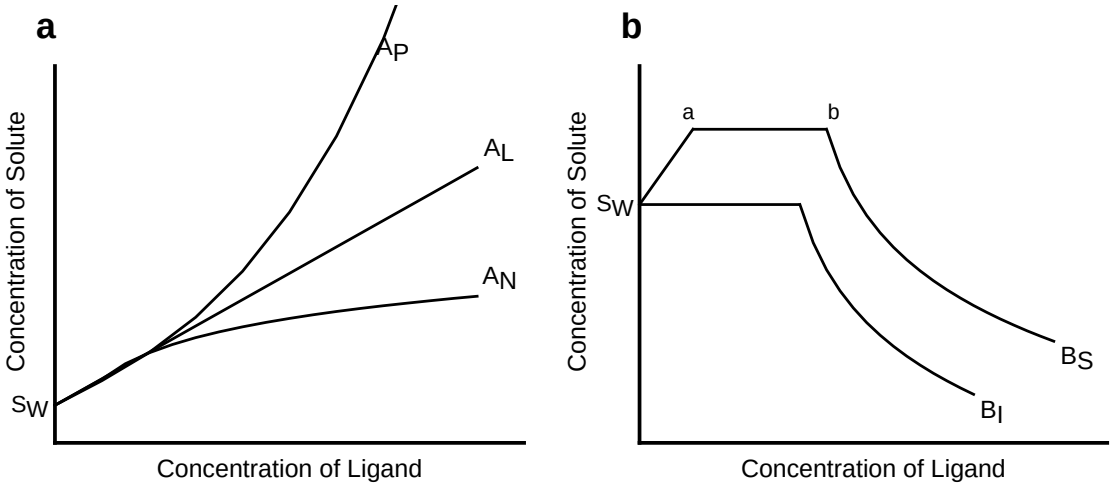

Figure 1-4. Phase solubility diagrams of **(a)** Type A and **(b)** Type B systems.

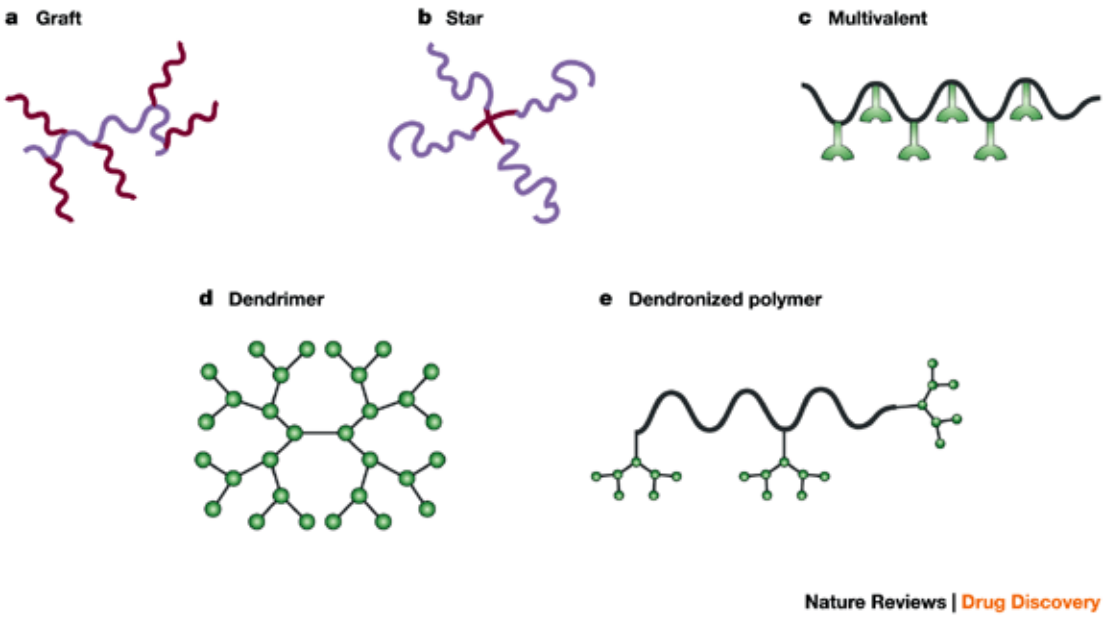

Figure 1-5. Novel polymeric architectures now being explored as the polymer therapeutics of the future.[36] Reproduced with permission from Springer Nature.

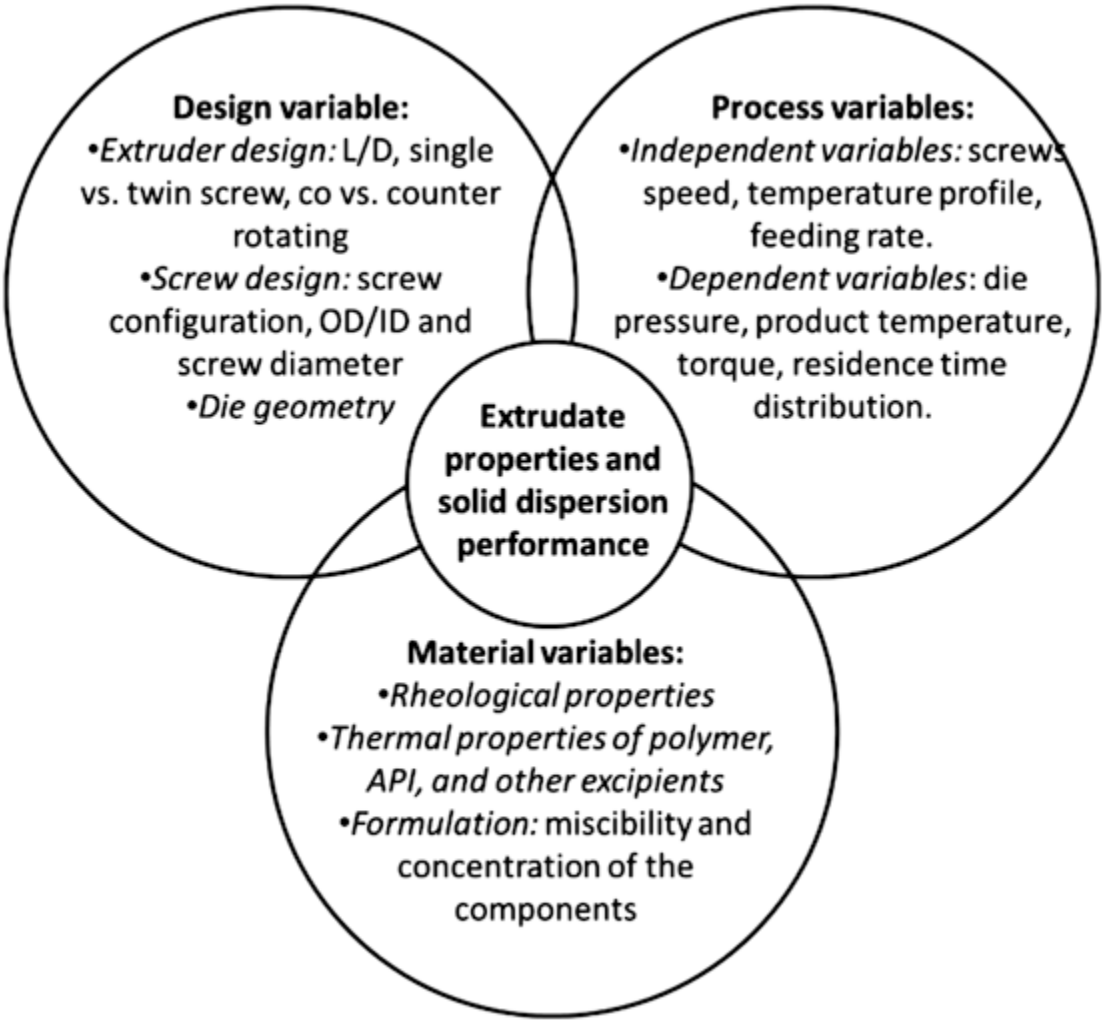

Figure 1-6. Summary of the variables that affect the properties and performance of the extrudate or HME product.[84] Reproduced with permission from Springer Nature.

1.5 References

1. J. Maincent and R. O. Williams. 2018. Sustained-release amorphous solid dispersions. *Drug Delivery and Translational Research*.
2. S. H. Yalkowsky. *Solubility and solubilization in aqueous media*, American Chemical Society, 1999.
3. C. Tanford. *The hydrophobic effect: Formation of micelles and biological membranes*, John Wiley & Sons, Inc., New York, 1973.
4. D. S. Mishra and S. H. Yalkowsky. 1990. Solubility of organic compounds in non-aqueous systems: Polycyclic aromatic hydrocarbons in benzene. *Industrial & Engineering Chemistry Research* **29**: 2278-2283.
5. D. S. Mishra and S. H. Yalkowsky. 1992. Ideal solubility of a solid solute: Effect of heat capacity assumptions. *Pharmaceutical Research* **9**: 958-959.
6. E. McLaughlin and H. A. Zainal. 1959. 177. The solubility behaviour of aromatic hydrocarbons in benzene. *Journal of the Chemical Society (Resumed)* 863-867.
7. G. Pifferi and P. Restani. 2003. The safety of pharmaceutical excipients. *Il Farmaco* **58**: 541-550.
8. A. S. Narang and S. H. S. Boddu. Excipient applications in formulation design and drug delivery. In A. S. Narang and S. H. S. Boddu (eds), *Excipient applications in formulation design and drug delivery* (A. S. Narang and S. H. S. Boddu, eds), Springer International Publishing, Cham, 2015, pp. 1-10.
9. M. Lesney. 2001. More than just the sugar in the pill. *Today's Chemist at Work* **10**: 38-43.
10. G. Pifferi, P. Santoro, and M. Pedrani. 1999. Quality and functionality of excipients. *Il Farmaco* **54**: 1-14.
11. A. Kamran, Q. Xin, and T. R. F. 2011. Use of carbohydrates, including dextrins, for oral delivery. *Starch - Stärke* **63**: 424-431.
12. H. O. Ammar, M. Ghorab, S. A. el-Nahhas, S. M. Omar, and M. M. Ghorab. 1995. Improvement of some pharmaceutical properties of drugs by cyclodextrin complexation. 4. Chlorpromazine hydrochloride. *Die Pharmazie* **50**: 805-808.
13. P. Crowley and L. Martini. Drug-excipient interactions, *Pharmaceutical Technology Europe*, Vol. 13, 2001, pp. 26.
14. D. C. Dubost, M. J. Kaufman, J. A. Zimmerman, M. J. Bogusky, A. B. Coddington, and S. M. Pitzenberger. 1996. Characterization of a solid state reaction product from a lyophilized formulation of a cyclic heptapeptide. A novel example of an excipient-induced oxidation. *Pharmaceutical Research* **13**: 1811-1814.
15. D. A. Adkin, S. S. Davis, R. A. Sparrow, P. D. Huckle, and I. R. Wilding. 1995. The effect of mannitol on the oral bioavailability of cimetidine. *Journal of Pharmaceutical Sciences* **84**: 1405-1409.
16. U.S. Food and Drug Administration. Guidance for industry: Nonclinical studies for the safety evaluation of pharmaceutical excipients, Rockville, MD, 2005.
17. W. C. Griffin. 1949. Classification of surface-active agents by" hlb". *Journal of the Society of Cosmetic Chemists* **1**: 311-326.
18. M. J. Rosen and J. T. Kunjappu. Characteristic features of surfactants, *Surfactants and interfacial phenomena*, John Wiley & Sons, Inc., 2012.
19. B. R. Bluestein and C. L. Hilton. *Amphoteric surfactants*, New York : M. Dekker, New York, 1982.

20. A. Florence. Drug solubilization in surfactant systems. In S. H. Yalkowsky (ed), *Techniques of solubilization of drugs* (S. H. Yalkowsky, ed), Marcel Dekker, Inc., New York, 1981, pp. 15-89.
21. A. T. Florence and J. M. N. Gillan. 1975. Non-ionic surfactants and membrane transport of thioridazine in goldfish. *Journal of Pharmacy and Pharmacology* **27**: 152-159.
22. A. B. G. Lansdown and P. Grasso. 1972. Physico-chemical factors influencing epidermal damage by surface active agents. *British Journal of Dermatology* **86**: 361-378.
23. C. Gloxhuber. 1974. Toxicological properties of surfactants. *Archives of Toxicology* **32**: 245-269.
24. T. F. Tadros. Surfactants in pharmaceutical formulations, *Applied surfactants: Principles and applications*, Wiley-VCH Verlag GmbH & Co. KGaA, Weinheim, Germany, 2005, pp. 433-502.
25. H. Klevens. 1950. The solubilization of polycyclic hydrocarbons. *The Journal of Physical Chemistry* **54**: 283-298.
26. T. Loftsson and M. E. Brewster. 2012. Cyclodextrins as functional excipients: Methods to enhance complexation efficiency. *Journal of Pharmaceutical Sciences* **101**: 3019-3032.
27. J. C. Verhoef, N. G. M. Schipper, S. G. Romeijn, and F. W. H. M. Merkus. 1994. The potential of cyclodextrins as absorption enhancers in nasal delivery of peptide drugs. *Journal of Controlled Release* **29**: 351-360.
28. Q. Zhao, J. Temsamani, and S. Agrawal. 1995. Use of cyclodextrin and its derivatives as carriers for oligonucleotide delivery. *Antisense Research and Development* **5**: 185-192.
29. I. Tetsumi and U. Kaneto. 1997. Pharmaceutical applications of cyclodextrins. Iii. Toxicological issues and safety evaluation. *Journal of Pharmaceutical Sciences* **86**: 147-162.
30. Y. Matsui and K. Mochida. 1979. Binding forces contributing to the association of cyclodextrin with alcohol in an aqueous solution. *Bulletin of the Chemical Society of Japan* **52**: 2808-2814.
31. M. V. Rekharsky and Y. Inoue. 1998. Complexation thermodynamics of cyclodextrins. *Chemical Reviews* **98**: 1875-1918.
32. K.-H. Frömming and J. Szejtli. *Cyclodextrins in pharmacy*, Springer Science & Business Media, 1993.
33. K. H. Frömming, V. Wedelich, and W. Mehnert. 1987. Nitrosation of mefenorex in the presence of cyclodextrins. *Journal of inclusion phenomena* **5**: 625-629.
34. R. Sanghvi, D. Evans, and S. H. Yalkowsky. 2007. Stacking complexation by nicotinamide: A useful way of enhancing drug solubility. *International Journal of Pharmaceutics* **336**: 35-41.
35. K. Connors and T. Higuchi. 1965. Phase solubility techniques. *Advances in Analytical Chemistry and Instrumentation* **4**: 117-212.
36. R. Duncan. 2003. The dawning era of polymer therapeutics. *Nature Reviews Drug Discovery* **2**: 347-360.
37. R. Duncan. 2014. Polymer therapeutics: Top 10 selling pharmaceuticals - what next? *Journal of Controlled Release* **190**: 371-380.

38. R. Duncan and M. J. Vicent. 2013. Polymer therapeutics-prospects for 21st century: The end of the beginning. *Advanced Drug Delivery Reviews* **65**: 60-70.
39. J. M. Frechet. 1994. Functional polymers and dendrimers: Reactivity, molecular architecture, and interfacial energy. *Science* **263**: 1710.
40. B. Říhová. 1996. Biocompatibility of biomaterials: Hemocompatibility, immunocompatiblity and biocompatibility of solid polymeric materials and soluble targetable polymeric carriers. *Advanced Drug Delivery Reviews* **21**: 157-176.
41. K. Knop, R. Hoogenboom, D. Fischer, and U. S. Schubert. 2010. Poly(ethylene glycol) in drug delivery: Pros and cons as well as potential alternatives. *Angewandte Chemie International Edition* **49**: 6288-6308.
42. M. Christensen, P. Johansen, and C. Hau. 1978. Storage of polyvinylpyrrolidone (pvp) in tissues following long-term treatment with a pvp-containing vasopressin preparation. *Acta Medica Scandinavica* **204**: 295-298.
43. S. Salunke, G. Giacoia, and C. Tuleu. 2012. The step (safety and toxicity of excipients for paediatrics) database. Part 1 - a need assessment study. *International Journal of Pharmaceutics* **435**: 101-111.
44. M. G. A. Vieira, M. A. da Silva, L. O. dos Santos, and M. M. Beppu. 2011. Natural-based plasticizers and biopolymer films: A review. *European Polymer Journal* **47**: 254-263.
45. V. K. Thakur and M. K. Thakur. *Handbook of polymers for pharmaceutical technologies, biodegradable polymers*, John Wiley & Sons, 2015.
46. S. Mizrahy and D. Peer. 2012. Polysaccharides as building blocks for nanotherapeutics. *Chemical Society Reviews* **41**: 2623-2640.
47. I. Wijesekara, R. Pangestuti, and S.-K. Kim. 2011. Biological activities and potential health benefits of sulfated polysaccharides derived from marine algae. *Carbohydrate Polymers* **84**: 14-21.
48. J. M. J. Fréchet, C. J. Hawker, I. Gitsov, and J. W. Leon. 1996. Dendrimers and hyperbranched polymers: Two families of three-dimensional macromolecules with similar but clearly distinct properties. *Journal of Macromolecular Science, Part A* **33**: 1399-1425.
49. S. R. Beeren and O. Hindsgaul. 2013. Nature's dendrimer: Characterizing amylopectin as a multivalent host. *Angewandte Chemie International Edition* **52**: 11265-11268.
50. H. Lundqvist, A.-C. Eliasson, and G. Olofsson. 2002. Binding of hexadecyltrimethylammonium bromide to starch polysaccharides. Part i. Surface tension measurements. *Carbohydrate Polymers* **49**: 43-55.
51. H. Lundqvist, A.-C. Eliasson, and G. Olofsson. 2002. Binding of hexadecyltrimethylammonium bromide to starch polysaccharides. Part ii. Calorimetric study. *Carbohydrate Polymers* **49**: 109-120.
52. L. Bi, L. Yang, G. Narsimhan, A. K. Bhunia, and Y. Yao. 2011. Designing carbohydrate nanoparticles for prolonged efficacy of antimicrobial peptide. *Journal of Controlled Release* **150**: 150-156.
53. Y. Xie and Y. Yao. 2018. Octenylsuccinate hydroxypropyl phytoglycogen enhances the solubility and in-vitro antitumor efficacy of niclosamide. *International Journal of Pharmaceutics* **535**: 157-163.

54. P. Serge and B. Eric. 2010. The molecular structures of starch components and their contribution to the architecture of starch granules: A comprehensive review. *Starch - Stärke* **62**: 389-420.
55. J.-L. Putaux, A. Buléon, R. Borsali, and H. Chanzy. 1999. Ultrastructural aspects of phytoglycogen from cryo-transmission electron microscopy and quasi-elastic light scattering data. *International Journal of Biological Macromolecules* **26**: 145-150.
56. J. D. Nickels, J. Atkinson, E. Papp-Szabo, C. Stanley, S. O. Diallo, S. Perticaroli, B. Baylis, P. Mahon, G. Ehlers, J. Katsaras, and J. R. Dutcher. 2016. Structure and hydration of highly-branched, monodisperse phytoglycogen nanoparticles. *Biomacromolecules* **17**: 735-743.
57. M. Grossutti and J. R. Dutcher. 2016. Correlation between chain architecture and hydration water structure in polysaccharides. *Biomacromolecules* **17**: 1198-1204.
58. M. C. Sweedman, M. J. Tizzotti, C. Schäfer, and R. G. Gilbert. 2013. Structure and physicochemical properties of octenyl succinic anhydride modified starches: A review. *Carbohydrate Polymers* **92**: 905-920.
59. M. Kuentz, P. Egloff, and D. Röthlisberger. 2006. A technical feasibility study of surfactant-free drug suspensions using octenyl succinate-modified starches. *European Journal of Pharmaceutics and Biopharmaceutics* **63**: 37-43.
60. C. Ratchanee, J. Anuvat, J. Kamolwan, H. Thepkunya, N. Onanong, and M. D. Julian. 2011. Influence of biopolymer emulsifier type on formation and stability of rice bran oil-in-water emulsions: Whey protein, gum arabic, and modified starch. *Journal of Food Science* **76**: E165-E172.
61. P. Vita, F. Takeshi, and Y. Hidefumi. 2012. High-oil-load encapsulation of medium-chain triglycerides and d-limonene mixture in modified starch by spray drying. *Journal of Food Science* **77**: E38-E44.
62. A. H. Goldberg, M. Gibaldi, and J. L. Kanig. 1966. Increasing dissolution rates and gastrointestinal absorption of drugs via solid solutions and eutectic mixtures iii: Experimental evaluation of griseofulvin—succinic acid solid solution. *Journal of Pharmaceutical Sciences* **55**: 487-492.
63. M. Thommes, D. R. Ely, M. T. Carvajal, and R. Pinal. 2011. Improvement of the dissolution rate of poorly soluble drugs by solid crystal suspensions. *Molecular Pharmaceutics* **8**: 727-735.
64. K. Sekiguchi and N. Obi. 1961. Studies on absorption of eutectic mixture. I. A comparison of the behavior of eutectic mixture of sulfathiazole and that of ordinary sulfathiazole in man. *Chemical & Pharmaceutical Bulletin* **9**: 866-872.
65. A. H. Goldberg, M. Gibaldi, and J. L. Kanig. 1965. Increasing dissolution rates and gastrointestinal absorption of drugs via solid solutions and eutectic mixtures i. Theoretical considerations and discussion of the literature. *Journal of Pharmaceutical Sciences* **54**: 1145-1148.
66. A. H. Goldberg, M. Gibaldi, and J. L. Kanig. 1966. Increasing dissolution rates and gastrointestinal absorption of drugs via solid solutions and eutectic mixtures ii: Experimental evaluation of a eutectic mixture: Urea-acetaminophen system. *Journal of Pharmaceutical Sciences* **55**: 482-487.

67. C. Leuner and J. Dressman. 2000. Improving drug solubility for oral delivery using solid dispersions. *European Journal of Pharmaceutics and Biopharmaceutics* **50**: 47-60.
68. M. Efentakis, A. Koutlis, and M. Vlachou. 2000. Development and evaluation of oral multiple-unit and single-unit hydrophilic controlled-release systems. *AAPS PharmSciTech* **1**: 62-70.
69. M. M. Crowley, F. Zhang, M. A. Repka, S. Thumma, S. B. Upadhye, S. Kumar Battu, J. W. McGinity, and C. Martin. 2007. Pharmaceutical applications of hot-melt extrusion: Part i. *Drug Development and Industrial Pharmacy* **33**: 909-926.
70. R. Bodmeier and O. Paeratakul. 1991. Constant potassium chloride release from microporous membrane-coated tablets prepared with aqueous colloidal polymer dispersions. *Pharmaceutical Research* **8**: 355-359.
71. A. T. M. Serajuddin. 1999. Solid dispersion of poorly water-soluble drugs: Early promises, subsequent problems, and recent breakthroughs. *Journal of Pharmaceutical Sciences* **88**: 1058-1066.
72. L. S. Taylor and G. Zografi. 1997. Spectroscopic characterization of interactions between pvp and indomethacin in amorphous molecular dispersions. *Pharmaceutical Research* **14**: 1691-1698.
73. S. Shah and M. A. Repka. Melt extrusion in drug delivery: Three decades of progress. In M. A. Repka, N. Langley, and J. DiNunzio (eds), *Melt extrusion: Materials, technology and drug product design* (M. A. Repka, N. Langley, and J. DiNunzio, eds), Springer New York, New York, NY, 2013, pp. 3-46.
74. S. Bialleck and H. Rein. 2011. Preparation of starch-based pellets by hot-melt extrusion. *European Journal of Pharmaceutics and Biopharmaceutics* **79**: 440-448.
75. J. Liu, F. Zhang, and J. W. McGinity. 2001. Properties of lipophilic matrix tablets containing phenylpropanolamine hydrochloride prepared by hot-melt extrusion. *European Journal of Pharmaceutics and Biopharmaceutics* **52**: 181-190.
76. A. Melocchi, G. Loreti, M. D. Del Curto, A. Maroni, A. Gazzaniga, and L. Zema. 2015. Evaluation of hot-melt extrusion and injection molding for continuous manufacturing of immediate-release tablets. *Journal of Pharmaceutical Sciences* **104**: 1971-1980.
77. M. Fukuda, N. A. Peppas, and J. W. McGinity. 2006. Properties of sustained release hot-melt extruded tablets containing chitosan and xanthan gum. *International Journal of Pharmaceutics* **310**: 90-100.
78. A. Gryczke, S. Schminke, M. Maniruzzaman, J. Beck, and D. Douroumis. 2011. Development and evaluation of orally disintegrating tablets (odts) containing ibuprofen granules prepared by hot melt extrusion. *Colloids and Surfaces B: Biointerfaces* **86**: 275-284.
79. M. A. Repka and J. W. McGinity. 2001. Bioadhesive properties of hydroxypropylcellulose topical films produced by hot-melt extrusion. *Journal of Controlled Release* **70**: 341-351.
80. C. R. Palem, S. Kumar Battu, S. Maddineni, R. Gannu, M. A. Repka, and M. R. Yamsani. 2013. Oral transmucosal delivery of domperidone from immediate release films produced via hot-melt extrusion technology. *Pharmaceutical Development and Technology* **18**: 186-195.

81. P. K. Mididoddi, S. Prodduturi, and M. A. Repka. 2006. Influence of tartaric acid on the bioadhesion and mechanical properties of hot-melt extruded hydroxypropyl cellulose films for the human nail. *Drug Development and Industrial Pharmacy* **32**: 1059-1066.
82. Z. Ghalanbor, M. Körber, and R. Bodmeier. 2010. Improved lysozyme stability and release properties of poly(lactide-co-glycolide) implants prepared by hot-melt extrusion. *Pharmaceutical Research* **27**: 371-379.
83. L. Schenck, G. M. Troup, M. Lowinger, L. Li, and C. McKelvey. Achieving a hot melt extrusion design space for the production of solid solutions. In D. J. a. Ende (ed), *Chemical engineering in the pharmaceutical industry* (D. J. a. Ende, ed), John Wiley & Sons, Inc., New Jersey, 2010.
84. C. Brown, J. DiNunzio, M. Eglesia, S. Forster, M. Lamm, M. Lowinger, P. Marsac, C. McKelvey, R. Meyer, L. Schenck, G. Terife, G. Troup, B. Smith-Goettler, and C. Starbuck. Hot-melt extrusion for solid dispersions: Composition and design considerations. In N. Shah, H. Sandhu, D. S. Choi, H. Chokshi, and A. W. Malick (eds), *Amorphous solid dispersions: Theory and practice* (N. Shah, H. Sandhu, D. S. Choi, H. Chokshi, and A. W. Malick, eds), Springer New York, New York, NY, 2014, pp. 197-230.
85. J.-M. Bouvier and O. H. Campanella. *Extrusion processing technology: Food and non-food biomaterials*, John Wiley & Sons, 2014.
86. J. C. DiNunzio, F. Zhang, C. Martin, and J. W. McGinity. Melt extrusion. In R. O. Williams III, A. B. Watts, and D. A. Miller (eds), *Formulating poorly water soluble drugs* (R. O. Williams III, A. B. Watts, and D. A. Miller, eds), Springer New York, New York, NY, 2012, pp. 311-362.
87. M. Mollan. Historical overview. In I. Ghebre-Sellassie and C. Martin (eds), *Pharmaceutical extrusion technology* (I. Ghebre-Sellassie and C. Martin, eds), Drugs and the pharmaceutical sciences, Marcel Dekker, Inc., New York, 2003.
88. J. C. DiNunzio and D. A. Miller. Formulation development of amorphous solid dispersions prepared by melt extrusion. In M. A. Repka, N. Langley, and J. DiNunzio (eds), *Melt extrusion: Materials, technology and drug product design* (M. A. Repka, N. Langley, and J. DiNunzio, eds), Springer New York, New York, NY, 2013, pp. 161-203.
89. C. Nikitine, E. Rodier, M. Sauceau, and J. Fages. 2009. Residence time distribution of a pharmaceutical grade polymer melt in a single screw extrusion process. *Chemical Engineering Research and Design* **87**: 809-816.
90. S. J. Kapp and P. A. Palmer. Controls and instrumentation. In I. Ghebre-Sellassie and C. Martin (eds), *Pharmaceutical extrusion technology* (I. Ghebre-Sellassie and C. Martin, eds), Drugs and the pharmaceutical sciences, Marcel Dekker, Inc., New York, 2003.
91. M. M. Crowley, F. Zhang, J. J. Koleng, and J. W. McGinity. 2002. Stability of polyethylene oxide in matrix tablets prepared by hot-melt extrusion. *Biomaterials* **23**: 4241-4248.
92. A. Dreiblatt. Process design. In I. Ghebre-Sellassie and C. Martin (eds), *Pharmaceutical extrusion technology* (I. Ghebre-Sellassie and C. Martin, eds), Drugs and the pharmaceutical sciences, Marcel Dekker, Inc., New York, 2003.

93. G. Verreck, K. Six, G. Van den Mooter, L. Baert, J. Peeters, and M. E. Brewster. 2003. Characterization of solid dispersions of itraconazole and hydroxypropylmethylcellulose prepared by melt extrusion—part i. *International Journal of Pharmaceutics* **251**: 165-174.
94. E. Verhoeven, T. R. M. De Beer, G. Van den Mooter, J. P. Remon, and C. Vervaet. 2008. Influence of formulation and process parameters on the release characteristics of ethylcellulose sustained-release mini-matrices produced by hot-melt extrusion. *European Journal of Pharmaceutics and Biopharmaceutics* **69**: 312-319.
95. D. Leister, T. Geilen, and T. Geissler. Twin-screw extruders for pharmaceutical hot-melt extrusion: Technology, techniques and practices. In D. Douroumis (ed), *Hot-melt extrusion: Pharmaceutical applications* (D. Douroumis, ed), John Wiley & Sons, Ltd, United Kingdom, 2012.
96. G. Verreck. The influence of plasticizers in hot-melt extrusion. In D. Douroumis (ed), *Hot-melt extrusion: Pharmaceutical applications* (D. Douroumis, ed), John Wiley & Sons Ltd, Chichester, West Sussex, U.K., 2012.
97. M. Rahman and C. S. Brazel. 2004. The plasticizer market: An assessment of traditional plasticizers and research trends to meet new challenges. *Progress in Polymer Science* **29**: 1223-1248.
98. K. Kolter. Properties and applications of polyvinyllactam polymers. In M. A. Repka, N. Langley, and J. DiNunzio (eds), *Melt extrusion: Materials, technology and drug product design* (M. A. Repka, N. Langley, and J. DiNunzio, eds), Springer New York, New York, NY, 2013, pp. 83-105.
99. A. N. Ghebremeskel, C. Vemavarapu, and M. Lodaya. 2007. Use of surfactants as plasticizers in preparing solid dispersions of poorly soluble api: Selection of polymer–surfactant combinations using solubility parameters and testing the processability. *International Journal of Pharmaceutics* **328**: 119-129.
100. Y. Seung-uk, K. S. L., W. Zeren, and T. Chitra. 2009. Miscibility/stability considerations in binary solid dispersion systems composed of functional excipients towards the design of multi-component amorphous systems. *Journal of Pharmaceutical Sciences* **98**: 4711-4723.
101. S. P. Chamarthy and R. Pinal. 2008. Plasticizer concentration and the performance of a diffusion-controlled polymeric drug delivery system. *Colloids and Surfaces A: Physicochemical and Engineering Aspects* **331**: 25-30.
102. C. Aitken-Nichol, F. Zhang, and J. W. McGinity. 1996. Hot melt extrusion of acrylic films. *Pharmaceutical Research* **13**: 804-808.
103. M. M. Crowley, A. Fredersdorf, B. Schroeder, S. Kucera, S. Prodduturi, M. A. Repka, and J. W. McGinity. 2004. The influence of guaifenesin and ketoprofen on the properties of hot-melt extruded polyethylene oxide films. *European Journal of Pharmaceutical Sciences* **22**: 409-418.
104. F. Angus, H. John, and R. Thomas. 2001. Characterization of glass solutions of poorly water-soluble drugs produced by melt extrusion with hydrophilic amorphous polymers. *Journal of Pharmacy and Pharmacology* **53**: 303-315.
105. C. d. Brabander, G. v. d. Mooter, C. Vervaet, and J. P. Remon. 2002. Characterization of ibuprofen as a nontraditional plasticizer of ethyl cellulose. *Journal of Pharmaceutical Sciences* **91**: 1678-1685.

106. J. G. Lyons, M. Hallinan, J. E. Kennedy, D. M. Devine, L. M. Geever, P. Blackie, and C. L. Higginbotham. 2007. Preparation of monolithic matrices for oral drug delivery using a supercritical fluid assisted hot melt extrusion process. *International Journal of Pharmaceutics* **329**: 62-71.
107. A. Streubel, J. Siepmann, and R. Bodmeier. 2006. Drug delivery to the upper small intestine window using gastroretentive technologies. *Current Opinion in Pharmacology* **6**: 501-508.
108. K. Ito, C. T. Moynihan, and C. A. Angell. 1999. Thermodynamic determination of fragility in liquids and a fragile-to-strong liquid transition in water. *Nature* **398**: 492.
109. K. J. Crowley and G. Zografi. 2002. Water vapor absorption into amorphous hydrophobic drug/poly(vinylpyrrolidone) dispersions. *Journal of Pharmaceutical Sciences* **91**: 2150-2165.
110. R. M. Hodge, T. J. Bastow, G. H. Edward, G. P. Simon, and A. J. Hill. 1996. Free volume and the mechanism of plasticization in water-swollen poly(vinyl alcohol). *Macromolecules* **29**: 8137-8143.
111. E. Reitz, C. Vervaet, R. H. H. Neubert, and M. Thommes. 2013. Solid crystal suspensions containing griseofulvin – preparation and bioavailability testing. *European Journal of Pharmaceutics and Biopharmaceutics* **83**: 193-202.
112. S. Hülsmann, T. Backensfeld, S. Keitel, and R. Bodmeier. 2000. Melt extrusion – an alternative method for enhancing the dissolution rate of 17β-estradiol hemihydrate. *European Journal of Pharmaceutics and Biopharmaceutics* **49**: 237-242.
113. S. L. James, C. J. Adams, C. Bolm, D. Braga, P. Collier, T. Friscic, F. Grepioni, K. D. M. Harris, G. Hyett, W. Jones, A. Krebs, J. Mack, L. Maini, A. G. Orpen, I. P. Parkin, W. C. Shearouse, J. W. Steed, and D. C. Waddell. 2012. Mechanochemistry: Opportunities for new and cleaner synthesis. *Chemical Society Reviews* **41**: 413-447.
114. M. K. Beyer and H. Clausen-Schaumann. 2005. Mechanochemistry: The mechanical activation of covalent bonds. *Chemical Reviews* **105**: 2921-2948.
115. T. Grecu, R. Prohens, J. F. McCabe, E. J. Carrington, J. S. Wright, L. Brammer, and C. A. Hunter. 2017. Cocrystals of spironolactone and griseofulvin based on an in silico screening method. *CrystEngComm* **19**: 3592-3599.
116. M. C. Etter and D. A. Adsmond. 1990. The use of cocrystallization as a method of studying hydrogen bond preferences of 2-aminopyrimidine. *Journal of the Chemical Society, Chemical Communications* 589-591.
117. C. C. Sun and H. Hou. 2008. Improving mechanical properties of caffeine and methyl gallate crystals by cocrystallization. *Crystal Growth & Design* **8**: 1575-1579.
118. N. Qiao, M. Li, W. Schlindwein, N. Malek, A. Davies, and G. Trappitt. 2011. Pharmaceutical cocrystals: An overview. *International Journal of Pharmaceutics* **419**: 1-11.
119. D. Daurio, C. Medina, R. Saw, K. Nagapudi, and F. Alvarez-Núñez. 2011. Application of twin screw extrusion in the manufacture of cocrystals, part i: Four case studies. *Pharmaceutics* **3**: 582.
120. K. Boksa, A. Otte, and R. Pinal. 2014. Matrix-assisted cocrystallization (mac) simultaneous production and formulation of pharmaceutical cocrystals by hot-melt extrusion. *Journal of Pharmaceutical Sciences* **103**: 2904-2910.

121. C. Saal and A. Becker. 2013. Pharmaceutical salts: A summary on doses of salt formers from the orange book. *European Journal of Pharmaceutical Sciences* **49**: 614-623.
122. P. H. Stahl, C. G. Wermuth, and International Union of Pure and Applied Chemistry. *Handbook of pharmaceutical salts : Properties, selection, and use*, VHCA : Wiley-VCH, Weinheim ; New York, 2002.
123. D. Daurio, K. Nagapudi, and F. Alvarez-Núñez. Manufacture of pharmaceutically relevant materials by mechanochemistry using twin screw extrusion. In A. M. Repka, N. Langley, and J. DiNunzio (eds), *Melt extrusion: Materials, technology and drug product design* (A. M. Repka, N. Langley, and J. DiNunzio, eds), Springer New York, New York, NY, 2013, pp. 223-242.
124. K. S. R. Vaka, M. M. Bommana, D. Desai, J. Djordjevic, W. Phuapradit, and N. Shah. Excipients for amorphous solid dispersions. In N. Shah, H. Sandhu, S. D. Choi, H. Chokshi, and W. A. Malick (eds), *Amorphous solid dispersions: Theory and practice* (N. Shah, H. Sandhu, S. D. Choi, H. Chokshi, and W. A. Malick, eds), Springer New York, New York, NY, 2014, pp. 123-161.

CHAPTER 2. DRUG SOLUBILIZATION BY MEANS OF A SURFACE-MODIFIED EDIBLE BIOPOLYMER ENABLED BY HOT MELT EXTRUSION*

2.1 Abstract

A coprocessing/formulation approach for increasing the solubility of poorly soluble drugs using solid dispersions is presented, whereby the active pharmaceutical ingredients (API) retain its crystalline state. The approach uses a biopolymer naturally produced as dendrimeric nanoparticles that has been surface-modified to act as a solubilizing agent. The solubilizing agent is enabled by hot melt extrusion to produce the solid dispersions. Four APIs, phenytoin (PHT), griseofulvin, ibuprofen, and loratadine were used as model compounds to evaluate solubility enhancement. The rank order in solubility enhancement follows that of the hydrophobicity of the APIs. The APIs remained predominantly crystalline after hot melt extrusion processing. However, APIs with weak crystal structure (ibuprofen and loratadine) underwent measurable crystallinity loss. The solubilizing power of the modified biopolymer increases with increasing hydrophobicity and strength of the crystal structure. The solubility is described in terms of a parallel liquid-phase partition-association. For one API (PHT), solubility enhancement was minimal. The dissimilar behavior of PHT is discussed in terms of the polarity match between the API and the hydrophobic microenvironment in the solubilizing agent. This approach is expected to apply to a large number of poorly soluble drugs, offering a complementary approach to existing processing and formulation drug solubilization methods.

* H. J. Ong and R. Pinal. 2018. Drug solubilization by means of a surface-modified edible biopolymer enabled by hot melt extrusion. *Journal of Pharmaceutical Sciences* **107**: 402-411.

2.2 Introduction

With the advent of high-throughput and combinatorial screening tools, the number of potent drug candidates has been rapidly increasing.[1] Despite their high potency, a significant portion of new drug candidates exhibit limited aqueous solubility, and thereby low oral bioavailability.[2] Consequently, the enhancement of aqueous solubility and in vivo dissolution rate of poorly water-soluble compounds continue to be one of the most common yet challenging aspects of pharmaceutical development to date.

The solubilization of a crystalline, hydrophobic organic compound in an aqueous medium involves 2 energetically distinct processes: the breaking of the crystal lattice into molecules, and the solvation of the freed solute molecules by the solvent. These processes contribute independently to the free energy of solution, hence to the observed solubility value, quantitatively represented as follows:

$$\log X = \log X_{ideal} - \log \gamma \qquad 2.1$$

where X is the observed (mole fraction) solubility, X_{ideal} is the ideal solubility, and γ is the activity coefficient of the solute in the particular solvent medium. The first term on the right-hand side of Equation 2.1 represents the energy barrier to freeing the solute molecules from the crystal and is given by:

$$\log X_{ideal} = -\frac{\Delta S_f \left(T_m - T\right)}{2.303RT} + \frac{\Delta C_p \left(T_m - T\right)}{2.303RT} - \frac{\Delta C_p}{2.303R}\log\left(\frac{T_m}{T}\right) \qquad 2.2$$

where ΔS_f and T_m are the entropy and temperature of melting of the solute, respectively, ΔC_p is the difference in heat capacity between the liquid and solid forms of the solute, T is the absolute temperature of the measurement, and R is the gas constant. Yalkowsky[3] conducted an analysis of the 2 simplifying assumptions of Equation 2.2 commonly used for quantifying the ideal solubility. One assumption is that $\Delta C_p = 0$, or more accurately, that the last 2 terms on the right-hand side of Equation 2.2 cancel each other, such that $\frac{\Delta C_p \left(T_m - T\right)}{2.303RT} - \frac{\Delta C_p}{2.303R}\log\left(\frac{T_m}{T}\right) \approx 0$. Note that the summation of the 2 heat capacity terms on the right-hand side of Equation 2.2 can be arbitrarily small, but it must be finitely different from zero.[4] The other simplifying assumption is that $\Delta C_p = \Delta S_f$. Yalkowsky[3]

found the former assumption to be more meaningful. Accordingly, Equation 2.2 can be simplified as follows:

$$\log X_{ideal} \approx -\frac{\Delta S_f \left(T_m - T\right)}{2.303RT} \qquad 2.3$$

which has become the standard expression for estimating the ideal solubility of organic compounds. The ideal solubility is an intrinsic property of the solid solute and it is the same regardless of the solvent. It is solely dependent on the crystal lattice energy of the solid. Strictly speaking, the ideal solubility corresponds to the solubility that would be observed if the solute and solvent form an ideal mixture, namely, with zero heat of mixing and with constant partial molar volumes, with the latter equal to the molar volume of each of the pure liquid components making the mixture. Ideal solutions are rather a theoretical construct. Therefore, in practice, a nearly ideal solution is one where the solute and solvent are completely miscible in the liquid state and their mixture is nearly athermal.[5] This situation arises when the solute and solvent molecules have similar size and shape, and where solute-solute, solvent-solvent, and solute-solvent interactions are of similar nature and magnitude.[5] A good rule-of-thumb indicator of crystal lattice energy is the melting point.[6] The higher the melting point of the solute, the greater its crystal lattice energy is expected to be. Consequently, drug candidates with high melting point often display extremely low aqueous solubility.[7] From the standpoint of solution phenomena, the quantitative measure of the lattice energy of the crystal corresponds, precisely, to Equation 2.2, so that Equation 2.3 provides a close approximation.

The second term on the right-hand side of Equation 2.1 is a property characteristic of the solute-solvent mixture and quantifies the energy barrier to the mixing of the solute and solvent molecules in the liquid phase. The activity coefficient (γ) in Equation 2.1 accounts for the deviation from ideal mixing as the solvent molecules solvate the solute molecules. Thus, the activity coefficient reflects the free energy cost (or the difficulty) associated with the solvation of the solute molecules by the solvent. As the solute and solvent approach ideal (athermal and isochoric) mixing, $\gamma \rightarrow 1$ and $\log \gamma \rightarrow 0$, so that Equation 2.1 approaches Equation 2.3. Therefore, the ideal solubility quantifies the maximum solubility achievable for a solute if dissolved in a perfect (ideal) solvent. Highly nonideal mixtures result in large

activity coefficient values (orders of magnitude greater than unity). This results in solubility values that are commensurately (several orders of magnitude) lower than the ideal solubility. Hydrophobic solutes form highly nonideal mixtures with water, such that $\gamma \gg 1$, thus imposing an additional and large limitation on Equation 2.1, and consequently, on the solubility of the compound in aqueous media. For dilute solutions (poorly soluble drugs), the observed aqueous solubility can be approximated as follows[8]:

$$\log S_m = -\frac{\Delta S_f \left(T_m - T\right)}{2.303RT} - \log \gamma + c \qquad 2.4$$

where S_m is the molar solubility of the compound and c is a constant accounting for the change in units used for expressing solubility, from mole fraction to the more commonly used in practice mass/volume units.[5]

Solubilization approaches can be broadly divided into 2 categories: solvent modification and solute modification.[5, 9] Solvent modification typically involves the use of solubility enhancers such as pH adjustment, cosolvents, emulsifiers, surfactants, complexing and hydrotropic agents.[10] Drug solubilization is achieved by creating a favorable solvating environment, capable of maintaining discrete hydrophobic molecules in aqueous media, by means of decreasing the magnitude of the (negative) contribution of the activity coefficient in Equation 2.1, without affecting the contribution of the crystal lattice effect. While these approaches are effective in producing a thermodynamically stable enhancement in solubility, these techniques are limited by the maximum solubility that can be obtained for a given concentration of the solubilizing agent.[5] Solute modification strategies typically involve either the alteration of the physical characteristics of the crystal by means of mechanical methods or the incorporation of a secondary component into the solute phase, such as the use of eutectic mixtures, solid solutions, or glass solutions.[9, 11] These approaches frequently lead to the formation of metastable crystalline and amorphous phases, thereby reducing or even eliminating, at least in theory, the limitation imposed by the crystal lattice energy (ideal solubility), without altering the contribution of the hydrophobicity effect of the solute.[12] Solute modification methods are generally effective in increasing the solubility and dissolution rate of organic compounds. However, the enhancement in apparent solubility (solute concentration) may only last temporarily and

eventually revert to the equilibrium solubility of the most stable form.[13] Clearly, these solubility enhancement techniques are not always adequate to deal with the current challenges in pharmaceutical development.

Rationale

As stated above, solvent modification approaches for increasing drug solubility produce a favorable solvation environment for the solute, thus increasing the capacity of the system to maintain the solute in liquid state, relative to that of pure water. Solvent modification has the effect of reducing the value of γ in Equation 2.1, thus increasing the observed solubility without altering the ideal solubility (crystallinity effect). However, such approaches require a formulated vehicle in order to achieve the increase in solubility sought. Solid dosage forms, taken with plain water, is the most common way drugs are taken by patients. Therefore, a means of increasing drug solubility from a solid formulation reconstituted with plain water or a predominantly aqueous medium would be advantageous for numerous poorly soluble drugs.

Taking Equation 2.1 as starting point, one way of increasing the observed solubility without altering either of the 2 terms on the right-hand side, is to incorporate an additional equilibrium, such as partitioning or complexation. The underlying concept consists of creating an intimate solid mixture of the crystalline drug with a solid component excipient, which upon hydration provides a liquid medium of reduced polarity available to drug molecules dislodged from the crystal, thus increasing the total concentration of drug in the solution phase. The property requirements for such solid excipient include the following:

(1) Readily hydrated by plain water

(2) Having high surface area

(3) Provides a low polarity (hydrophobic) environment when hydrated

Although requirements **1** and **3** above can be considered mutually exclusive in many instances, the issue can be resolved by means of a modified hydrophilic biopolymer, as described below.

In this chapter, we present a combined formulation/process, i.e. coprocessing platform approach for generating solid dispersions (SDs) that by virtue of being nonamorphous are thermodynamically stable. The SDs generated do not involve the obliteration of the crystal lattice structure of the API in order to increase the solubility. These nonamorphous SD systems are capable of enhancing the drug-release performance while maintaining the physical stability of the API in solid oral formulations.

This study also evaluates the potential of a low-cost, biocompatible phytoglycogen polymer of vegetal origin, naturally produced as dendrimeric nanoparticles. These attributes of the biodendrimeric (BD) material satisfy the property requirements **1** and **2** enumerated above. In order to provide a hydrated environment of lower polarity than that of water (requirement **3**), their surface of the BD material is modified by means of covalently linked octenylsuccinate (OS) groups. The result is a polymeric carrier matrix with solubility-enhancing properties. The nonamorphous dispersions of this study use the BD material as carrier matrix. Accordingly, they are referred to as biodendrimeric solid dispersions (BDSDs) throughout this chapter.

Phytoglycogen is a glycogen-like α-D-glucan found in plant mutants such as those of maize, sorghum, and algae. Phytoglycogen nanoparticles are naturally produced with roughly spherical shape with typical size range of 30 to 100 nm.[14] Phytoglycogen nanoparticles readily hydrate, and the presence of covalently linked hydrophobic OS groups on the dendrimer-like biopolymer (DLB) results in a hydrated microenvironment containing an organic region formed by aliphatic chains that are locked in place. A similar situation is responsible for the partition phenomenon responsible for chromatographic retention in reversed-phase HPLC, where the stationary-phase microparticles (silica in this case) are covalently covered with hydrophobic chains. A graphic representation of the solubilization process of the approach presented here is depicted in Figure 2-1. By themselves, the hydrophilic native-DLB nanoparticles have a negligible effect, if any, on solubility, such that the solubility of the drug is virtually the same as its aqueous solubility. The presence of hydrophobic chains on the OS-modified DLB (OS-DLB) provides the nonpolar microenvironment necessary for producing the secondary (partitioning) equilibrium

responsible for the increase in the total amount of solute present in solution. It should be pointed out that the nanoscale of the OS-DLB particles is relevant in 2 ways. From the theoretical point of view, the high (hydrophobically modified) surface area helps maximize the contribution of the secondary (partition) phenomenon per unit mass of OS-DLB. From the practical point of view, the hydrated system is a colloidal dispersion with bulk and handling properties like those of a normal liquid solution. Brownian motion prevents the settling of the suspensions for indefinite time periods. In addition, their liquid-like handling is such that they pass unchanged through 0.22 μm filter membranes. The effect of this new type of BDSD is expected to be 2-fold: increasing the apparent aqueous solubility of these drugs, and potentially enhancing the permeability and retention effect in vivo, owing to the nanoscale of the complexes (noting that in this context, the term "complex" broadly refers to molecular association between the hydrophobic solute and the OS-modified phytoglycogen particles).[15, 16] The present study focuses on the solubilizing properties of the surface-modified (OS) DLB, that is, the OS-DLB and not on the native-DLB. For simplicity, throughout the subsequent text in this chapter, the plain "DLB" designation is reserved for the OS-DLB, while the native DLB is referred to as "native-DLB."

Hot melt extrusion (HME) was chosen as an enabling processing technology for preparing the coprocessed BDSDs because it offers significant advantages over other traditional pharmaceutical processing techniques, such as short processing time, intimate mixing, and highly controllable processing conditions.[17] Four poorly water-soluble compounds were used as model drugs. These are, phenytoin (PHT), griseofulvin (GSF), ibuprofen (IBU), and loratadine (LOR). The model drugs were used to assess the solubility enhancement based on the BDSD coprocessing platform. The first 2 model drugs (PHT and GSF) cover the case where poor solubility is primarily the result of the high lattice energy of the crystalline solute (first term on the right-hand side of Equation 2.1). The other 2 drugs (IBU and LOR) cover the case where the solubility is primarily limited through the second term of Equation 2.1, that is, by virtue of their hydrophobicity.

2.3 Experimental

2.3.1 Materials

PHT was obtained from Spectrum (Gardena, CA), GSF from Hawkins (Minneapolis, MN), IBU from BASF (Bishop, TX), and LOR from Mallinckrodt (St. Louis, MO). All drug substances were used as received. Poloxamer 338 (PLX) was obtained from BASF (North Mount Olive, NJ) and was gently ground with mortar and pestle and screened through a US 100 mesh sieve (aperture size of 150 μm) before use. OS-DLB was prepared by Professor Yuan Yao's laboratory as described elsewhere.[16] All solvents were of HPLC grade and were obtained from Fisher Chemical (Fair Lawn, NJ).

2.3.2 Methods

2.3.2.1 Quantification of drug association

The amount of API associated with OS-DLB in solution was quantified following a 3-step procedure. This was necessary because the drug-loaded OS-DLB particles are so small that they cannot be separated from the aqueous solution by simple means such as filtration (0.22 μm) or even by ultracentrifugation. Note that because the OS-DLB colloidal dispersions handle like a normal liquid, we use the term “solution” when referring to DLB-water mixtures. First, 500 μL of dimethyl sulfoxide was added to an equal volume of aqueous solution of API, DLB, and PLX and agitated at room temperature for 30 min, to extract the drug molecules from the colloidal DLB particles. Following the extraction of the API from the DLB, 500 μL of 20% (w/w) sodium chloride solution was added to the mixture and agitated at room temperature for 30 min to precipitate the DLB nanoparticles. Finally, the mixture was centrifuged at 12,000 rpm for 20 min, and the amount of drug in the supernatant was assayed using HPLC. A control study was performed (data not shown) to determine the efficiency of removal of the drug associated in the DLB particles. The efficiency of extraction of DLB-associated drug was at least 95%.

2.3.2.2 Phase solubility measurements

Solubility measurements were carried out according to the method described by Connors and Higuchi.[18] Briefly, excess amounts of API were added to aqueous solutions containing either DLB or PLX at varying concentrations and agitated at constant temperature (25°C ± 0.5°C). After 24 h, an aliquot was removed and filtered through a 0.45 μm surfactant-free cellulose acetate membrane. The samples were treated and analyzed using HPLC, following the extraction and DLB separation procedure described in the preceding section.

2.3.2.3 Hot melt extrusion

In a typical HME experiment, 4 g of API, DLB, and processing aid (3:1:1 weight) were first blended by gentle vortexing for approximately 1 min. The mixture was then fed into a Thermo Scientific HAAKE MiniLab micro compounder (Waltham, MA), equipped with dual conical corotating screws (screw diameter of 14 to 5 mm, 11 cm length), and with a valve for controlling the residence time of the sample through the extruder chamber. Direct extrusion of a solid mixture containing only the crystalline API and the DLB powder was not possible. The torque generated was exceedingly high, such that it triggered the safety shut-off mechanism of the extruder. Therefore, a processing aid was necessary. If the objective of the processing aid were solely to reduce the torque generated during extrusion, a number of different materials could serve such function. However, because the purpose of the present study was to investigate the solubilizing properties of the DLB material, the choice of processing aid was limited. Specifically, the processing aid chosen had to be one that does not act as solubilizer for the drugs used in the study. If the processing aid also acts as a solubilizer, its presence would produce a large confounding effect on the solubilizing properties of DLB. Therefore, the processing aid had to be a material capable of reducing the torque during extrusion, but at the same time, a material that by itself did not have a solubilizing effect on the drugs. Based on these considerations, PLX was selected as processing aid in this study. PLXs are known to have surface activity, which makes them potential solubilizing agents. However, the PLX 338 concentrations used throughout this study fall below the critical micelle concentration,[19] such that PLX 338 acts as a wetting agent but not as a solubilizer. PLX 338 was found to have no appreciable

solubilizing effect on any of the model drugs included in this study (data not shown), hence PLX was selected as processing aid for this particular study. Preliminary experiments showed that 20% (w/w) PLX provided a suitable processing aid for extrusion. The feeding step into the extruder was completed within 5 min. The SDs were prepared using screw speed of 60 rpm, residence time of 15 min, and barrel temperature of 100°C for PHT and GSF, 30°C for IBU, and 65°C for LOR, well below the melting temperature of the API in each case.

2.3.2.4 Differential scanning calorimetry

Thermal analysis was performed using a PerkinElmer DSC 7 (Waltham, MA) equipped with a PerkinElmer Intercooler 1. Samples (2-4 mg) were hermetically sealed in aluminum pans (20 μL) and heated at 10°C/min under dry nitrogen purge with a flow rate of 20 mL/min. Data analysis was performed using the Pyris™ data analysis software.

2.3.2.5 X-ray diffraction

Powder X-ray diffraction was performed using a Rigaku SmartLab X-ray diffractometer (Tokyo, Japan). Measurements were taken using CuKα radiation at 40 kV and 44 mV over a 2θ angle range of 5°-40°, with a scan rate of 4°/min and a step size of 0.02°. The percent crystallinity of the API in the BDSD was estimated with respect to its corresponding physical mixture (PM) using PONKCS (partial or no known crystal structure), a Rietveld refinement method described by Scarlett and Madsen.[20] Data analysis was conducted using Panalytical X'Pert HighScore Plus 4 (Almelo, the Netherlands).[21] First, an *hkl* file that best fit the observed amorphous halo was generated for each, DLB and PLX, based on the diffraction pattern of the pure material. The diffraction pattern of the APIs was refined using the crystal structure information obtained from the Cambridge Structural Database. Subsequently, the peak files were incorporated into the quantification of the phases present in the PMs, where the pseudo-formula mass of DLB and PLX was scaled according to their known weight fractions. Finally, the values determined for the pseudo-formula mass were used in all subsequent analyses of corresponding BDSDs. The percent crystallinity of the

API in the BDSD is defined as the ratio of the API phase in the BDSD relative to that present in the PM.

2.3.2.6 Time-concentration profile

The dissolution study was performed by suspending a sample equivalent to 2.5 ± 0.2 mg of API into the barrel of a 30 mL syringe, filled with 28 mL of deionized water and fitted with a 0.45 μm surfactant-free cellulose acetate syringe filter. The syringe was placed on a rotating shaker set at 10 rpm at room temperature. A 2 mL aliquot was collected from the mixing solution at the first time point, and 1 mL aliquots were withdrawn at subsequent time points. The samples were treated and analyzed according to the extraction and HPLC quantification procedure described above.

2.4 Results and Discussion

2.4.1 Solubilization effect

The experimentally determined melting properties and the calculated solubility properties, crystallinity (ideal solubility) and hydrophobicity (activity coefficient) of the model drugs used in this study, are listed in Table 2-1. The relative contributions of the crystallinity and hydrophobicity effects on the solubility of the solutes (Equation 2.1) are graphically represented in Figure 2-2. The black portion of the bars represents solubility limit imposed by the crystal properties of the solute (log X_{ideal}). The white portion of the bars represents the additional solubility limit imposed by the hydrophobicity of the solute (–log γ). Based on log X_{ideal} values, the order of crystal lattice energy of the solutes is IBU < LOR < GSF < PHT. Based on log γ values, which is the thermodynamic parameter that best quantifies hydrophobicity, the order of hydrophobicity of the model drugs is PHT < GSF < IBU < LOR.

Figure 2-3 shows the solubility values (S), relative to the aqueous solubility (S_o), for the model drugs as a function of the concentration of DLB dispersed in water at 25°C ± 0.5°C. The solubilizing effect of DLB ranges from substantial (LOR) to marginal (PHT). It is

noteworthy that the rank order in solubilizing effect of DLB matches the rank order in hydrophobicity of the drugs (Table 2-1). The more hydrophobic the solute, the greater the solubilizing effect of DLB. These results indicate that while the OS-modified surface of DLB is necessarily saturated with water, the microenvironment produced remains predominantly hydrophobic, hence favoring association (partitioning) of the more hydrophobic solute molecules. The profiles in Figure 2-3 correspond to the type of solubilization profile observed when a parallel equilibrium process involving the solute takes place in the solution phase, in addition to the solid-liquid equilibrium.[22] Accordingly,

Main equilibrium: $A_{solid} \rightleftharpoons A^{aq.}_{solution}$

Parallel equilibrium: $A^{aq.}_{solution} \rightleftharpoons A^{org.}_{solution}$

where *A* denotes the solute and the superscripts *aq.* and *org.* denote the liquid-phase solute present in the aqueous (solvent) environment and in the organic microenvironment of the (OS-modified) DLB, respectively. The partition-association equilibrium constant (*K*) for the parallel equilibrium is given by

$$K = \frac{[A]^{org.}_{solution}}{[A]^{aq.}_{solution}} \qquad 2.5$$

and the solubility value resulting from the combined equilibria can be expressed as

$$S = S_o\left(1 + K \cdot M\right) \qquad 2.6$$

Alternatively,

$$S/S_o = 1 + K \cdot M \qquad 2.7$$

where *S* and S_o are as defined above and *M* is the amount of DLB present in the system. Rough but nevertheless useful estimates of the *K* values for the different solutes can be obtained by fitting Equation 2.6 to the initial linear portions of the data in Figure 2-3. The estimated values for K are 1.15, 3.67, 3.82, and 17.02 L/g for PHT, GSF, IBU, and LOR, respectively. Yalkowsky et al.[23] have pointed out that equilibrium partition constants such as the octanol-water partition coefficient are defined as the ratio of concentrations in the 2 phases in dilute solution. The data in Figure 2-3 correspond to solutions that are numerically dilute (low concentration) but thermodynamically concentrated (at full

saturation). As the solute concentration approaches saturation, effects like self-association begin to take place, making the partition constant concentration dependent.[23]

It is noteworthy that despite the high hydrophobicity of the IBU molecule, a relatively small solubilizing effect of DLB on IBU (compared to LOR) is observed. The solubilization profile of IBU is closer to that of GSF than to LOR. One plausible explanation for this seemingly anomalous behavior is that while IBU is roughly 10-fold more hydrophobic than GSF (see Table 2-1), LOR is roughly 40-fold more hydrophobic than IBU. The C_8 chains in the OS groups covalently linked to DLB are quite hydrophobic, creating a solvating microenvironment that even if saturated with water, has very low polarity. The ability of a liquid environment to accommodate solute molecules is maximal when the hydrophobicity of the solute most closely matches the polarity of the solvating environment and decreases on either side of the polarity scale.[24, 25] The data indicate that the nonpolar microenvironment of the (OS-modified) DLB more closely matches the hydrophobicity of LOR, relative to the other solutes.

2.4.2 Characterization of the BDSD coprocessed formulations

The differential scanning calorimetry (DSC) thermograms of the individual components, their PM, and the BDSD of equal composition (3:1:1 API:DLB:PLX by weight) are shown for each model drug in Figure 2-4. The melting of IBU and LOR in the BDSDs exhibit noticeable melting point depression and decrease in ΔH_f, relative to the pure drug. These results indicate appreciable miscibility of the low melting drugs with PLX at their melting points. With the exception of IBU, which undergoes substantial melting point depression, the close similarity between the DSC thermograms of the PM and the BDSD suggests that the HME process preserved the original solid phase of the drugs.

Figure 2-5 shows the binary melting phase diagrams for the 4 model drugs with DLB and PLX. The negligible melting point depression of the model APIs by DLB indicates negligible miscibility between the 4 drugs and DLB. This result indicates that the mere presence of DLB does not induce the disruption of the crystal structure of the model

compounds. Therefore, the solubilizing effect of DLB takes place upon the presence of water, making it a solution-phase phenomenon. On the other hand, the melting temperature of the model drugs undergoes appreciable depression by the processing aid (PLX), especially as PLX starts to become the major component in the binary mixture. This observation shows that PLX has some potential to disperse the drugs at the molecular level, thus reducing the crystallinity of the API. The API:PLX ratio used in the BDSDs of this study is 3:1. The data in Figure 2-5 show that as the proportion of PLX exceeds this ratio, the potential for partial disruption of the crystalline structure of the API increases. In the investigation presented here, the ideal processing aid is one that is present as a component that is nonmiscible with either the DLB or the API (the sole role of the processing aid here is to reduce the torque generated during extrusion). PLX is immiscible with DLB but begins to show some miscibility with the API at concentrations around 20% (w/w) or greater, especially for IBU. However, as explained above, PLX was chosen for this study because by itself, it does not have a solubilizing effect on any of the model drugs in aqueous solution. This makes it possible to investigate the solubilizing effect of DLB without any confounding solubilization effect from the processing aid. It is expected that optimization of the HME process toward minimizing the amount of processing aid used will reduce the miscibility effect with the APIs. In addition, as stated above, the processing temperature used for generating BDSDs by HME is well below the melting point of the API, in all 4 cases, much lower than the temperature required to induce partial miscibility of the drug with PLX. This condition is likely to reduce the potential for disruption of the crystalline structure of the API, as seen from the X-ray diffraction results.

Figure 2-6 shows the X-ray diffractograms of the individual components, as well as their PMs and the corresponding BDSD with equal composition as the PM. The estimated percent crystallinity of PHT, GSF, IBU, and LOR in their BDSD with respect to their corresponding PM is 97%, 98%, 66.3%, and 84.1%, respectively. These results indicate that the original crystalline phase of the API in the BDSD is mostly preserved for all 4 model drugs. However, IBU, which has the weakest crystal structure among the 4 model compounds (see Figure 2-2), lost about one-third of its crystallinity during the process. These results indicate that the crystal disruption effect exerted by the processing aid is

insignificant for those drugs with high melting point and strong crystal lattice, and the effect becomes appreciable for drugs with weaker crystal lattice.

Figure 2-7 shows the time-concentration profile for the dissolution of each of the model APIs from the BDSDs, as well as from the corresponding PMs. With the notable exception of PHT, the dissolution rate from the BDSDs is markedly greater than those from the PMs of equal composition. The initial fast dissolution is likely due to the wetting effect of the processing aid, rather than from the solubilizing effect of the DLB. The effect of the latter is reflected on the supersaturated plateau values obtained, as discussed below.

Comparison of the results from PHT and the other 3 solutes in Figure 2-7 is informative. The PMs and corresponding BDSDs have the same composition. Thermodynamic equilibrium requires that given sufficient time, the final concentration for each API be the same, whether the PM or the BDSD was used in the experiment. This is the case for PHT, but not for the other 3 APIs within the time of the experiment. Furthermore, the final (at 120 min) concentration of PHT is the same for the plain API, the PM, and the BDSD. This result shows that DLB has a negligible, if any, solubilization effect on PHT, and that DLB only accelerates the dissolution of PHT. This is strong indication that thermodynamic equilibrium was achieved for PHT within the timeframe of the experiment. The results in Figure 2-7 also demonstrate that for the other 3 APIs – GSF, IBU, and LOR – dissolution from the BDSDs results in drug concentrations that significantly exceed the solubility of the API. The phase solubility results (see Figure 2-3) show that the rank order of the equilibrium solubilizing effect of DLB on the 3 APIs is LOR > IBU > GSF. In contrast, the rank order of the plateau values in Figure 2-7, relative to the aqueous solubility of the API, is LOR > GSF > IBU. The different concentrations obtained from the PMs and BDSDs in Figure 2-7 and the difference in rank order between the phase solubility and the time-dissolution profiles indicate that thermodynamic equilibrium has not been reached for GSF, IBU, and LOR after 120 min. Thus, the BDSDs produce high levels of supersaturation and the plateau concentration value is an apparent, rather than thermodynamic solubility. It is noteworthy that BDSDs produce long-lived supersaturation, that is, a protracted spring-and-parachute effect.[26, 27] HME processing has

been shown to produce high and long-lasting supersaturation, even in relation to PMs in other applications.[28] The impact of the manufacturing process on the solubilization profile is evident from the different time-concentration profiles of the PM and the corresponding BDSD. Subjecting the same solid blend to HME results in higher and more quickly attained supersaturated concentrations of the API. Childs et al.[29] have demonstrated the critical role that formulation plays on increasing bioavailability by means of increasing solubility. Additional studies are needed in order to elucidate the underlying reasons for the pronounced effect of the HME process. However, it is appropriate to say that BDSDs are coprocessed formulations (composites) produced by the distinctive type of intimate mixing characteristic of HME, which helps increase the efficiency of the solubilizing agent.

The rank order of the supersaturation plateau values in Figure 2-7 obtained from the BDSDs matches that of the hydrophobicity of the APIs (see Table 2-1). This indicates that the increase in drug concentration, relative to its solubility, obtained from the BDSDs is primarily a reflection of the solubilizing effect of the DLB. One question is whether the behavior observed for PHT is a reflection of the properties and potential solubilizing limitations of DLB, or of restrictions imposed by the specific solute molecule. The experimental measurements needed to fully answer this question are beyond the scope of the present report, but it is possible to roughly outline a plausible approach. If the observed behavior for PHT is primarily attributable to the properties of DLB, the likely fundamental cause is the hydrophobicity of the microenvironment created by the OS groups. PHT is the least hydrophobic among the model drugs included in this study, and the OS group contains C_8 aliphatic chains, making it highly hydrophobic. It is conceivable that even though both PHT and the C_8 chains are hydrophobic, there is not an adequate polarity match between the two, such that the hydrophobic microenvironment created by the C_8 chains is suboptimal, if not inadequate, to accommodate a molecule of comparatively low hydrophobicity like PHT. This type of situation is imposed by the inherent properties of the DLB, and one can expect a hydrophobicity ($\log \gamma$) cutoff value for the solute molecule, in order for DLB to exert the desirable solubilizing power. Under these circumstances, replacing the surface substitution to a shorter aliphatic chain would make the (less hydrophobic) modified-DLB more effective in solubilizing drugs that are, relatively

speaking, not very hydrophobic. There is a caveat however, to the use of an aliphatic chain with length other than C_8. The OS-modification chemistry has been in wide use by the food industry for several decades and falls within the generally recognized as safe (GRAS) classification by the FDA.[30] It goes without saying that in the pharmaceutical field, the difference in the regulatory hurdle for adopting a GRAS versus a non-GRAS type of chemistry for use in functional excipients is by no means trivial.

Another possibility is that the behavior observed for PHT is in fact a limitation imposed by the drug molecule itself and not by the DLB. In such case, the likely reason would be the existence of specific interactions between the PHT molecule and the OS groups that hinder the uptake of the hydrophobic PHT by the also hydrophobic microenvironment present in DLB. In such a case, one can expect that drugs other than PHT, but of similar hydrophobicity, will be effectively solubilized by DLB without the need of changing the surface-modification chemistry.

In any case, from a practical point of view, assessing whether or not DLB is an effective solubilizing agent for a particular drug of interest is a rather simple matter. A small set of simple phase solubility measurements provides a quantitative answer.

2.5 Conclusions

The use of (surface-modified) DLB nanoparticles as a carrier and solubilizing agent, coprocessed along with a suitable processing aid using HME, demonstrates the potential for increasing the apparent solubility and enhancing the dissolution rate of poorly soluble drugs, resulting in high and long-lasting supersaturation, while retaining a predominantly crystalline (hence physically stable) state of the drug. Furthermore, with their surface polarity modified by means of OS groups, DLB nanoparticles are very well suited for solubilizing drugs that in addition to possessing a strong crystal structure in the solid state, consist of molecules exhibiting extreme hydrophobic character. This new pharmaceutical application of HME offers a complementary approach to the existing repertoire of processing techniques used in product development for poorly water-soluble drugs.

Specifically, this approach is useful for drugs that are not good glass formers and that are difficult to stabilize in the amorphous state. Taking this notion one step further, it is expected that through rational design and optimization of the extrusion processing parameters, thermodynamically stable nonamorphous dispersion systems can be achieved for a large number of poorly soluble drugs.

2.6 Acknowledgments

Financial support from the Dane O. Kildsig Center for Pharmaceutical Processing Research (CPPR), Purdue Research Foundation, and the National Science Foundation (NSF DMR 1310475) is gratefully acknowledged. We thank Prof. Yuan Yao's laboratory for providing the DLB material used in the study.

Table 2-1. Physicochemical and solubility properties (crystallinity and hydrophobicity) of the solutes used in this study. (n = 3, ± *S.D.*)

Compound	T_m **(°C)**	S_m **(mg/L)**	ΔH_f **(J/g)**	**log** X_{ideal}	**log** γ
Phenytoin	296.23 ± 0.04	17.91 ± 0.61	157.85 ± 0.21	–3.32	2.57
Griseofulvin	216.86 ± 0.15	9.86 ± 0.42	112.37 ± 0.65	–2.72	3.57
Ibuprofen	74.79 ± 0.25	55.12 ± 1.52	125.58 ± 1.10	–0.65	4.66
Loratadine	134.06 ± 0.15	0.59 ± 0.03	72.63 ± 0.33	–1.30	6.25

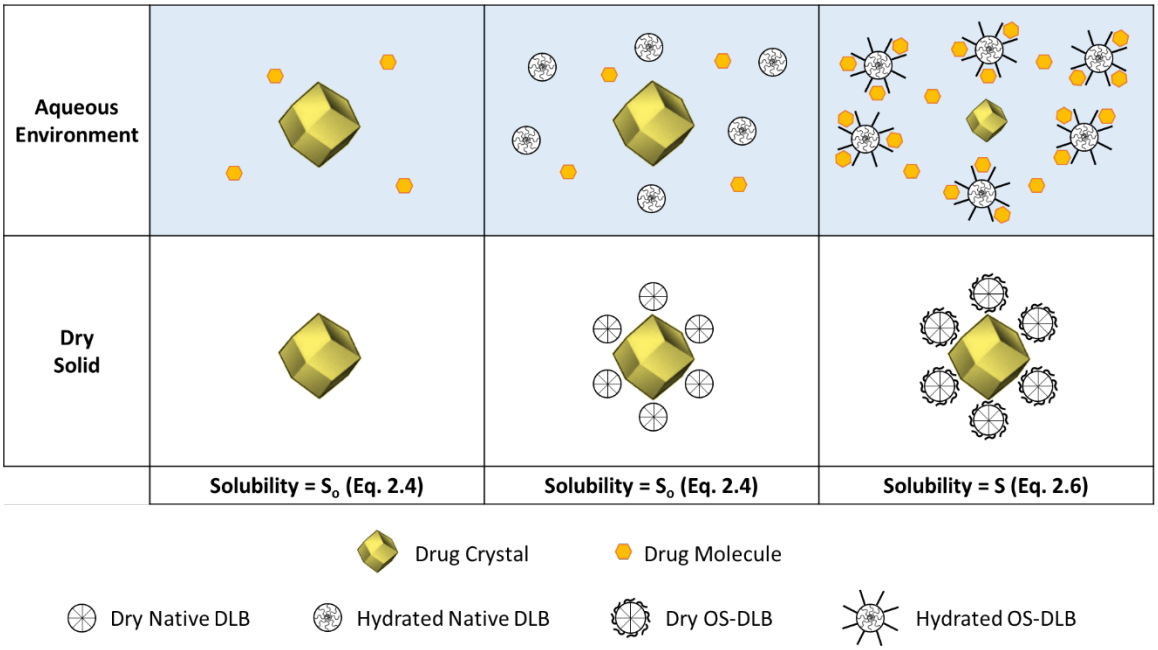

Figure 2-1. Depiction of the drug solubilization effect exerted by the native glycogen-like α-D-glucan, native-DLB, and surface-modified DLB (OS-DLB).

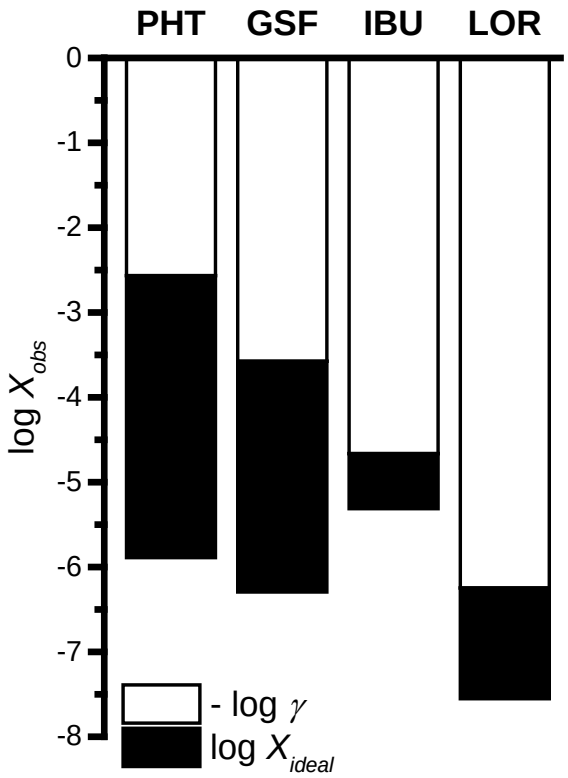

Figure 2-2. Graphical representation of the experimental aqueous solubility according to Equation 2.1. Contributions to the observed aqueous solubility for the model drugs included in the study. The black portion of the bars represents the solubility limit imposed by the crystal lattice energy of the solute (ideal solubility). The white portion of the bars represents the decrease in solubility, relative to the ideal solubility, imposed by the hydrophobicity of the drug.

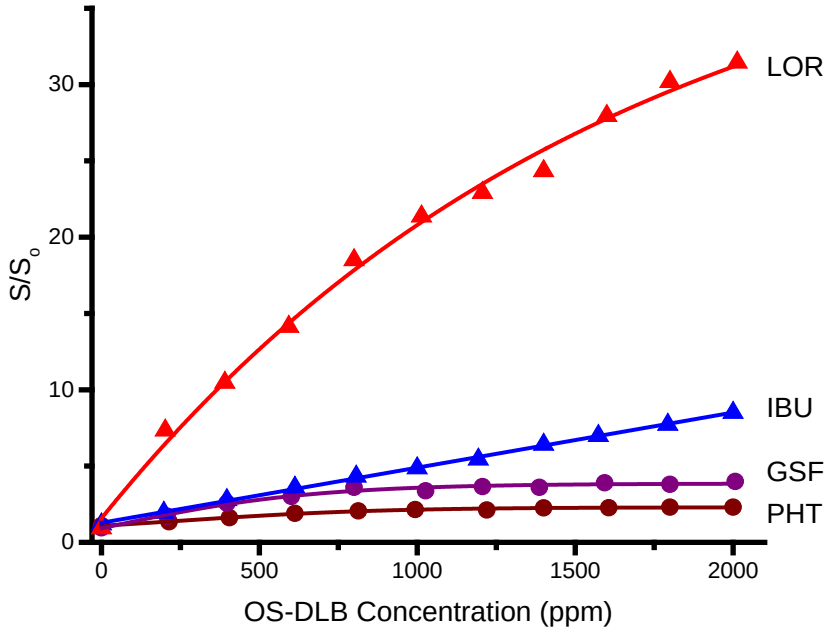

Figure 2-3. Solubility enhancement of the model drugs in aqueous OS-DLB solutions of different concentrations at 25°C ± 0.5°C. *S* and S_o represent the equilibrium solubility of the drug in the presence of OS-DLB in solution and the solubility in plain water, respectively.

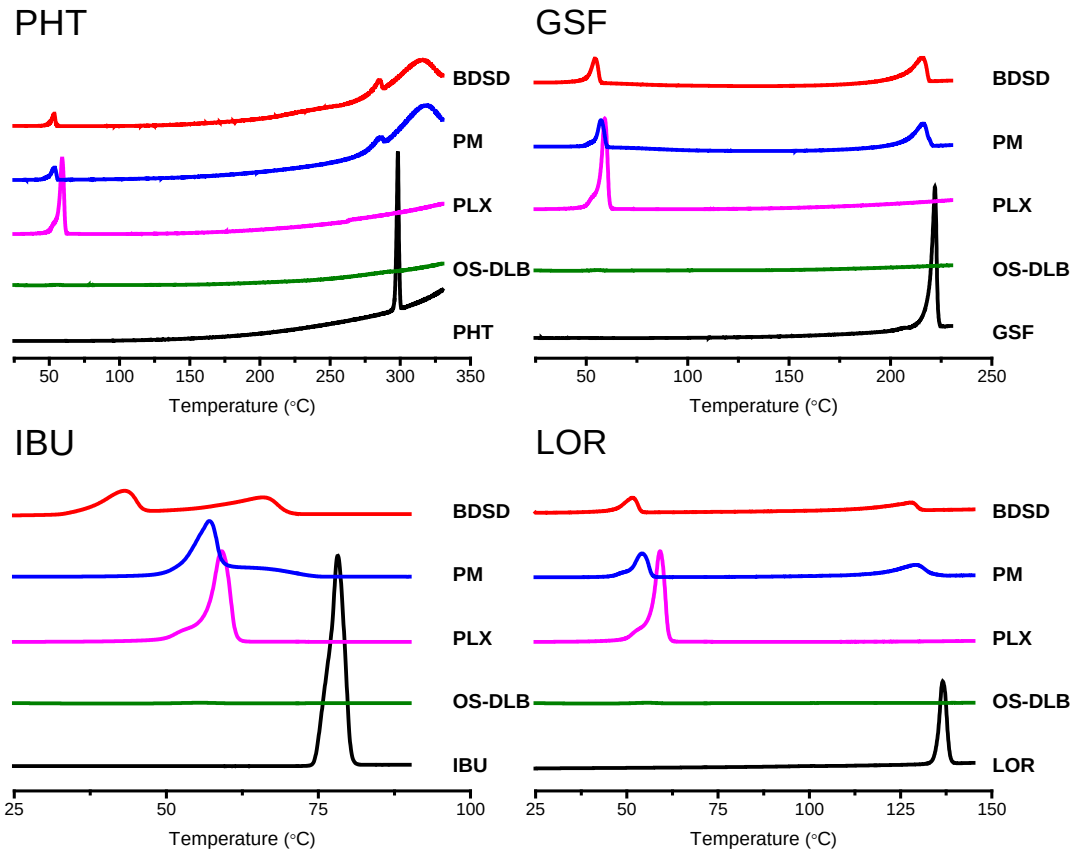

Figure 2-4. DSC thermograms of the individual components, the PM, and the BDSD for each API. The PMs and BDSDs have the same composition (3:1:1 API:DLB:PLX by weight).

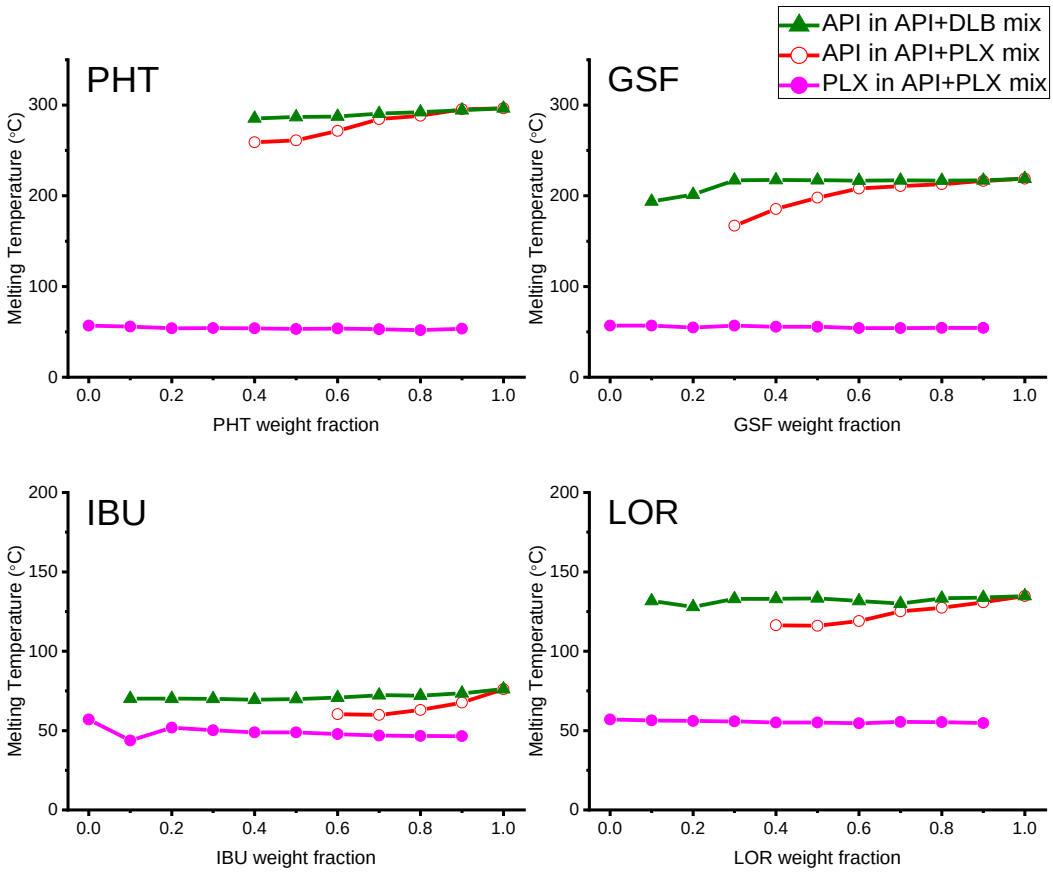

Figure 2-5. Melting phase diagrams for binary mixtures of each model drug with OS-DLB and PLX. For simplicity, OS-DLB has the designation DLB in the figure.

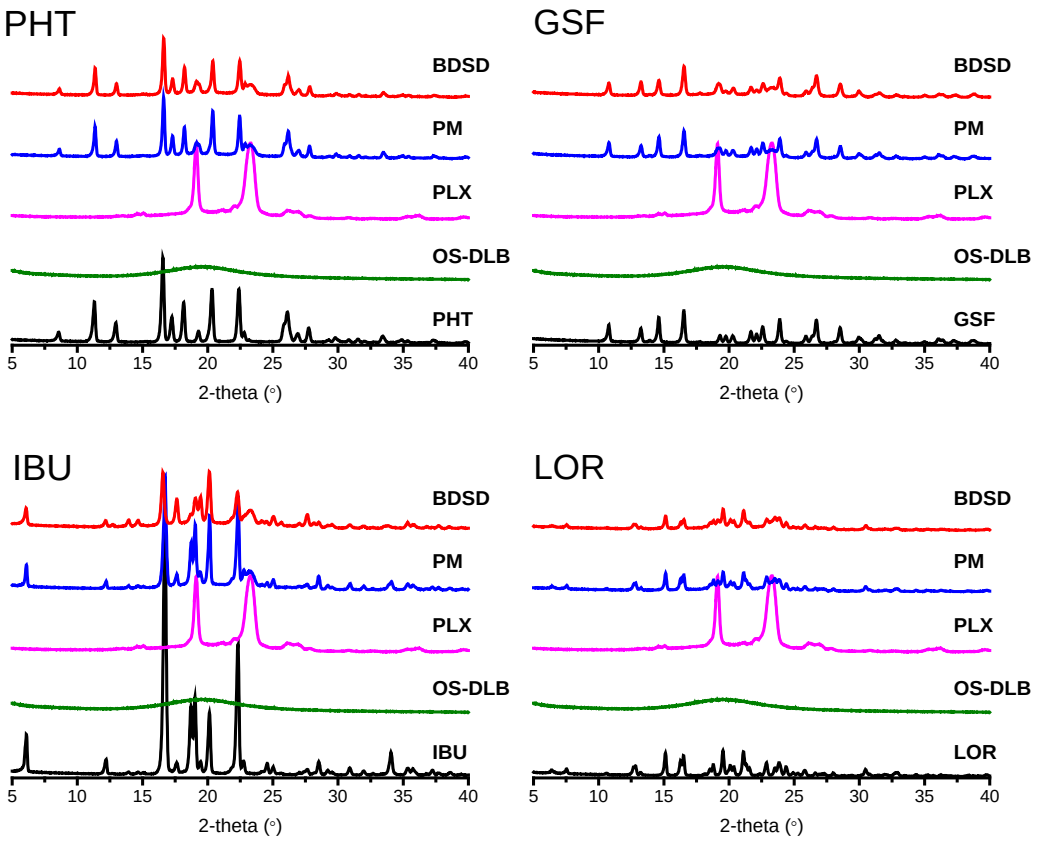

Figure 2-6. X-ray diffractograms of the individual components, the PM, and the BDSD for each API. The PMs and BDSDs have the same composition (3:1:1 API:DLB:PLX by weight).

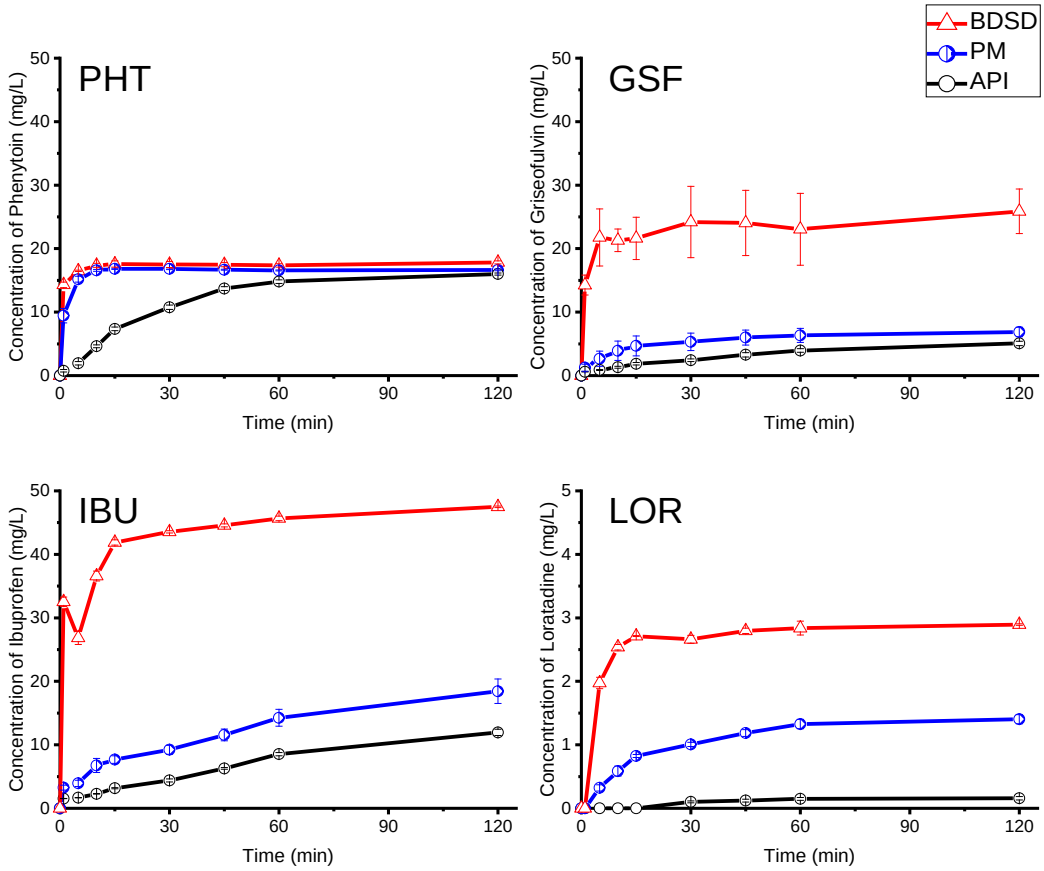

Figure 2-7. Time-concentration profiles of model drug compounds from BDSDs and their corresponding PMs (n = 3, ± *S.D.*).

2.7 References

1. C. A. Lipinski, F. Lombardo, B. W. Dominy, and P. J. Feeney. 2001. Experimental and computational approaches to estimate solubility and permeability in drug discovery and development settings. *Advanced Drug Delivery Reviews* **46**: 3-26.
2. M. Thommes, D. R. Ely, M. T. Carvajal, and R. Pinal. 2011. Improvement of the dissolution rate of poorly soluble drugs by solid crystal suspensions. *Molecular Pharmaceutics* **8**: 727-735.
3. S. H. Yalkowsky. 1981. Solubility and partitioning v: Dependence of solubility on melting point. *Journal of Pharmaceutical Sciences* **70**: 971-973.
4. R. Pinal. 2004. Effect of molecular symmetry on melting temperature and solubility. *Organic & Biomolecular Chemistry* **2**: 2692-2699.
5. S. H. Yalkowsky. *Solubility and solubilization in aqueous media*, American Chemical Society, 1999.
6. R.-M. Dannenfelser and S. H. Yalkowsky. 1996. Estimation of entropy of melting from molecular structure: A non-group contribution method. *Industrial & Engineering Chemistry Research* **35**: 1483-1486.
7. S. H. Yalkowsky and S. C. Valvani. 1980. Solubility and partitioning i: Solubility of nonelectrolytes in water. *Journal of Pharmaceutical Sciences* **69**: 912-922.
8. Y. Miyako, N. Khalef, K. Matsuzaki, and R. Pinal. 2010. Solubility enhancement of hydrophobic compounds by cosolvents: Role of solute hydrophobicity on the solubilization effect. *International Journal of Pharmaceutics* **393**: 48-54.
9. S. Janssens and G. Van den Mooter. 2009. Review: Physical chemistry of solid dispersions. *Journal of Pharmacy and Pharmacology* **61**: 1571-1586.
10. S. H. Yalkowsky. *Techniques of solubilization of drugs*, New York : M. Dekker, New York, 1981.
11. C. Leuner and J. Dressman. 2000. Improving drug solubility for oral delivery using solid dispersions. *European Journal of Pharmaceutics and Biopharmaceutics* **50**: 47-60.
12. A. M. Kaushal, P. Gupta, and A. K. Bansal. 2004. Amorphous drug delivery systems: Molecular aspects, design, and performance. *Critical Reviews™ in Therapeutic Drug Carrier Systems* **21**: 133-193.
13. A. T. M. Serajuddin. 1999. Solid dispersion of poorly water-soluble drugs: Early promises, subsequent problems, and recent breakthroughs. *Journal of Pharmaceutical Sciences* **88**: 1058-1066.
14. J.-L. Putaux, A. Buléon, R. Borsali, and H. Chanzy. 1999. Ultrastructural aspects of phytoglycogen from cryo-transmission electron microscopy and quasi-elastic light scattering data. *International Journal of Biological Macromolecules* **26**: 145-150.
15. S. Mizrahy and D. Peer. 2012. Polysaccharides as building blocks for nanotherapeutics. *Chemical Society Reviews* **41**: 2623-2640.
16. S. L. Scheffler, L. Huang, L. Bi, and Y. Yao. 2010. In vitro digestibility and emulsification properties of phytoglycogen octenyl succinate. *Journal of Agricultural and Food Chemistry* **58**: 5140-5146.
17. I. Ghebre-Sellassie. *Pharmaceutical extrusion technology*, M. Dekker, New York, 2003.

18. K. Connors and T. Higuchi. 1965. Phase solubility techniques. *Advances in Analytical Chemistry and Instrumentation* **4**: 117-212.
19. P. Alexandridis, T. Nivaggioli, and T. A. Hatton. 1995. Temperature effects on structural properties of pluronic p104 and f108 peo-ppo-peo block copolymer solutions. *Langmuir* **11**: 1468-1476.
20. N. V. Y. Scarlett and I. C. Madsen. 2006. Quantification of phases with partial or no known crystal structures. *Powder diffraction* **21**: 278-284.
21. T. Degen, M. Sadki, E. Bron, U. König, and G. Nénert. 2014. The highscore suite. *Powder Diffraction* **29**: S13-S18.
22. E. H. Lee, S. R. Byrn, and R. Pinal. 2012. The solution properties of mefenamic acid and a closely related analogue are indistinguishable in polar solvents but significantly different in nonpolar environments. *Journal of Pharmaceutical Sciences* **101**: 4529-4539.
23. S. H. Yalkowsky, S. C. Valvani, and T. J. Roseman. 1983. Solubility and partitioning vi: Octanol solubility and octanol–water partition coefficients. *Journal of Pharmaceutical Sciences* **72**: 866-870.
24. J. T. Rubino. Cosolvents and cosolvency, *Encyclopedia of pharmaceutical technology*, Vol. 3, Marcel Dekker, New York, NY, 1988, pp. 375-398.
25. Y. Miyako, H. Tai, K. Ikeda, R. Kume, and R. Pinal. 2008. Solubility screening on a series of structurally related compounds: Cosolvent-induced changes on the activity coefficient of hydrophobic solutes. *Drug Development and Industrial Pharmacy* **34**: 499-505.
26. H. R. Guzmán, M. Tawa, Z. Zhang, P. Ratanabanangkoon, P. Shaw, C. R. Gardner, H. Chen, J. P. Moreau, Ö. Almarsson, and J. F. Remenar. 2007. Combined use of crystalline salt forms and precipitation inhibitors to improve oral absorption of celecoxib from solid oral formulations. *Journal of Pharmaceutical Sciences* **96**: 2686-2702.
27. R. Vandecruys, J. Peeters, G. Verreck, and M. E. Brewster. 2007. Use of a screening method to determine excipients which optimize the extent and stability of supersaturated drug solutions and application of this system to solid formulation design. *International Journal of Pharmaceutics* **342**: 168-175.
28. K. Boksa, A. Otte, and R. Pinal. 2014. Matrix-assisted cocrystallization (mac) simultaneous production and formulation of pharmaceutical cocrystals by hot-melt extrusion. *Journal of Pharmaceutical Sciences* **103**: 2904-2910.
29. S. L. Childs, P. Kandi, and S. R. Lingireddy. 2013. Formulation of a danazol cocrystal with controlled supersaturation plays an essential role in improving bioavailability. *Molecular Pharmaceutics* **10**: 3112-3127.
30. M. C. Sweedman, M. J. Tizzotti, C. Schäfer, and R. G. Gilbert. 2013. Structure and physicochemical properties of octenyl succinic anhydride modified starches: A review. *Carbohydrate Polymers* **92**: 905-920.

CHAPTER 3. EFFECT OF COSOLUTES ON SOLUBILITY OF POORLY WATER SOLUBLE DRUGS

3.1 Abstract

The objective of this study is to understand the combined effects of an octenylsuccinate-modified dendrimer-like biopolymer (OS-DLB) and poloxamer (PLX) on the solubility of poorly water-soluble compounds. Phenytoin (PHT), griseofulvin (GSF), ibuprofen (IBU), and loratadine (LOR) were used as model compounds. Phase solubility measurements were conducted to determine the relative proportions of API, OS-DLB and PLX that result in the most stable nanocomplexes. By itself, the solubilizing power of OS-DLB increases with increasing hydrophobicity of the solute. In the presence of PLX, the solubilization effect of OS-DLB on the model dugs is accentuated to varying degrees. For IBU and LOR whose molecules exhibit extreme hydrophobic character, the solubilization of IBU and LOR by OS-DLB is practically insensitive to the presence of PLX. In the case of GSF whose aqueous solubility is primarily limited by its strong crystal lattice energy, the solubilization profiles are characteristic of hydrotropic solubilization. Despite a hydrophobicity close to GSF, the solubilization profile of PHT in mixtures of OS-DLB and PLX is similar to that of OS-DLB alone. The difference in solubilization profiles is attributable to the polarity match between the API and the hydrophobic microenvironment created by the synergistic effect of OS-DLB and PLX.

3.2 Introduction

Solubility is one of the most persistent challenges in pharmaceutical development. Traditional solubilization approaches can be broadly divided in two categories: solvent modification and solute modification. Solute modification strategies typically involve either the alteration of the physical properties of the crystal, such as salt formation, polymorphism and amorphization, or the incorporation of a second component in the solute phase in small concentration as an impurity, in comparable amounts as a eutectic, or in large excess as a carrier.[1] These strategies are effective in enhancing the apparent solubility and dissolution rate of organic compounds in water. However, the increase in apparent solubility is a thermodynamically unstable condition; if the solution is supersaturated, the solubilized solute will eventually precipitate.[2]

The solvent modification is comparatively more effective in producing thermodynamically stable enhancement in solubility.[1] Solvent modification approaches typically involve the use of solubilizing agents such as cosolvents, buffers, complexing ligands, and surfactants. The use of cosolvents is one of the most powerful means of altering the solubility of a crystalline organic compound in aqueous media. Cosolvents facilitate drug-solvent mixing in the liquid phase by decreasing the activity coefficient, γ, of the solute in a particular solvent mixture, thus decreasing the free energy of mixing. Mechanistically, cosolvents disrupt water structure, such that the less strongly water self-associates, the less likely it will “squeeze out” nonpolar solutes, and therefore, the higher the solubility (easier mixing) of the nonpolar solutes in the water-cosolvent mixture. Solubilization by buffers, complexing ligands and surfactants is attained through the creation of an additiional parallel liquid phase equilibrium. The use of buffers to control the pH of a system provides a means of increasing the solubility of a weak electrolyte in aqueous media by incorporating the acid-base equilibrium as a contributor toward the overall solubility equilibrium. At surfactant concentrations above the critical micelle concentration (CMC), surfactant-based solubilization of nonpolar solutes in aqueous media is achieved via incorporation of solute molecules into the nonpolar core of the micelle, which is largely composed of the hydrocarbon chains of the surfactant. Solubilization by complexation is achieved by “reversible (noncovalent), stoichiometric association of two or more

molecules into a distinct, well-defined structural entity".[3] The driving force for forming (inclusion and stacking) complexes is identical to the driving force for forming micelles in that the nonpolar solute is arranged to reduce its interfacial contact area with water. Both micelles and complexing agents (inclusion and stacking compounds) provide a favorable nonpolar microenvironment (a secondary equilibrium) that is well-suited to accommodate nonpolar molecules being squeezed out of water. However, a major limitation of these solvent modification techniques is that there is a maximum solubility enhancement that can be achieved for a given concentration of a solubilizing agent.

One way to circumvent the abovementioned limitation of solvent modification techniques is the use of multiple of solubilizing agents, either multiple solubilizing agents, each from a different class, or different solubilizing agents all from the same class.[1] The use of combinations of solubilizing agents allows the formulation scientist to minimize the unfavorable characteristics of any single solubilizing agent, as well as to expand the solubilization range of the solubilizing agents. Hoye and Myrdal[4] demonstrated the versatility of ethanol as cosolvent in hydrofluoroalkane (HFA)-based metered dose inhalers, with the solubility enhancement for various solutes ranging from 1.2 to 99.4 times when 20% (w/w) ethanol was added compared to pure HFA-134a. He et al.[5] showed that the solubility of fluasterone can be increased or decreased by varying the concentrations of cosolvent and cyclodextrin, as well as the type of cosolvent. Li et al.[6] found that pH control, when used in combination with cosolvents, surfactants or complexing ligands, is effective in enhancing the solubility of both the ionized and unionized forms of flavopiridol.

The present study is an extension of the study presented in Chapter 2 and is aimed at understanding the combined effects of an octenylsuccinate-modified dendrimer-like biopolymer (OS-DLB) and poloxamer (PLX) on the solubility of poorly water soluble compounds in aqueous medium. Four poorly soluble compounds were used as model compounds. They are phenytoin (PHT), griseofulvin (GSF), ibuprofen (IBU), and loratadine (LOR). Their experimentally determined melting properties and calculated solubility properties (crystallinity and hydrophobicity) are discussed in Chapter 2. PLX was used as a processing aid for enabling the extrusion of biodendrimeric solid dispersions

(BDSDs). Direct extrusion of a solid mixture of API and DLB is not possible due to the exceedingly high torque generated during the hot melt extrusion (HME) process. A number of different materials could have served as a processing aid. However, in this particular investigation, the choice of processing aid is limited to one that does not act as a solubilizer for the model compounds. PLX 338 was selected as a processing aid because PLX does not have an appreciable solubilizing effect on any of the model drugs in this study, as shown in Figure 3-1, where $[A]_t$ and $[A]_o$ denote the equilibrium solubility of the drug in aqueous mixture containing PLX, and in plain water, respectively. The lack of solubilizing effect of PLX is due to its concentrations being below the CMC value.[7] This situation eliminates any potential PLX-related confounding effects on the solubilizing effect of OS-DLB, which is the solubilizing agent of interest in this study.

3.3 Experimental

3.3.1 Materials

PHT was obtained from Spectrum (Gardena, CA), GSF from Hawkins (Minneapolis, MN), IBU from BASF (Bishop, TX), and LOR from Mallinckrodt (St. Louis, MO). All drug substances were used as received. Poloxamer 338 (PLX) was obtained from BASF (North Mount Olive, NJ) and was gently ground with mortar and pestle and screened through a US 100 mesh sieve (aperture size of 150 μm) before use. OS-DLB was prepared by Professor Yuan Yao's laboratory as described elsewhere.[8] All solvents were of HPLC grade and were obtained from Fisher Chemical (Fair Lawn, NJ).

3.3.2 Methods

3.3.2.1 Quantification of drug association

The amount of API associated with OS-DLB in solution was quantified following a 3-step procedure. First, in order to extract the drug molecules from the colloidal DLB particles, 500 μL of dimethyl sulfoxide was added to an equal volume of aqueous solution of API, DLB, and PLX and agitated at room temperature for 30 min. Following the extraction of

the API from the DLB, 500 μL of 20% (w/w) sodium chloride solution was added to the mixture and agitated at room temperature for 30 min in order to precipitate the DLB nanoparticles. Finally, the mixture was centrifuged at 12,000 rpm for 20 min. The amount of drug in the supernatant was quantified by HPLC assay, using a Shimadzu SCL-10AVP HPLC system (Kyoto, Japan), equipped with an Applied Biosystems 783A UV detector (Foster City, CA) and an Agilent Zorbax SB-C_{18} column (Santa Clara, CA). The mobile phase flow rate was set at 1 mL/min and the injection volume was 20 μl. Key parameters of the HPLC analysis method pertaining to the model drugs are summarized in Table 3-1.

3.3.2.2 Phase solubility measurements

Solubility measurements were carried out according to the method described by Connors and Higuchi[9], where excess amounts of API were added to aqueous solutions containing either DLB or PLX, as well as combinations of DLB and PLX, at concentrations ranging from 0 to 2000 ppm. After 24 h of constant agitation at 25 °C, an aliquot was removed and filtered through a 0.45 μm surfactant-free cellulose acetate membrane. The samples were treated and analyzed as described in the preceding section. Microsoft Excel (2013) Solver was used to perform nonlinear least-squares curve fitting of the experimental data.

3.4 Results and Discussion

Figure 3-2 shows the solubilization enhancement of the model compounds as a function of the concentration of OS-DLB dispersed in water at 25 °C ±0.5 °C, where $[A]_t$ and $[A]_o$ represent the equilibrium solubility of the drug in aqueous mixture containing DLB and PLX, and in plain water, respectively. The solid curves show the fit to the solubility models (described below), while the broken curves are for visualization purposes only. The solubilization models describing the solubilization of the drugs are described below. The full derivation of the solubilization models is provided in Appendix A.

3.4.1 Solubilization effect of OS-DLB

Briefly, as discussed in Chapter 2, the rank order in solubilizing effect of OS-DLB matches the rank order in hydrophobicity of the drugs (Figure 2-3). The more hydrophobic the drug molecule, the greater the solubilizing effect of OS-DLB. It is possible that the hydrophobic C_8 chains, covalently bonded to the surface of DLB, create a nonpolar microenvironment that most closely matches to the hydrophobicity of LOR, relative to the other model compounds. As a result, a substantial solubilizing effect of OS-DLB on LOR is observed. Conversely, the minimal solubilizing effect of OS-DLB on PHT – the least hydrophobic compound among the four model drugs in this study – is attributable to the poorest polarity match of PHT with the C_8-rich microenvironment of the OS-DLB.

It is noteworthy from Figure 3-2 that the solubilization curves for PHT and GSF exhibit a plateau, suggesting the formation of insoluble nanocomplexes at high concentrations of OS-DLB. Here, the term “complex” broadly refers to the intermolecular associations between the drug solutes and OS-DLB. Figure 3-3 shows the theoretical estimation of the spatial distance between nanocomplexes in water at 25 °C, where a power-law decay of the interparticle separation is observed. It is likely that as the interparticle separation distance decreases, the frequency of close-proximity interactions between drug-loaded colloidal particles increase to such an extent that precipitation of the nanocomplexes occurs. Whether or not the precipitation of the nanocomplexes involves the crystallization of the drug contained within is not clear, but an unambiguous fact is that for some drugs such as GSF and PHT, the nanocomplex itself exhibits a solubility limit. Since the nanocomplexes precipitate, an upper limit to the attainable solubilizing effect of OS-DLB is observed. Based on log X_{ideal} values, the rank order in crystal lattice energy of the solutes is PHT > GSF > LOR > IBU. It is reasonable to expect that PHT has the greatest tendency to crystallize among the four compounds, while IBU has the weakest tendency to form a crystal from the solution state. This relation corresponds precisely to the results in Figure 2-3, where the formation of insoluble nanocomplexes of PHT and OS-DLB occurs even at low concentrations of OS-DLB, while only soluble nanocomplexes of IBU were formed over the entire range of OS-DLB concentration studied.

3.4.2 Combined solubilization effect of OS-DLB and PLX

Interestingly, the solubilization effect of OS-DLB on the model dugs is accentuated by the presence of PLX to varying degrees. For IBU and LOR, whose molecules exhibit extreme hydrophobic character, the solubilization by OS-DLB is minimally influenced by the presence of PLX. This is can be attributed to a closer polarity match between these types of molecules and the solvating microenvironment present in OS-DLB. The solubilization profiles of IBU and LOR are linear, indicating the formation of soluble nanocomplexes over the range of OS-DLB concentration studied. In the case of GSF, whose aqueous solubility is primarily limited by its strong crystal lattice energy, the solubilizing effect of OS-DLB is accentuated by the presence of PLX. This is a potentiation effect; the combined effect of OS-DLB and PLX is superior in solubilizing GSF than the sum of the individual components. The solubilization profiles of GSF assume a sigmoidal shape – analogous to that of hydrotrope-induced solubilization, where the apparent solubility of a compound increases sharply at a minimum hydrotrope concentration (MHC) and reaches a plateau at high hydrotrope concentrations.[10] Hydrotropy is defined as "the nonstoichiometric solubilization of an insoluble (often aromatic) solute by a partially water miscible aromatic solute", and is often loosely used to describe a variety of solubilization approaches, such as complexation, micellization, or even cosolvency (as described below).[1] To date, hydrotropic cooperativity is still not well understood from a mechanistic point of view.[1, 10] However, due to the apparent similarity between MHC and CMC, the molecular basis of hydrotropic cooperatively has been largely attributed to the self-aggregation of the hydrotrope, analogous to the aggregation of surfactant molecules to form micellar aggregates.[11, 12] The initial portion of the solubilization profile, showing an increasingly steeper slope is likely related to a PLX-induced modification (decrease) in the hydrophobicity of the OS-created hydrophobic microenvironment in the OS-DLB. The result is a microenvironment that is better suited to solvate GSF than that provided by plain OS-DLB without any PLX. As a result, the solubilization capacity of OS-DLB for GSF increases in a manner that resembles that of the cosolvency effect (see Figure 3-5). Poloxamers are nonionic surface active agents commonly used as solubilizing and emulsifying agents. However, poloxamer surfactants can also behave as cosolvents.[13] Although most cosolvents are liquids, solids that are highly soluble in the main solvent can

also function as cosolvents. Examples of solid cosolvents in aqueous solutions are sorbitol, polyvinylpyrrolidone and high molecular weight hydrophilic polymers such as polyethylene glycol.[13] In hydrophobic solvents, paraffin ($C_{40}H_{82}$) can function as a cosolvent.[13] The less polar moieties in the structure of these solid compounds help reduce the overall polarity of the solvent environment relative to that of plain water, which in turn diminishes the squeezing out of the nonpolar solutes and consequently increases the solubility of the latter in the aqueous media. However, as discussed in the preceding section, there is a limitation to the combined solubilizing effect of OS-DLB and PLX on GSF. Precipitation of nanocomplexes is expected to occur at higher concentrations of OS-DLB where the concentration of the nanocomplex exceeds its solubility limit. In comparison, the combined solubilization effect of OS-DLB and PLX on PHT is almost identical to that of OS-DLB alone. Unlike GSF, the solubilization profiles of PHT do not exhibit a sigmoidal shape. These observations indicate that the solubility limit of the nanocomplex is determined by the simultaneous presence of the drug and OS-DLB, and not a property of the concentration of OS-DLB alone. In other words, the solubility limit of the nanocomplex is the manifestation of a solubility product, rather than that of a maximum concentration limit. Despite the lowering of the hydrophobicity of the microenvironment of OS-DLB mediated by PLX, it is apparent that the polarity match between PHT molecules and the microenvironment of OS-DLB is still inadequate, hence negligible solubility enhancement of PHT is observed. To summarize, the difference in solubilization profiles is most likely attributable to the polarity match (IBU and LOR) or mismatch (PHT and GSF) between the hydrophobic solutes and the nonpolar microenvironment of OS-DLB.

3.4.3 Solubilization models

3.4.3.1 Solution behavior of IBU and LOR

The solubilization profiles of IBU and LOR correspond to the type of solubilization profile observed when, in addition to the main solid-liquid equilibrium, a secondary parallel solution phase equilibrium is present. The parallel solution phase equilibrium in a mixture containing API and OS-DLB can be represented as follows:

$$A + D \overset{K_p}{\rightleftharpoons} \langle AD \rangle \qquad \text{Equilibrium 1}$$

where A and D represent API and OS-DLB, respectively, $\langle AD \rangle$ represents the nanocomplex of API and OS-DLB, and K_p represents the partition-association equilibrium constant,

$$K_p = \frac{[A]_{\langle AD \rangle}}{[A]} \qquad 3.1$$

where $[A]$ and $[A]_{\langle AD \rangle}$ are the concentration of the molecularly free drug in solution and the concentration of the drug in the $\langle AD \rangle$ phase, respectively. Accordingly, the solubility enhancement of IBU and LOR by OS-DLB is

$$\frac{[A]_t}{[A]_o} = 1 + K_p [D] \qquad 3.2$$

where $[A]_t$ and $[A]_o$ denote the total and molecularly free concentrations of API, respectively, and $[D]$ is the concentration of OS-DLB in solution. Note that in a saturated solution, the value of $[A]$ in Equation 3.1 is constant and equal to the aqueous solubility limit of the API, $[A]_o$. It is further noted that PLX does not directly participate in the secondary equilibrium. However, by its effect of modifying the polarity of OS-DLB, PLX indirectly modifies the value of K_p to different extent, depending on the polarity of the drug, as discussed in a subsequent section. The linear solubility model of Equation 3.2, as indicated by the solid lines in Figure 3-2, is in good agreement with the experimental data. The partition-association equilibrium constants (Table 3-2) obtained by fitting the data to Equation 3.2 show that the effect of PLX on the solubility enhancement of IBU and LOR by OS-DLB is minimal, with roughly 1.2 and 1.5-fold increase, respectively, at PLX concentration of 2000 ppm. Additionally, the solubility enhancement does not increase with PLX concentration, suggesting that PLX exerts a negligible effect on the solubility enhancement of IBU and LOR.

3.4.3.2 Solution behavior of PHT and GSF

Based on the solubilization profiles of PHT and GSF in Figure 3-2, it is evident that in addition to the solution phase equilibrium (Equilibrium 1), an additional secondary

equilibrium involving the formation of insoluble nanocomplexes of API and OS-DLB is present:

$$A + \langle AD \rangle \underset{\leftarrow}{\overset{K_{sp}}{\rightleftharpoons}} \langle AD \rangle_s \qquad \text{Equilibrium 2}$$

where $\langle AD \rangle_s$ denotes the solid (insoluble) nanocomplex and K_{sp} represents the solubility product of the equilibrium. K_{sp} is therefore the solubility maximum of the $\langle AD \rangle$ nanocomplex, and is given by the product of the equilibrium concentration of the free drug solute and OS-DLB in the formation of the nanocomplexes:

$$K_{sp} = [A]_o [D]_{\max} \qquad 3.3$$

where $[D]_{\max}$ denotes the limiting concentration value of OS-DLB at which the $\langle AD \rangle$ nanocomplex precipitates. The value of $[D]_{\max}$ was determined from the solubility curves by applying piecewise linear approximation. The solubility product, K_{sp}, is analogous to the solubility product of a sparingly soluble salt, where the concentration of the ions in solution is in equilibrium with the solid. The solubility product of a salt, which is given by the product of the ionized solute and counterion concentrations, represents the solubility maximum of the salt. Since the solubility product of $\langle AD \rangle$ nanocomplex is constant, at high concentrations of OS-DLB (analogous to the counterion of a salt), for any given concentration of free *A*, there is a $[D]_{\max}$ for which $\langle AD \rangle$ formation reaches its solubility product, leading to the precipitation of the nanocomplex. Accordingly, the solubility enhancement of PHT and GSF by OS-DLB is given by

$$\frac{[A]_t}{[A]_o} = \begin{cases} 1 + K_p [D] & [A][D] < K_{sp} \\ 1 + \dfrac{K_p K_{sp}}{[A]_o} & [A][D] \geq K_{sp} \end{cases} \qquad 3.4$$

The predicted solubilization effect of OS-DLB on PHT and GSF, as indicated by the solid curves in Figure 3-4 and Figure 3-5 (PLX 0 ppm), respectively, is in good agreement with the experimental data. The solubility enhancement of PHT and GSF by OS-DLB is proportional to the concentration of OS-DLB when the concentration of $\langle AD \rangle$ nanocomplex is below its solubility product. Further addition of the OS-DLB beyond the

K_{sp} limits causes the $\langle AD \rangle$ nanocomplex to precipitate, thereby producing a ceiling to the solubilizing effect of OS-DLB. It is observed that the solubility ceiling is not flat, but has a shallow slope. This feature is not surprising since the value of the solubility product depends on the physical properties of DLB, a naturally-occurring nano-dendrimeric polysaccharide that may exhibit some degree of structural variability. Properties such as the size and drug loading capacity of the nanoparticles are not fixed numbers but rather exhibit distributions. The calculated solubility products of PHT-DLB nanocomplex are shown in Table 3-3. As stated previously, one of the criteria for the use of PLX in this study was its inability to act as a solubilizer for the drugs. Even though by itself PLX does not solubilize PHT, the data in Table 3-3 show that PLX has a moderate potentiating effect on the solubilizing power of OS-DLB.

3.4.3.3 Solution behavior of GSF in the presence of OS-DLB and PLX

Quantitatively, the initial increasingly steeper portion of the solubilization profile of GSF in the ternary system of GSF, OS-DLB and PLX represents a positive deviation from the solubilization profile described by Equilibrium 1. As a first approximation, such positive deviation can be described using the log-linear model proposed by Yalkowsky and coworkers.[14-16] Analogous to Equilibrium 1, the solution phase equilibrium in a mixture containing GSF, OS-DLB and PLX, can be represented as follows:

$$A + D \overset{K_p^{'}}{\rightleftharpoons} \langle AD \rangle \qquad \text{Equilibrium 3}$$

where $K_p^{'}$ represents the equilibrium constant for the nanocomplex formation, under the influence of a cosolvency-like solubilization effect. Accordingly:

$$K_p^{'} = 10^{\sigma[D]} K_p \qquad 3.5$$

where σ is the solubilization power of PLX over the inherent solubilization power of OS-DLB. That is, the solubilization parameter, σ, denotes the overall solubilizing power of OS-DLB and PLX for GSF solute. The value of σ, as shown in Table 3-4, increases with PLX concentration, in analogous fashion to the cosolvency effect. It is important to point in a true cosolvent system, i.e., one consisting of a mixture of two true liquid solvents, the

exponential increase in solubility observed corresponds to that of the molecularly free drug. Conversely, in the complexing system of this study, the exponential increase in solubility produced by PLX does not reside on $[A]_o$, the concentration of the molecularly free drug, but rather on the magnitude of $[A]_{\langle AD \rangle}$ from Equation 3.1, the concentration of the API in the organic OS-DLB phase. The concentration of free GSF remains constant at $[A]_o$, its intrinsic aqueous solubility, since the bulk solvent phase is still predominantly water. Furthermore, PLX was found to have no appreciable solubilizing effect on GSF (Figure 3-1). The main contribution of increased solubility is the enhancement in the partition-association (K_p) of the hydrophobic solute molecules and the microenvironment created by the combined effect of OS-DLB and PLX, as indicated by the values of σ in Table 3-4. As the concentration of PLX in the solubilizing medium increases, the exponential solubilization profile becomes more pronounced. The results indicate that when mixed with water, PLX has no appreciable solubilizing effect on GSF. However, when mixed with the hydrophobic chains of the OS groups of OS-DLB, PLX has an exponential (cosolvency) effect on enhancing the ability of the OS environment to solvate GSF.

As observed with PHT, the solubility product of the nanocomplex, K_{sp}, increases with PLX concentration, but only up to a limit; at sufficiently high $[D]$ values, the solubility of $\langle AD \rangle$ is reached. Similarly, the additional secondary equilibrium involving the formation of insoluble nanocomplexes can be represented by:

$$A + \langle AD \rangle \rightleftharpoons \langle AD \rangle_s \qquad \text{Equilibrium 4}$$

The equilibrium constant, K_{sp}, is the maximum solubility of $\langle AD \rangle$ nanocomplex, and is given by

$$K_{sp} = [A]_o [D]_{\max} \qquad 3.6$$

Accordingly, the relative enhancement of apparent solubility of GSF by OS-DLB and PLX is given by

$$\frac{[A]_t}{[A]_o} = \begin{cases} 1 + 10^{\sigma[D]} K_p [D] & [A][D] < K_{sp} \\ 1 + \dfrac{10^{\sigma[D]_{\max}} K_p K_{sp}}{[A]_o} & [A][D] \geq K_{sp} \end{cases} \qquad 3.7$$

Figure 3-5 shows the predicted solubilization effect of OS-DLB and PLX on GSF, as indicated by the solid curves. The proposed model is in general good agreement with the experimental data. The exponential increase in the apparent solubility of GSF is attributable to the increase in polarity in the solvating environment in OS-DLB facilitated by PLX, thereby increasing the solubilizing power of OS-DLB for GSF. However, at high concentrations of OS-DLB, the concentration of $\langle AD \rangle$ nanocomplex exceeds its solubility product, resulting in the plateau in the solubility curves.

The proposed model provides a useful understanding of cooperative solubilization by OS-DLB and PLX, functioning in a fashion analogous to that of hydrotropes. Shimizu and Matubayasi[10, 17] have successfully modeled hydrotropic solubilization through the combination of statistical thermodynamics with computer simulations; however, such type of analysis is beyond the scope of the present study.

3.5 Conclusions

The effect of OS-DLB and PLX on the solubilization of poorly water-soluble compounds depends strongly on the hydrophobicity of the solute, as well as the concentrations of OS-DLB and PLX. The synergistic effect of OS-DLB and PLX is particularly prominent for the most hydrophobic drug molecules, indicating a closer polarity match between this type of molecules and the mixture of OS-DLB and PLX. While the shake-flask method is a straightforward method for determining the apparent solubility of the API in phase solubility systems, it only leads to a partial understanding of the nature of the intermolecular interactions in solution. Calorimetry-based methods, on the other hand, offer a complementary approach for the quantitative analysis of interactions, derived from the fact that heat evolution invariably occurs in all processes. Nevertheless, the preliminary findings of this study set the foundation for the thermodynamic studies of the molecular interactions between the components in a BDSD formulation by isothermal titration calorimetry in the subsequent chapter.

3.6 Acknowledgments

Financial support from the Dane O. Kildsig Center for Pharmaceutical Processing Research (CPPR), Purdue Research Foundation, and the National Science Foundation (NSF DMR 1310475) is gratefully acknowledged. We thank Prof. Yuan Yao's laboratory for providing the DLB material used in the study.

Table 3-1. Key parameters of the HPLC method for the analysis of the model compounds.

Compound	**Mobile Phase (Volume Parts)**	**Wavelength (nm)**
Phenytoin	38 acetonitrile, 62 water	220
Griseofulvin	35 acetonitrile, 60 water, 5 tetrahydrofuran	295
Ibuprofen	60 acetonitrile, 40 water, 0.01 trifluoroacetic acid	220
Loratadine	68 acetonitrile, 32 water	248

Table 3-2. Estimation of solubilization parameters of IBU and LOR in the presence of OS-DLB and PLX.

Compound	Parameter	Concentration of PLX (ppm)			
		0	200	1000	2000
Ibuprofen	K_p (L g^{-1})	3.82	4.67	4.78	4.69
Loratadine	K_p (L g^{-1})	17.02	26.23	28.08	29.08

Table 3-3. Estimation of solubilization parameters of PHT in the presence of OS-DLB and PLX. The equilibrium constant K_p is estimated by a straight line tangent to the solubility curve at zero OS-DLB concentration, and it is assumed to be the same in all cases (shaded areas).

Parameter	Concentration of PLX (ppm)			
	0	200	1000	2000
K_p (L g^{-1})	1.15	1.15	1.15	1.15
$K_{sp} \times 10^4$ (mg L^{-1})^2	1.34	1.52	1.95	1.80

Table 3-4. Estimation of solubilization parameters of GSF in the presence of OS-DLB and PLX. The equilibrium constant K_P is estimated by a straight line tangent to the solubility curve at zero OS-DLB concentration, and it is assumed to be the same in all cases (shaded areas).

Parameter	Concentration of PLX (ppm)			
	0	200	1000	2000
K_p (L g^{-1})	3.67	3.67	3.67	3.67
$K_{sp} \times 10^3$ (mg L^{-1})^2	5.55	7.16	8.70	7.37
σ (L g^{-1})	N.A.	0.09	0.29	0.44

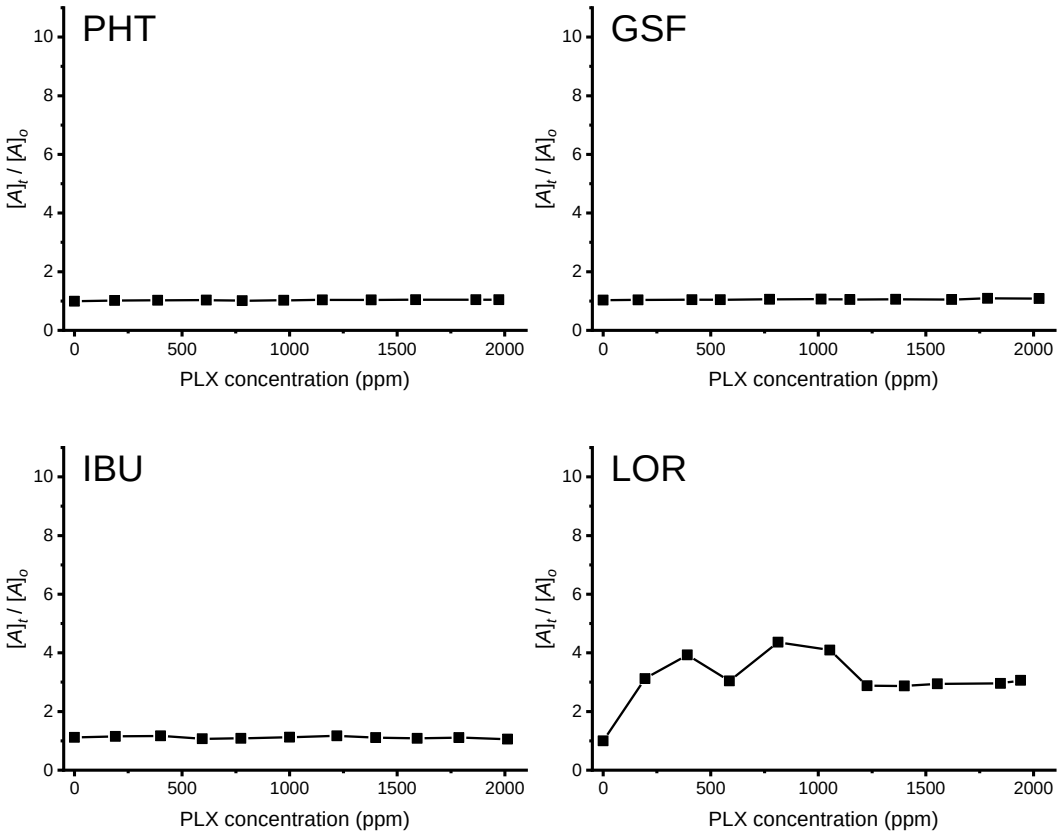

Figure 3-1. Solubility enhancement of the model drugs in aqueous PLX solutions of different concentrations at 25 °C ± 0.5 °C. $[A]_t$ and $[A]_o$ represent the equilibrium solubility of the drug in the presence of PLX in solution and the solubility in plain water, respectively.

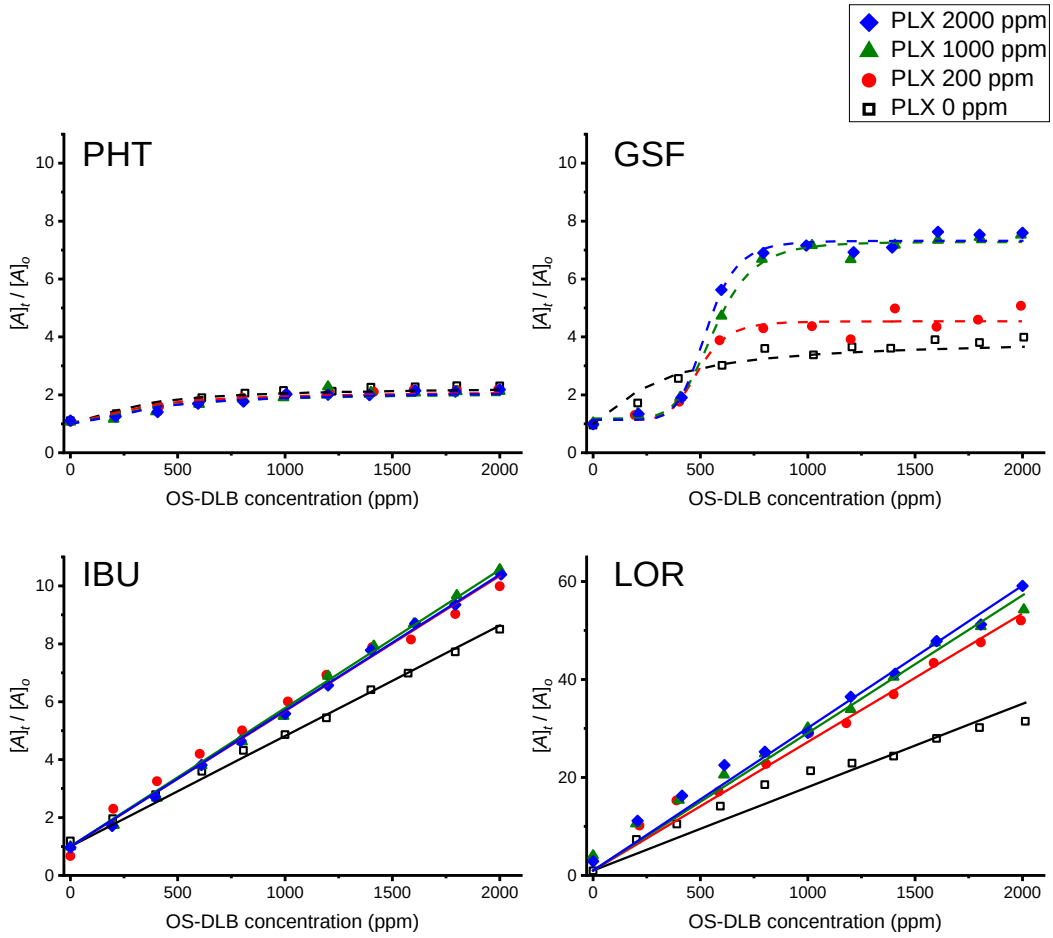

Figure 3-2. Solubility enhancement of the model drugs in aqueous solutions of OS-DLB and PLX solutions of different concentrations at 25 °C ± 0.5 °C. $[A]_t$ and $[A]_o$ represent the equilibrium solubility of the drug in the presence of OS-DLB and PLX in solution and the solubility in plain water, respectively. The solid curves represent the predicted solubility enhancement, and the broken curves are for visualization purposes only.

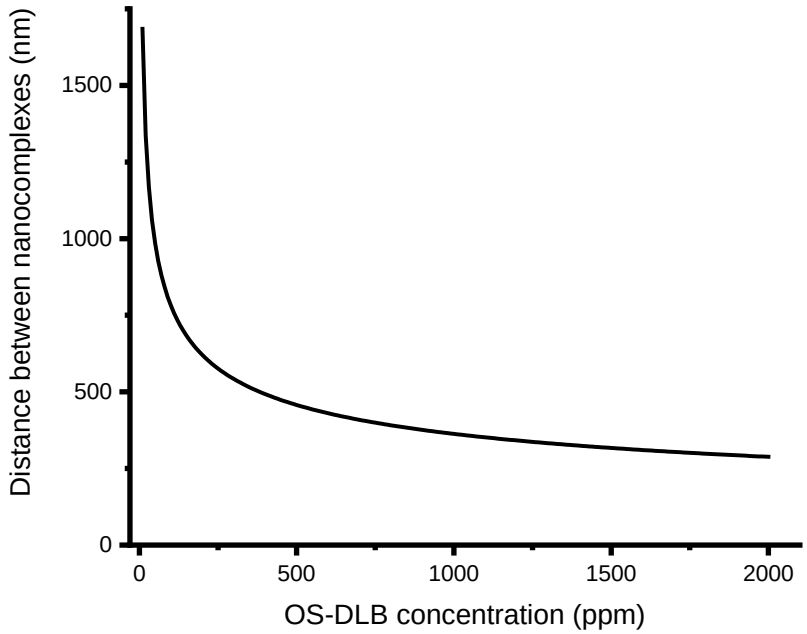

Figure 3-3. Theoretical prediction of spatial separation between API-DLB nanocomplexes in water at 25°C.

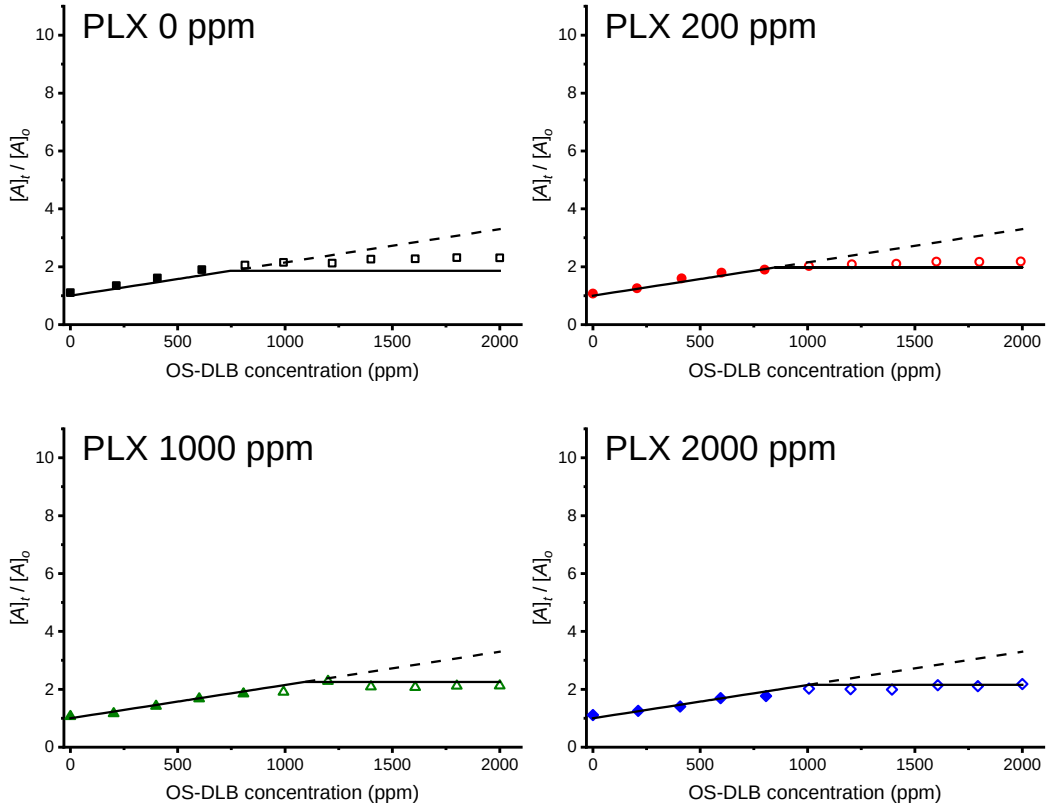

Figure 3-4. Solubility enhancement of PHT in aqueous solutions of OS-DLB and PLX solutions of different concentrations at 25 °C ± 0.5 °C. $[A]_t$ and $[A]_o$ represent the equilibrium solubility of PHT in the presence of OS-DLB and PLX in solution and the solubility in plain water, respectively. The symbols and solid curves represent the observed and predicted solubility enhancement, respectively. The open symbols indicate the possibility of insoluble nanocomplexes formation. The broken lines represent the solubility enhancement of PHT if the solubility product of the nanocomplex is not exceeded.

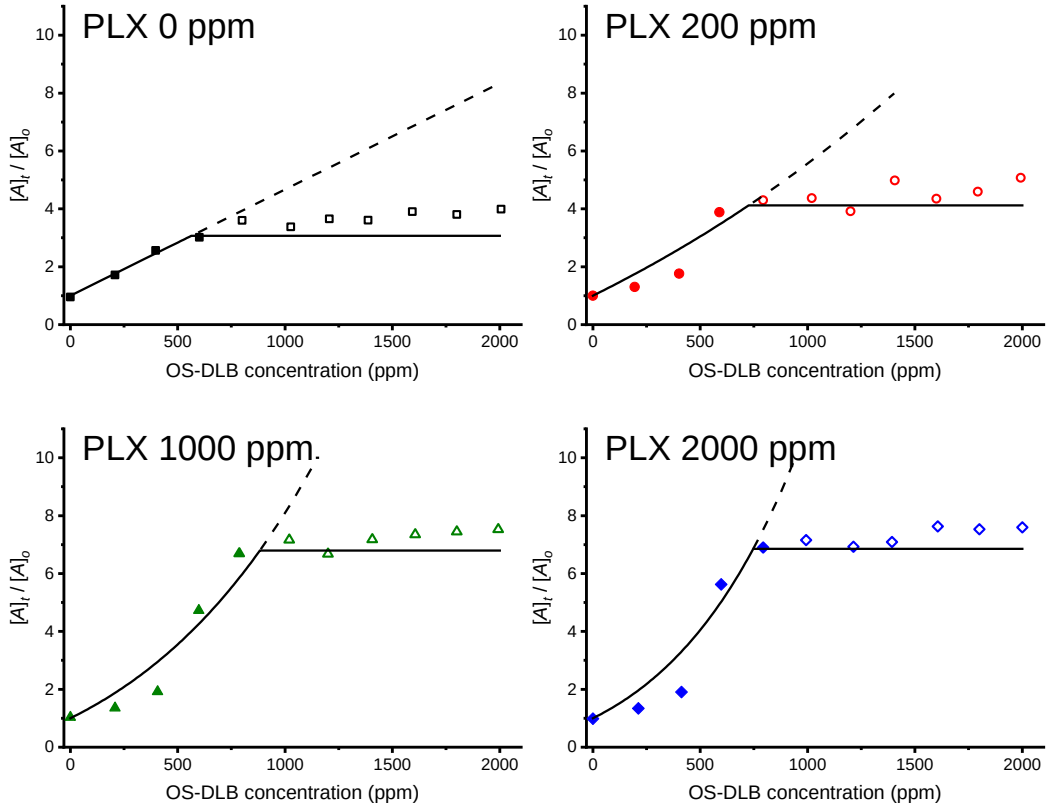

Figure 3-5. Solubility enhancement of GSF in aqueous solutions of OS-DLB and PLX solutions of different concentrations at 25 °C ±0.5 °C. $[A]_t$ and $[A]_o$ represent the equilibrium solubility of GSF in the presence of OS-DLB and PLX in solution and the solubility in plain water, respectively. The symbols and solid curves represent the observed and predicted solubility enhancement, respectively. The open symbols indicate the possibility of insoluble nanocomplexes formation. The broken lines represent the solubility enhancement of GSF if the solubility product of the nanocomplex is not exceeded.

3.7 References

1. S. H. Yalkowsky. Overview and strategy for solubilization, *Solubility and solubilization in aqueous media*, American Chemical Society, 1999, pp. 417-439.
2. S. H. Yalkowsky. *Techniques of solubilization of drugs*, New York : M. Dekker, New York, 1981.
3. S. H. Yalkowsky. Solubilization by complexation, *Solubility and solubilization in aqueous media*, American Chemical Society, 1999, pp. 321-396.
4. J. A. Hoye and P. B. Myrdal. 2008. Measurement and correlation of solute solubility in hfa-134a/ethanol systems. *International Journal of Pharmaceutics* **362**: 184-188.
5. Y. He, P. Li, and S. H. Yalkowsky. 2003. Solubilization of fluasterone in cosolvent/cyclodextrin combinations. *International Journal of Pharmaceutics* **264**: 25-34.
6. P. Li, S. E. Tabibi, and H. Yalkowsky Samuel. 2000. Solubilization of flavopiridol by ph control combined with cosolvents, surfactants, or complexants. *Journal of Pharmaceutical Sciences* **88**: 945-947.
7. P. Alexandridis, T. Nivaggioli, and T. A. Hatton. 1995. Temperature effects on structural properties of pluronic p104 and f108 peo-ppo-peo block copolymer solutions. *Langmuir* **11**: 1468-1476.
8. S. L. Scheffler, L. Huang, L. Bi, and Y. Yao. 2010. In vitro digestibility and emulsification properties of phytoglycogen octenyl succinate. *Journal of Agricultural and Food Chemistry* **58**: 5140-5146.
9. K. Connors and T. Higuchi. 1965. Phase solubility techniques. *Advances in Analytical Chemistry and Instrumentation* **4**: 117-212.
10. S. Shimizu and N. Matubayasi. 2016. The origin of cooperative solubilisation by hydrotropes. *Physical Chemistry Chemical Physics* **18**: 25621-25628.
11. J. Y. Kim, S. Kim, M. Papp, K. Park, and R. Pinal. 2010. Hydrotropic solubilization of poorly water-soluble drugs. *Journal of Pharmaceutical Sciences* **99**: 3953-3965.
12. J. Y. Kim, S. Kim, R. Pinal, and K. Park. 2011. Hydrotropic polymer micelles as versatile vehicles for delivery of poorly water-soluble drugs. *Journal of Controlled Release* **152**: 13-20.
13. S. H. Yalkowsky. Solubilization by cosolvents, *Solubility and solubilization in aqueous media*, American Chemical Society, 1999, pp. 180-235.
14. S. H. Yalkowsky, G. L. Flynn, and G. L. Amidon. 1972. Solubility of nonelectrolytes in polar solvents. *Journal of Pharmaceutical Sciences* **61**: 983-984.
15. S. H. Yalkowsky, G. L. Amidon, G. Zografi, and G. L. Flynn. 1975. Solubility of nonelectrolytes in polar solvents iii: Alkyl p-aminobenzoates in polar and mixed solvents. *Journal of Pharmaceutical Sciences* **64**: 48-52.
16. S. H. Yalkowsky, S. C. Valvani, and G. L. Amidon. 1976. Solubility of nonelectrolytes in polar solvents iv: Nonpolar drugs in mixed solvents. *Journal of Pharmaceutical Sciences* **65**: 1488-1494.
17. S. Shimizu and N. Matubayasi. 2017. Unifying hydrotropy under gibbs phase rule. *Physical Chemistry Chemical Physics* **19**: 23597-23605.

CHAPTER 4. STUDY OF DRUG-EXICIPIENT INTERMOLECULAR INTERACTIONS IN SOLUTION USING ISOTHERMAL TITRATION CALORIMETRY

4.1 Abstract

The aim of this study is to assess the role of drug hydrophobicity on the energetics of intermolecular interactions with an OS-DLB - octenylsuccinate-modified (OS) dendrimer-like biopolymer (DLB) - and poloxamer (PLX) using isothermal titration calorimetry (ITC). Phenytoin (PHT), griseofulvin (GSF) and ibuprofen (IBU) were used as model compounds. The results indicate that the intermolecular interaction between IBU and OS-DLB in solution exhibits very small energy change upon mixing but a stronger effect on entropy. In comparison, the intermolecular interaction between the less hydrophobic GSF and OS-DLB have significant effects on both enthalpy and entropy. Consequently, in terms of solubilization enhancement, it was found that the interaction between IBU and OS-DLB is entropy-driven (more favorable), while in the case of GSF, the interacting molecules are arranged to maximize enthalpic interaction. The very low solubilizing effect on PHT is attributable to two factors, one general and one solute specific. In a general sense, the microenvironment of the hydrated OS-DLB does not offer an ideal polarity match with PHT. In addition, the very low solubilizing effect on PHT suggests that solubilization involves specific interactions.

4.2 Introduction

The aqueous solubility of organic crystalline compounds is one of the most important physicochemical properties in pharmaceutical product development. It is an important consideration for 1) controlling the dissolution rate and maximum amount of drug that can be dissolved when administered as a solid, 2) determining the strategy for solubilizing a drug, 3) providing a reasonable guarantee of accurate dose, particularly when small amounts of potent drugs are to be delivered, and 4) controlling and optimizing the therapeutic efficacy of a drug. Solubility measurements are typically performed using the conventional shake-flask method, where an excess amount of the solid drug is mixed with excipients and solvent of interest, and shaken in a closed "flask" for a period of time (typically 24 h or longer) at a specific temperature, until equilibrium is achieved.[1] While the shake-flask method is a straightforward method for determining the solubility of the API (active pharmaceutical ingredient) with high accuracy, it provides limited insight into the intermolecular interactions between the components in solution. As Hvidt[2] aptly noted, "aqueous solutions of non-polar molecules are notorious because of their eccentric thermodynamic properties and because of our limited understanding of the molecular interactions in the solutions." The importance of understanding the thermodynamic factors that govern the process of solubilization cannot be understated.

Calorimetry-based methods offer a complementary approach for the quantitative analysis of intermolecular interactions, derived from the fact that heat is an invariable component of both physical and chemical processes. The analysis of thermodynamic parameters provides a means of determining drug solubility in organic and aqueous solvents in situations where the shake-flask method becomes challenging or unreliable[3], understanding the energetics of the different stages of the dissolution process that are otherwise difficult or even impossible to ascertain by traditional dissolution methods[4], as well as elucidating the mechanisms of intermolecular interactions in the solid state[5] and in solution[6] which are paramount in the understanding of the factors that affect drug solubility. Isothermal titration calorimetry (ITC) has been long considered as a method of choice for characterizing the energetics and stoichiometry of intermolecular interactions with exquisite sensitivity.[7] The thermodynamic parameters governing the intermolecular

interactions can be accurately determined without immobilization or physical/chemical modifications of the interacting molecules. ITC has been widely used for studying aggregation behavior of micellar systems[8], protein-protein[9], protein-small molecule[10], protein-nanoparticle[11], protein-metal ion[12], complexing agent-small molecule[13], polymer-small molecule[14], and lipid-surfactant[15] interactions, to name some applications. A comprehensive review on the recent applications of ITC is provided by Falconer[16].

The present study is an extension of the study in Chapter 3 and is aimed at understanding the thermodynamic nature of the intermolecular interactions between the components in a biodendrimeric solid dispersion (BDSD) formulation – namely drug, octenylsuccinate modified dendrimer-like biopolymer (OS-DLB), and poloxamer 338 (PLX) – in solution. Three* poorly soluble compounds were used as model compounds. They are phenytoin (PHT), griseofulvin (GSF) and ibuprofen (IBU). The "release" protocol instead of the classic "incorporation" protocol[17] was adopted, and the experimental setup and procedure are described in Section 4.5.2. Briefly, the syringe was filled with a saturated aqueous mixture of drug solute and nanocomplex (OS-DLB preloaded with solute molecules). Each injection of the syringe content into the reaction cell filled with water resulted in the dilution of the nanocomplex, which in turn promoted the release of solute molecules into water. The "release" protocol is preferred to the classic "incorporation" protocol for the following reasons. First, the aqueous solubility of the model drugs in this study is extremely low; preparation of homogenous aqueous solutions of these compounds for binding experiments is challenging. Furthermore, given the relatively low concentrations of solute, the calorimetric signal obtained from classical binding experiment is weak and cannot be clearly distinguished from background noise. Unlike the conventional binding protocol, the release protocol can be pursued for virtually all solutes that are sparingly soluble in aqueous media, without compromising the ability to discriminate between background and true calorimetric signal. Second, the application of the release protocol allows the assessment of the release of solutes from the nanocomplexes upon dilution, which in turn offers insight into the diffusive transport of the solutes across the OS-DLB. This type of

* Data for loratadine is not included here. The reason is that loratadine precipitated in the calorimeter cell due to its extremely low aqueous solubility.

information cannot be obtained from a classical binding experiment.[15] Clearly, the application of the release protocol is superior to the classic incorporation protocol in this study.

4.3 Nomenclature

In this context, the term "complex" broadly refers to the intermolecular associations between the drug solute, OS-DLB, and PLX. The terms, OS-DLB and DLB, are used interchangeably to refer to octenylsuccinate-modified dendrimer-like biopolymer. The nanocomplex is defined according to the composition of the mixture from which it was prepared. For instance, API-DLB-PLX refers to a nanocomplex prepared from a mixture containing API, OS-DLB, and PLX. The term "complex" does not necessarily refer to the stoichiometric association of molecules into a distinct, well-defined structural entity. Each ITC experimental setup is defined according to the content in the syringe (left) and reaction cell (right), respectively. For example, the experimental setup IBU-DLB-PLX → H_2O indicates the injection of a mixture composed of IBU, OS-DLB and PLX into water.

4.4 Theory

The fitting model presented here pertains to a solubilization process represented as follows:

$$A + D \underset{}{\overset{K_p}{\rightleftharpoons}} \langle AD \rangle \qquad \text{Equilibrium 1}$$

where A and D represent API and OS-DLB, respectively, $\langle AD \rangle$ represents the nanocomplex of API and OS-DLB, and K_p represents the partition-association equilibrium constant.

In a typical ITC system, the total heat of the system Q is given by

$$Q = Q^{syr} + Q^{cell} \qquad 4.1$$

where the superscripts *syr* and *cell* refer to the syringe and reaction cell of the isothermal titration calorimeter, respectively. The enthalpy variation of the syringe and cell contents upon an injection are

$$Q^{syr} = -\Delta V\left(A_W^{syr}h_W^A + A_{\langle AD\rangle}^{syr}h_{\langle AD\rangle}^A + D_t^{syr}h^D\right) \quad 4.2$$

$$Q^{cell} = V_o\left[\Delta A_t h_W^A + \Delta D_t h^D + \left(\frac{\partial A_{\langle AD\rangle}}{\partial A_t}\Delta A_t + \frac{\partial A_{\langle AD\rangle}}{\partial D_t}\Delta D_t\right)\left(h_{\langle AD\rangle}^A - h_W^A\right)\right] \quad 4.3$$

where ΔV and V_o denote the volume of injection and cell volume, respectively, the subscripts W and $\langle AD\rangle$ denote the different environments (W: water, $\langle AD\rangle$: API-DLB nanocomplex) in which the component (indicated by the superscript) is located in, the subscript t denotes the total concentration of the component, and h denotes the partial molar enthalpy of the component. It is assumed that h_W^A, $h_{\langle AD\rangle}^A$, and h^D are constant, regardless of the composition in the syringe and reaction cell. The total amount of heat evolved (released or absorbed) upon an injection is

$$Q = -\Delta V A_{\langle AD\rangle}^{syr}\left(h_{\langle AD\rangle}^A - h_W^A\right) + V_o\left(\frac{\partial A_{\langle AD\rangle}}{\partial A_t}\Delta A_t + \frac{\partial A_{\langle AD\rangle}}{\partial D_t}\Delta D_t\right)\left(h_{\langle AD\rangle}^A - h_W^A\right) \quad 4.4$$

where $\Delta h_{W\to\langle AD\rangle}^A = h_{\langle AD\rangle}^A - h_W^A$ represents the enthalpy of transfer of API solute from water to OS-DLB to form nanocomplex. Accordingly, the partial derivatives of Equation 4.4 are

$$\frac{\partial A_{\langle AD\rangle}}{\partial A_t} = \frac{K_p D_t}{1 + K_p D_t} \quad 4.5$$

$$\frac{\partial A_{\langle AD\rangle}}{\partial D_t} = \frac{K_p A_t}{1 + K_p D_t}\left(1 - \frac{K_p D_t}{1 + K_p D_t}\right) \quad 4.6$$

The full derivation of the models is provided in Appendix B.

4.5 Experimental

4.5.1 Materials

PHT was obtained from Spectrum (Gardena, CA), GSF from Hawkins (Minneapolis, MN), and IBU from BASF (Bishop, TX). All drug substances were used as received. PLX was obtained from BASF (North Mount Olive, NJ) and was gently ground with mortar and pestle and screened through a US 100 mesh sieve (aperture size of 150 μm) before use. OS-DLB was prepared by Professor Yuan Yao's laboratory as described elsewhere.[18] All solvents were of HPLC grade and were obtained from Fisher Chemical (Fair Lawn, NJ).

4.5.2 Methods

4.5.2.1 Quantification of drug association

The amount of API associated with OS-DLB in solution was quantified following a 3-step procedure. First, 500 μL of dimethyl sulfoxide was added to an equal volume of aqueous solution of API, OS-DLB, and PLX and agitated at room temperature for 30 min, to extract the complexed drug from the colloidal OS-DLB particles. Following the extraction of the API from the OS-DLB, 500 μL of 20% (w/w) sodium chloride solution was added to the mixture and agitated at room temperature for 30 min to precipitate the DLB nanoparticles. Finally, the mixture was centrifuged at 12,000 rpm for 20 min, and the amount of drug in the supernatant was assayed using HPLC.

4.5.2.2 Preparation of aqueous solutions of nanocomplex

Excess amounts of API were added to aqueous solutions containing 2000 ppm OS-DLB. 200 ppm PLX was added as needed. After 24 h of constant agitation at 25°C, an aliquot was removed, filtered through a 0.22 μm surfactant-free cellulose acetate membrane, and degassed, prior to ITC measurements. The amount of drug in the solution was quantified as described in the preceding section.

4.5.2.3 Isothermal titration calorimetry

ITC measurements were carried out using a MicroCal ITC200 (Norhampton, MA). Deionized water was placed in the reference cell. In a typical ITC experiment, an aqueous solution of nanocomplexes was placed in the syringe and titrated into the reaction cell containing deionized water. The reaction cell was maintained at 25°C and 0.4 μl of solution was first injected into the reaction cell (200 μl), followed by a series of 13 injections of 3 μl each of solution. As recommended by the manufacturer, the observed heat corresponding to the first injection was neglected because it was likely subjected to somewhat larger errors. Each injection was delivered over 6 s at an interval of 150 s and with a stirring speed of 750 rpm. Each titration was performed at least in duplicate. The heats of dilution were determined in a control experiment whereby 2000 ppm OS-DLB aqueous solution was injected into water. The heats of dilution were then subtracted from the heats determined in the experiment, normalized with respect to the amount of injected API, and plotted as a function of the concentration of OS-DLB in the reaction cell. MicroCal Origin 7 was used to process the data and Microsoft Excel (2013) Solver was used to perform nonlinear least-squares curve fitting of the experimental data.

4.6 Results and Discussion

4.6.1 Kinetic entrapment of solute

The DLB material used in this study is phytoglycogen. Phytoglycogen is a naturally-occurring polysaccharide that is commonly found in plant mutants, such as those of sweet corn, sorghum, and algae. Phytoglycogen is roughly spherical and monodisperse with typical size range of 30 to 100 nm.[19] Phytoglycogen nanoparticles are composed of regularly and extensively branched, flexible linear chains of glucose.[20]

Over the time scale of sample preparation (24 h), solute molecules are likely to diffuse/translocate across the dense dendrimeric structure of phytoglycogen. However, it is conceivable that the relatively short recording time after each injection (150 s) may not provide sufficient time for the same translocation across the dendrimeric structure to the

surface of OS-DLB for redistribution between water and OS-DLB. In the context of ITC, the *non-entrapment* scenario refers to the situation in which all the solute molecules are available for redistribution between water and OS-DLB during the short time period after each injection. The *entrapment* scenario, on the other hand, refers to the case in which the solute molecules are kinetically entrapped in the dendrimeric structure of OS-DLB during the relatively short time frame of titration, thus the pertinent correction becomes necessary in the fitting procedure. Therefore, the effective concentration of API molecularly associated with OS-DLB, $A^{syr}_{\langle AD \rangle}$ is substituted by $\alpha A^{syr}_{\langle AD \rangle}$, where α is the fraction of API solutes that is free to leave OS-DLB dendrimeric structure within the time constraint, i.e. available for redistribution between water and OS-DLB after each injection. α is equivalent to 1 in the non-entrapment scenario, and $0 < \alpha < 1$ in the entrapment scenario. The value of α is likely dependent on the hydrophobicity and molecular size of the solute, as well as the presence of cosolutes in the mixture.

Figure 4-1 compares the non-entrapment and entrapment scenarios for two experimental setups: injection of IBU-DLB and IBU-DLB-PLX mixtures into water. In comparison to the non-entrapment scenario, the entrapment scenario provides better fit to the data. It is evident that a fraction of the drug solutes are entrapped in the dendrimeric structure of OS-DLB and not able to redistribute freely between water and OS-DLB within the recording time frame after each injection. In the experimental setup in which a mixture of IBU and OS-DLB was injected into water (Figure 4-1a), the effective concentration of IBU is approximately 83% of the total concentration molecularly associated (or “bound”) with OS-DLB. In the setup in which a mixture of IBU, OS-DLB and PLX was injected into water (Figure 4-1b), approximately 96% of bound IBU is available for redistribution between water and the nanocomplex. This is within expectation since PLX solutes are also likely to diffuse/translocate across the dendrimeric structure of OS-DLB and take the place of drug solutes, thus render a higher fraction of API available for redistribution during the experiment.

4.6.2 Interaction of PLX with API and OS-DLB

It is demonstrated in Chapter 3 that the solubilization effect of OS-DLB on the model drugs is accentuated by the presence of PLX to varying degrees. The question arises whether there is a definite stoichiometric interaction of PLX with API and OS-DLB. Assuming that the interaction between API, OS-DLB and PLX is stoichiometric, the equilibrium in a mixture containing IBU, OS-DLB and PLX can be represented as follows:

$$A + D + P \underset{}{\overset{K}{\rightleftharpoons}} \langle ADP \rangle \qquad \text{Equilibrium 3}$$

where $\langle ADP \rangle$ represents the concentration of the nanocomplex of API, OS-DLB and PLX. The total change in the enthalpy content of the system upon an injection is

$$Q = -\Delta V A^{syr}_{\langle ADP \rangle} \left(h^{A}_{\langle ADP \rangle} - h^{A}_{W} \right) + V_o \left(\frac{\partial A_{\langle ADP \rangle}}{\partial A_t} \Delta A_t + \frac{\partial A_{\langle ADP \rangle}}{\partial D_t} \Delta D_t + \frac{\partial A_{\langle ADP \rangle}}{\partial P_t} \Delta P_t \right) \left(h^{A}_{\langle ADP \rangle} - h^{A}_{W} \right) \quad 4.7$$

where the partial derivatives of Equation 4.7 are

$$\frac{\partial A_{\langle ADP \rangle}}{\partial A_t} = \frac{K D_t P_t}{1 + K D_t P_t} \qquad 4.8$$

$$\frac{\partial A_{\langle ADP \rangle}}{\partial D_t} = \frac{K A_t P_t}{1 + K D_t P_t} \left(1 - \frac{K D_t P_t}{1 + K D_t P_t} \right) \qquad 4.9$$

$$\frac{\partial A_{\langle ADP \rangle}}{\partial P_t} = \frac{K A_t D_t}{1 + K D_t P_t} \left(1 - \frac{K D_t P_t}{1 + K D_t P_t} \right) \qquad 4.10$$

Figure 4-2 compares the nonstoichiometric and stoichiometric models by fitting each model to the data obtained from the experimental setup in which a mixture of IBU, OS-DLB and PLX was injected into water. It is evident that the nonstoichiometric model provides a significantly better fit to the data, therefore it can be concluded that PLX plays a nonstoichiometric role in the solubilization effect of OS-DLB on the model drugs. These results are consistent with a partitioning mechanism for the uptake of the drug by OS-DLB. The concentrations of PLX used throughout this study fall below the critical micelle concentration [21], therefore it is unlikely that there is a stoichiometric interaction of PLX (as in the case of micellar surfactant) with API and OS-DLB. A plausible role of PLX in the solubilization of the model compounds by OS-DLB (as discussed in Chapter 3) is the

reduction in the hydrophobicity of the microenvironment created by the hydrophobic C_8 chains covalently linked on DLB. This improves the polarity match between the hydrophobic drug molecules and the microenvironment of OS-DLB, and in turn the solubilizing capacity of OS-DLB for the model compounds.

4.6.3 Sequential titration of API-DLB into water (API-DLB → H_2O)

The upper panel of Figure 4-3 shows the energetics of interaction from the sequential titration of API-DLB nanocomplex into water. The magnitude of heat evolution reflects the solubilizing capacity of OS-DLB for the model compounds. The rank order in the magnitude of heat evolution matches the rank order in hydrophobicity of the drugs. The more hydrophobic the drug molecule, the greater the magnitude of heat evolution. This result is in agreement with the study in Chapter 3. The lower panel shows the integrated heat of interaction normalized to the amount of API injected into the reaction cell. The proposed model, as indicated by the solid lines, are generally in good agreement with the experimental data. There are a few plausible explanations for the slight deviations of the fitting curves from the data for PHT and GSF. First, the heat of dilution, which cannot be measured directly for the experimental setup, could somewhat differ from that obtained from injecting pure OS-DLB into water. Second, the concentration of (solute-loaded) OS-DLB placed in the syringe in an actual experiment may be lower than that in a control experiment where 2000 ppm OS-DLB was injected. As determined empirically from the solubility measurements in Chapter 3, the maximum concentration of OS-DLB, $[D]_{max}$, at which the solubility product of the nanocomplex is attained is approximately 750 ppm and 563 ppm for PHT and GSF, respectively. Insoluble nanocomplexes are highly likely to be separated/filtered in the sample preparation stage. Consequently, the magnitude of discrepancy between the experimental data and proposed model is greater in the case of PHT and GSF than in the case of IBU.

The transfer of API from water to OS-DLB involves two energetically distinct processes. The first step involves the disruption of “iceberg”-like water cages around the nonpolar solutes and this step is invariably endothermic. Energy is required to disrupt the extensive

and strong hydrogen bond network that maintains the iceberg-like structure of water. The second step involves the molecular association of the API solute and OS-DLB. Energy is released as new (weak) attractive forces (hydrophobic interactions between the hydrophobic solute and C_8 chains on OS-DLB) are formed. As shown in Table 4-1, the enthalpy of transfer of API solute from water to OS-DLB to form nanocomplex $\Delta h^{A}_{W\rightarrow\langle AD\rangle}$ is positive for all 3 drugs, suggesting that water-water interactions (cohesive interactions) are stronger than interactions between drug solutes and C_8 chains on OS-DLB (adhesive interactions). Notably, the enthalpy of transfer of GSF solute from water to OS-DLB is significantly higher than that of PHT and IBU. This is due to the fact that GSF solute has the largest molecular size and has the greatest propensity to form hydrogen bonds (6 hydrogen bond acceptor groups) with water molecules, and therefore a significantly higher amount of energy is required to disrupt the extensive three-dimensional hydrogen bond network. Interestingly, only approximately 9% of bound PHT is available for redistribution between water and the nanocomplexes. A plausible explanation for such low availability of PHT is that the predominantly hydrophilic core of OS-DLB offers a more conducive microenvironment for PHT than the less polar microenvironment created by the abundance of C_8 chains on the surface of OS-DLB. Consequently, a large fraction of PHT molecules preferentially diffused to the more hydrophilic inner core of OS-DLB, entrapped in the dendrimeric structure of OS-DLB and are not able to redistribute freely between water and OS-DLB within the recording time frame after each injection.

The free energy of interaction between API and OS-DLB, ΔG, is defined as $\Delta G = \Delta H - T\Delta S$, where ΔH and ΔS are the enthalpy and entropy of interaction, respectively, and T is the temperature. Intermolecular interaction between API and OS-DLB occurs if and only when ΔG is negative. In the case of IBU, the interaction between IBU and OS-DLB is nearly athermal ($\Delta h^{A}_{W\rightarrow\langle AD\rangle} \approx 0$), suggesting that the sum of cohesive interactions between water molecules is nearly equivalent to the adhesive interactions between IBU and OS-DLB. Consequently, the entropy of mixing is expected to be moderately lower than the ideal entropy of mixing because for truly ideal mixing to occur, the molecular size of IBU and OS-DLB must be almost the same, such that the molecular

arrangement in the mixture can be truly random. Conversely, in the case of GSF, the interaction between GSF and OS-DLB is strongly endothermic, implying that the entropy of mixing is substantially lower than the ideal entropy of mixing. This is not surprising, since GSF solute and OS-DLB have very dissimilar molecular volumes as well as polarities. Recalling Chapter 3, a polarity mismatch between GSF solutes and the nonpolar microenvironment of OS-DLB is observed in the absence of PLX, but a substantial enhancement in the partition-association of the hydrophobic solute molecules and the microenvironment is created by the combined effect of OS-DLB and PLX. Entropy is the driving force toward unhindered mixing or randomness. The greater the number of arrangements of the interacting molecules, the more random the system, and therefore the greater the tendency for the molecules to interact to form a single phase rather than separate phases. In the case of GSF, it is conceivable that the interacting molecules (solute and OS-DLB) are not randomly arranged, resulting in an increase in the order of the mixture, which in turn produces a reduction in the entropy of interaction. In short, the entropy of interaction is an effect secondary to the enthalpic interaction. Consequently, the free energy of mixing between GSF and OS-DLB is substantially less negative than that of an ideal solution. This result is in agreement with the solubility study in Chapter 3, where a greater solubilizing effect of OS-DLB on IBU than on GSF is observed. The molecular association of IBU with OS-DLB is analogous to the opposing surfaces of Velcro® strips, where the interactions between the fuzzy surfaces are numerous and less restrictive in terms of orientation requirements. Conversely, the molecular association between OS-DLB and GSF is analogous to the two halves of a press-snap fastener, where they are interlocked in a specific orientation with a comparatively greater amount of energy of the "interaction." A similar situation was described by Carvajal and Staniforth[22], where a polymorph of an organic compound exhibits a greater number of weaker active sites for water on its surface as compared to the surface of a different polymorph.

4.6.4 Sequential titration of API-DLB-PLX into water (API-DLB-PLX → H_2O)

The upper panel of Figure 4-4 shows the heat evolution obtained from the sequential titration of API-DLB-PLX nanocomplex into water. Notably, the heat evolved from

titrating IBU-DLB-PLX nanocomplex into water is exothermic throughout, whereas for PHT and GSF, persistent asymmetric split peaks are observed. The endothermic component is relatively large and constant, while the exothermic component weakens over sequential injections. It is conceivable that energetically opposing and kinetically differing processes are present in PHT and GSF systems. It is plausible that each injection of the syringe content into the reaction cell promotes the dissociation, and subsequently the regeneration of the nanocomplex. Interestingly, unlike GSF and IBU, the integrated heat of interaction (lower panel) for PHT resembles a sigmoidal profile. Consequently, the fitting of the proposed model deviates substantially from the data for PHT. This result agrees with the results from the study in Chapter 2, where it is hypothesized that perhaps there are other less obvious, but significant specific interactions between the components in the mixture.

Table 4-2 lists the fitting parameters as well as the enthalpy of transfer of API solute from water to OS-DLB to form nanocomplex $\Delta h^{A}_{W\to\langle AD\rangle}$. Similar to the results in Table 4-1, the enthalpy of transfer of drug solute from water to OS-DLB to form nanocomplex, $\Delta h^{A}_{W\to\langle AD\rangle}$, is positive for the 3 model compounds. Notably, the enthalpy of transfer of GSF in the ternary system of API, OS-DLB and PLX is substantially lower than that in the binary system of API and OS-DLB. Consequently, it is expected that the entropy of mixing in the ternary system is higher than that in the binary system, but nonetheless lower than the ideal entropy of mixing. This result suggests that in the ternary system, the polarity difference between GSF solute and the microenvironment created by the C_8 chains on OS-DLB and PLX is closer, and therefore, molecular arrangement of the components is more random. This result is in agreement with the results in Chapter 3, where the synergistic solubilization of GSF by OS-DLB and PLX is more favorable than OS-DLB alone due to the enhancement in the partition-association of the hydrophobic solute molecules and the microenvironment.

Interestingly, the availability of drug solute for redistribution between water and OS-DLB is higher for PHT and IBU, compared with GSF. It is within expectation that the presence of PLX as cosolute would render a higher fraction of API available for redistribution during

the recording timeframe after each injection. However, in the case of GSF, it appears that the microenvironment of the hydrophilic core of OS-DLB, influenced by PLX, is equally favorable to GSF. Further experiments are required to fully understand the mechanism of kinetic entrapment of solutes in OS-DLB. However, the results from this study indicate that the bound (kinetically trapped) vs. unbound API in the nanocomplex provides a realistic description of the data.

4.7 Conclusions

The challenges associated with the solubilization of poorly water soluble compounds have become progressively more complex. The appreciation of fundamental thermodynamic principles that govern the process of solubilization is paramount in understanding the factors that influence solubility and in developing rational strategies for solubilizing organic crystalline compounds in water. This study demonstrates the use of ITC as a means of elucidating the underlying mechanism of solubilization by OS-DLB through the characterization of thermodynamic parameters that govern the intermolecular interactions in the mixture. It was found that solubilization of drugs, whose molecules exhibit extreme hydrophobic character, occurs by means of favorable entropy-driven interactions. On the other hand, solubilization of drugs whose aqueous solubility is primarily limited by its strong crystal lattice energy, occurs predominantly through the maximization of enthalpic interactions. From a practical point of view, it is recommended to evaluate the effectiveness of OS-DLB as a solubilizing agent for a particular drug candidate during the early stages of preformulation studies. This can be achieved by a set of simple phase solubility measurements and a preliminary evaluation of the thermodynamics associated with the solubilization process by OS-LDB. These preliminary studies can help save a great deal of time and effort in developing a formulation, and in determining the extent to which the OS-DLB approach is expected to serve such purpose.

4.8 Acknowledgments

Financial support from the Dane O. Kildsig Center for Pharmaceutical Processing Research (CPPR), Purdue Research Foundation, and the National Science Foundation (NSF DMR 1310475) is gratefully acknowledged. We thank Prof. Yuan Yao's laboratory for providing the DLB material used in the study. We also thank Dr. Jia Ma for running the isothermal titration calorimetry experiments.

Table 4-1. Thermodynamic properties for the sequential titration of API-DLB nanocomplex into water (API-DLB → H_2O). The partition-association constant, K_p, was obtained from solubility measurements in Chapter 3.

Compound	K_p **(L/g)**	α	$h^A_{\langle AD \rangle} - h^A_W$ **(J/g)**
Phenytoin	1.15	0.09	16.67
Griseofulvin	3.67	0.96	1579.34
Ibuprofen	3.82	0.83	82.56

Table 4-2. Thermodynamic properties for the sequential titration of API-DLB-PLX nanocomplex into water (API-DLB-PLX → H_2O). The partition-association constant, K_p, was obtained from solubility measurements in Chapter 3.

Compound	K_p **(L/g)**	α	$h^A_{\langle AD \rangle} - h^A_W$ **(J/g)**
Phenytoin	1.15	0.24	78.04
Griseofulvin	3.67	0.63	571.76
Ibuprofen	3.82	0.96	78.17

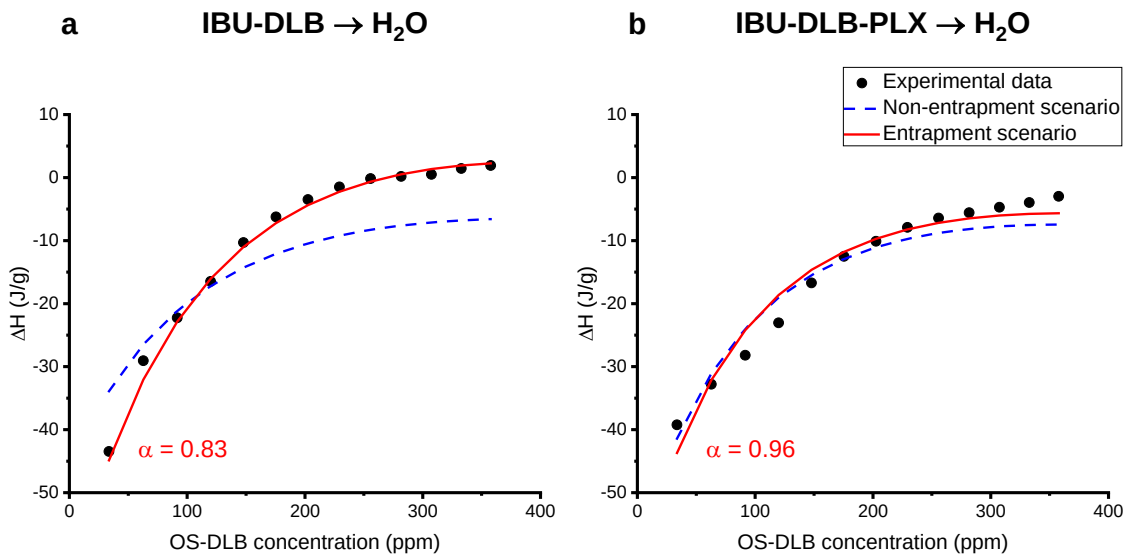

Figure 4-1. Sequential titration of **(a)** IBU-DLB and **(b)** IBU-DLB-PLX nanocomplex into water at 25°C. The heat of interaction is normalized to the amount of injected IBU. The solid and broken curves illustrate the best fit of the data to the entrapment and non-entrapment scenarios, respectively. The non-entrapment scenario is ruled out due to the poor fit of the data.

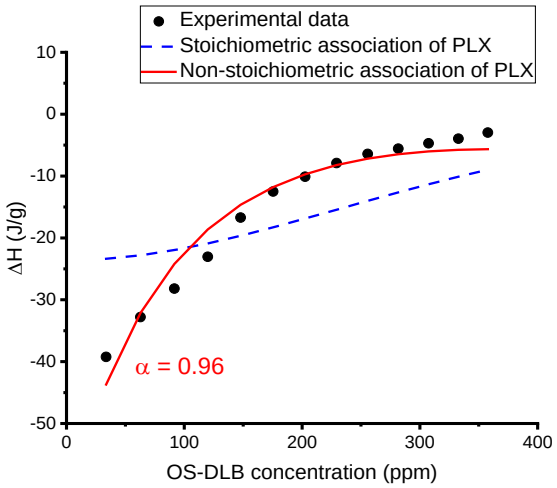

Figure 4-2. Sequential titration of IBU-DLB-PLX nanocomplex into water at 25°C. The heat of interaction is normalized to the amount of injected IBU. The solid and broken curves represent models in which PLX is non-stoichiometrically and stoichiometrically incorporated, respectively. The stoichiometric model is ruled out due to the poor fit of the data.

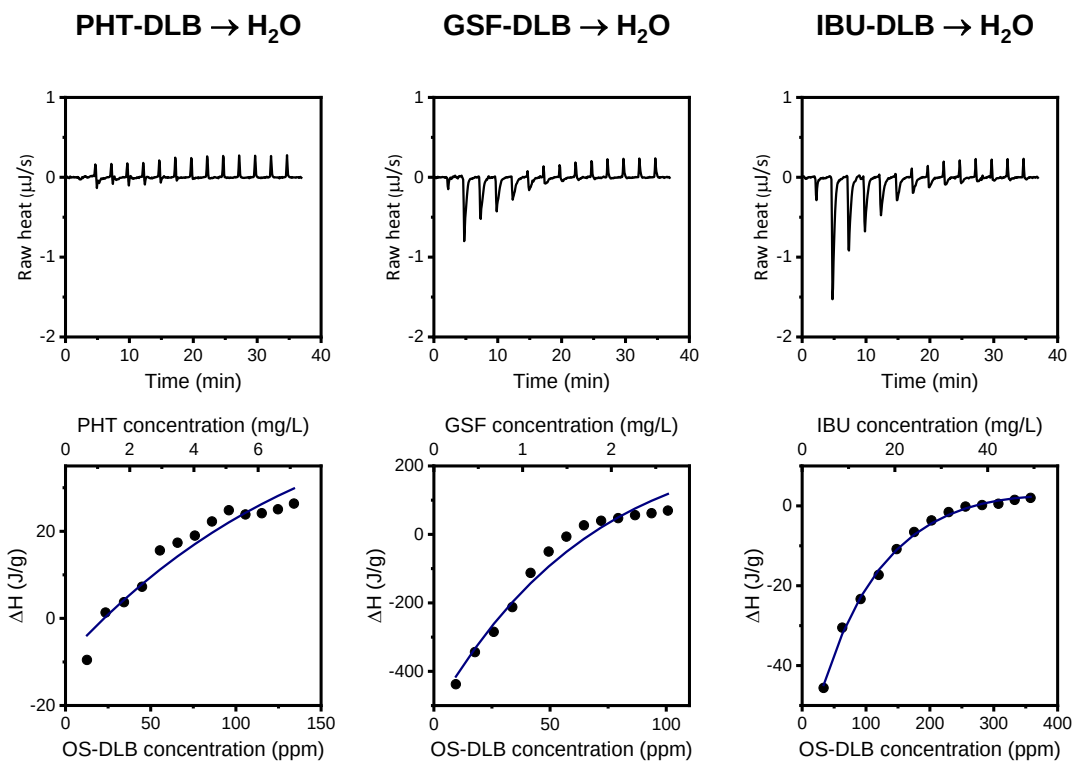

Figure 4-3. Sequential titration of API-DLB nanocomplex into water at 25°C. Upper panel: Raw calorimetric trace. Lower panel: Heat of interaction normalized to the amount of injected API. The solid lines are the non-linear least squares fit of the calorimetric data to the model.

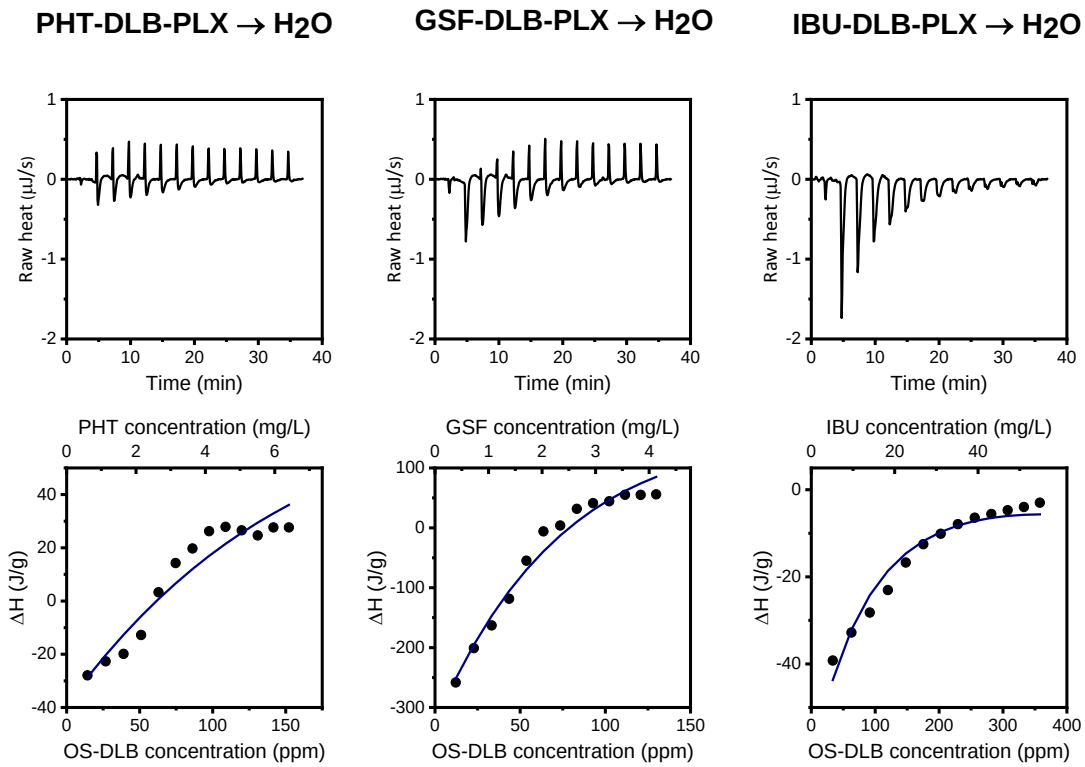

Figure 4-4. Sequential titration of API-DLB-PLX nanocomplex into water at 25°C. Upper panel: Raw calorimetric trace. Lower panel: Heat of interaction normalized to the amount of injected API. The solid lines are the non-linear least squares fit of the calorimetric data to the model.

4.9 References

1. K. Connors and T. Higuchi. 1965. Phase solubility techniques. *Advances in Analytical Chemistry and Instrumentation* **4**: 117-212.
2. A. Hvidt. 1983. Interactions of water with nonpolar solutes. *Annual Review of Biophysics and Bioengineering* **12**: 1-20.
3. H. M. Fadda, X. Chen, A. Aburub, D. Mishra, and R. Pinal. 2014. A novel method for determining the solubility of small molecules in aqueous media and polymer solvent systems using solution calorimetry. *Pharmaceutical Research* **31**: 1735-1743.
4. D. Q. M. Craig and J. M. Newton. 1991. Characterisation of polyethylene glycols using solution calorimetry. *International Journal of Pharmaceutics* **74**: 43-48.
5. R. J. Willson, A. E. Beezer, and J. C. Mitchell. 1996. Solid state reactions studied by isothermal microcalorimetry; the solid state oxidation of ascorbic acid. *International Journal of Pharmaceutics* **132**: 45-51.
6. R. Patel, G. Buckton, and S. Gaisford. 2007. The use of isothermal titration calorimetry to assess the solubility enhancement of simvastatin by a range of surfactants. *Thermochimica Acta* **456**: 106-113.
7. K. Bouchemal. 2008. New challenges for pharmaceutical formulations and drug delivery systems characterization using isothermal titration calorimetry. *Drug Discovery Today* **13**: 960-972.
8. B. B. Raju, F. M. Winnik, and Y. Morishima. 2001. A look at the thermodynamics of the association of amphiphilic polyelectrolytes in aqueous solutions: Strengths and limitations of isothermal titration calorimetry. *Langmuir* **17**: 4416-4421.
9. M. M. Pierce, C. S. Raman, and B. T. Nall. 1999. Isothermal titration calorimetry of protein–protein interactions. *Methods* **19**: 213-221.
10. W. F. de Azevedo Jr and R. Dias. 2008. Experimental approaches to evaluate the thermodynamics of protein- drug interactions. *Current Drug Targets* **9**: 1071-1076.
11. N. M. Eren, G. Narsimhan, and O. H. Campanella. 2016. Protein adsorption induced bridging flocculation: The dominant entropic pathway for nano-bio complexation. *Nanoscale* **8**: 3326-3336.
12. M. Sokołowska, M. Wszelaka-Rylik, J. Poznański, and W. Bal. 2009. Spectroscopic and thermodynamic determination of three distinct binding sites for co(ii) ions in human serum albumin. *Journal of Inorganic Biochemistry* **103**: 1005-1013.
13. M. Lovatt, A. Cooper, and P. Camilleri. 1996. Energetics of cyclodextrin-induced dissociation of insulin. *European Biophysics Journal* **24**: 354-357.
14. Y. Boonsongrit, B. W. Mueller, and A. Mitrevej. 2008. Characterization of drug–chitosan interaction by 1h nmr, ftir and isothermal titration calorimetry. *European Journal of Pharmaceutics and Biopharmaceutics* **69**: 388-395.
15. H. H. Heerklotz, H. Binder, and R. M. Epand. 1999. A “release” protocol for isothermal titration calorimetry. *Biophysical Journal* **76**: 2606-2613.
16. R. Ghai, J. Falconer Robert, and M. Collins Brett. 2011. Applications of isothermal titration calorimetry in pure and applied research—survey of the literature from 2010. *Journal of Molecular Recognition* **25**: 32-52.

17. A. D. Tsamaloukas, S. Keller, and H. Heerklotz. 2007. Uptake and release protocol for assessing membrane binding and permeation by way of isothermal titration calorimetry. *Nature Protocols* **2**: 695.
18. S. L. Scheffler, L. Huang, L. Bi, and Y. Yao. 2010. In vitro digestibility and emulsification properties of phytoglycogen octenyl succinate. *Journal of Agricultural and Food Chemistry* **58**: 5140-5146.
19. J.-L. Putaux, A. Buléon, R. Borsali, and H. Chanzy. 1999. Ultrastructural aspects of phytoglycogen from cryo-transmission electron microscopy and quasi-elastic light scattering data. *International Journal of Biological Macromolecules* **26**: 145-150.
20. J. D. Nickels, J. Atkinson, E. Papp-Szabo, C. Stanley, S. O. Diallo, S. Perticaroli, B. Baylis, P. Mahon, G. Ehlers, J. Katsaras, and J. R. Dutcher. 2016. Structure and hydration of highly-branched, monodisperse phytoglycogen nanoparticles. *Biomacromolecules* **17**: 735-743.
21. P. Alexandridis, T. Nivaggioli, and T. A. Hatton. 1995. Temperature effects on structural properties of pluronic p104 and f108 peo-ppo-peo block copolymer solutions. *Langmuir* **11**: 1468-1476.
22. M. T. Carvajal and J. N. Staniforth. 2006. Interactions of water with the surfaces of crystal polymorphs. *International Journal of Pharmaceutics* **307**: 216-224.

CHAPTER 5. QUALITY BY DESIGN: OPTIMIZATION OF HOT MELT EXTRUSION PROCESS FOR THE PREPARATION OF BIODENDRIMERIC SOLID DISPERSIONS

5.1 Abstract

An integrated approach involving experimental design, multivariate methods, and response surface modeling to aid in the understanding of the controlling factors affecting dissolution and crystallinity of biodendrimeric solid dispersions (BDSDs) prepared by hot melt extrusion (HME), is presented. BDSDs comprise of an octenylsuccinate-derivatized dendrimer-like biopolymer (OS-DLB) to act as both solubilizing agent and carrier matrix. Ibuprofen (IBU) and griseofulvin (GSF) were used as poorly water-soluble drugs. The primary solubilization mechanism of IBU is via molecular association of hydrophobic solutes with the non-polar solvating environment of the modified biopolymer. Consequently, changes in the processing parameters that alter the polarity of the microenvironment of the biopolymer result in discernible changes in the dissolution characteristics of IBU BDSDs. However, due to the polarity mismatch between the less hydrophobic GSF solutes and the OS (C_8) groups on OS-DLB, the performance of GSF BDSDs is less sensitive to the process variables. This is advantageous because it allows greater flexibility for formulation design and future process improvement, as well as processing at multiple operational scales.

5.2 Introduction

Hot melt extrusion (HME) is one of the most widely used processing technologies in the plastics industry. Over the last four decades, the science and technology of HME has been successfully exploited by the pharmaceutical industry as an alternative "platform technology" for preparing pharmaceutical solid dosage forms.[1] HME is currently one of the most active areas of research in the pharmaceutical field, with the number of patents issued and journal articles published increasing steadily since the early 1980's (Figure 5-1). To date, there is a wide array of marketed pharmaceutical dosage forms using melt extrusion technology (Table 5-1), demonstrating the versatility, feasibility and scalability of HME as an enabling processing technology.[1]

HME is a highly complex processing technology. It involves simultaneous process functions, such as transport, mixing and compression of particulate components, melting of polymeric materials, mechanochemical reactions, and shaping of a molten / dough-like material through a die.[2] It offers significant advantages over traditional pharmaceutical processing techniques, such as short processing (residence) time, intimate mixing, highly controllable processing conditions, and excellent process efficiency.[3] Furthermore, HME is a solvent-free, continuous process that can be scaled to manufacture industrially relevant amounts using quality by design (QbD) principles.[4] A major drawback of HME is the use of high processing temperatures – a processing requirement for improving the processability of the formulation and/or achieving an intended pharmaceutical formulation (e.g. amorphous solid dispersion) – thereby, presenting a significant limitation on the applicability of HME in processing thermolabile materials.

HME has been firmly established as a robust means of producing amorphous solid dispersions (ASDs) of poorly water-soluble drugs with improved dissolution rate and enhanced bioavailability.[5-7] In an ideal ASD system, the crystalline lattice of the drug is completely obliterated, and the drug molecules are randomly / molecularly dispersed within an amorphous polymer chain network. This typically entails the extrusion of a crystalline drug substance with a suitable polymeric carrier at processing temperatures higher than the melting temperature of the drug, to ensure complete obliteration of the

crystal lattice structure of the drug. Upon exposure to an aqueous medium, the drug in the ASD presents itself in solution form, whereby the energy typically required to break up the crystalline lattice of the drug is no longer a limitation to the solvation of the drug in aqueous conditions. However, the inherent physical instability of the amorphous state of the drug often diminishes the viability of ASDs as full-fledged pharmaceutical products. Depending on the solubility of the drug in the polymeric carrier as well as the crystallization kinetics of the drug, the drug may either remain molecularly dispersed in the solid solution or re-crystallize as a whole or in part on aging.[8] Moreover, when exposed to a volume of aqueous medium insufficient to dissolve all of the drug, the drug forms a supersaturated solution, which has an inherent tendency to precipitate, thereby losing the advantages of an amorphous molecular dispersion. Clearly, despite the potential benefits, amorphous systems are not viable in many cases due to the limitations just described.

Conversely, the development of poorly soluble drugs that does not involve the obliteration of the crystal lattice structure of the drug offers an alternative strategy for enhancing dissolution rate and oral bioavailability. However, this often requires the thoughtful combination of functional excipients (such as carrier matrices and processing aids) and processing conditions in order to produce non-amorphous systems that are equally, if not more capable of enhancing the dissolution rate of poorly soluble drugs. A limited number of non-amorphous systems prepared by HME have been reported. Thommes et al.[9] prepared “solid crystal suspensions” of griseofulvin, phenytoin and spironolactone wherein the drug particles were dispersed at the particulate level in crystalline mannitol by HME at processing temperatures above the melting point of mannitol but below that of the drugs. The result is a thermodynamically stable dispersion with fast dissolution rate, an effect that is largely attributed to the wetting effect of the highly hydrophilic carrier. Boksa et al. and several research groups[10-12] have studied extensively the concurrent production and formulation of cocrystals wherein the cocrystals were physically embedded in the carrier matrix. The effect of the carrier matrix is expected to be 2-fold. On the one hand, the carrier matrix promotes intimate mixing between the drug and the coformer, while reducing the amount of shear stress applied to the cocrystal. On the other hand, the carrier matrix provides a means for fine-tuning the apparent solubility and dissolution rate of the cocrystal.

The abovementioned cases demonstrate the potential of thermodynamically stable, non-amorphous dispersion systems for increasing the dissolution rate of poorly soluble drugs.

This study extends the study in Chapter 2, where it was demonstrated that a non-amorphous solid dispersion system, comprised of a octenylsuccinate-modified dendrimer-like biopolymer (OS-DLB) as a carrier matrix and poloxamer 338 (PLX) as a processing aid, was capable of increasing the apparent solubility and enhancing the dissolution rate of poorly water-soluble drugs, while retaining a predominantly crystalline state of the drug. Accordingly, the non-amorphous solid dispersion system is referred to as biodendrimeric solid dispersion (BDSD) throughout this report. A quality by design (QbD) approach is presented here to aid in the optimization of the extrusion processing parameters and in the understanding of the controlling factors that affect dissolution and crystallinity of the BDSDs.

The QbD paradigm of drug development, outlined in ICH *Q8(R2) Pharmaceutical Development*, was introduced to enhance pharmaceutical product and process understanding, which in turn provides a basis for greater degree of regulatory flexibility [13]. The flowchart in Figure 5-2 shows the main steps for the development of a pharmaceutical product using a QbD approach, as outlined in the ICH Q8(R2) guideline. Briefly, the QbD paradigm of drug development includes the following elements at a minimum:

1. Defining the quality target product profile (QTPP). Considerations for the QTPP include all factors that influence the quality, safety and efficacy of the drug product, ranging from the characteristics of the active pharmaceutical ingredient (API) and excipients, all the way to packaging. These factors can include the route of administration, type of dosage form, delivery system, dosage strength, and container closure system.
2. Identifying potential critical quality attributes (CQAs) of the drug product. A CQA is defined as “a physical, chemical, biological or microbiological property or characteristic that should be within an appropriate limit, range or distribution to

ensure the desired product quality". It is generally associated with the drug substance, excipients, intermediates and drug product.

3. Determining the design space. A design space describes the functional relationships between process inputs (material attributes and process parameters) and the CQAs of the drug product. It can be presented either in terms of ranges of material attributes and process parameters, or through complex mathematical models. A design space can be used to describe one or more unit operations, or the entire manufacturing process that spans multiple operations.
4. Defining a control strategy. The goal of a control strategy is to ensure that the QTPP can be achieved consistently. The elements of a control strategy can include, but is not limited to controls of input materials attributes (e.g. drug substance, excipients, intermediates, and packing materials), controls for unit operations, and in-process testing.
5. Continuous improvement. Throughout the lifecycle of the drug product, companies have the opportunity to evaluate innovative approaches to improve the quality of the drug product. This falls under the purview of ICH *Q10 Pharmaceutical Quality Systems*.[14]

The goal of this study is to define a HME design space and to illustrate the use of an integrated approach involving experimental design, multivariate methods and response surface modeling. HME, like many pharmaceutical processing technologies, still relies largely on experience and a trial-and-error approach toward finding a set of processing parameters that provides the desired product quality. The QbD approach to product development has been proven to be a more efficient strategy to studying the effects of multiple process parameters and in establishing a design space that will ensure product quality.[15, 16] While modeling and simulations methods can enhance the understanding of the complex interactions between material attributes and process parameters[17, 18], they are beyond the scope of the present study. Accordingly, ibuprofen (IBU) and griseofulvin (GSF) were used as model poorly soluble drugs in this study. The choice of these model compounds covers the case where low solubility results mainly from the high hydrophobicity of the molecule (IBU), as well as the case where poor solubility is mainly

the result of the high lattice energy of the crystalline solid (GSF). A three-step approach was employed in this study. First, the variables that influence the quality of BDSDs were determined from their variable influence on projection (VIP) and principal component analysis (PCA) plots. Second, a prediction profiler was used to examine the effect of the processing variables individually on each of the proposed outputs (CQAs), namely initial dissolution rate, supersaturated concentration, and crystallinity. Finally, a prospective design space was established for each model drug using a response surface methodology. The statistical analysis methods will be discussed in greater detail in Section 5.4.

5.3 Experimental

5.3.1 Materials

GSF was obtained from Hawkins (Minneapolis, MN) and IBU from BASF (Bishop, TX). All drug substances were used as received. Poloxamer 338 (PLX) was obtained from BASF (North Mount Olive, NJ) and was gently ground with mortar and pestle and screened through a US 100 mesh sieve (aperture size of 150 μm) before use. OS-DLB was prepared by Professor Yuan Yao's laboratory as described elsewhere.[19] All solvents were of HPLC grade and were obtained from Fisher Chemical (Fair Lawn, NJ).

5.3.2 Methods

5.3.2.1 Design of experiments

The Box-Behnken design was selected for the following three reasons. 1) The Box-Behnken design has been demonstrated to be efficient for studying the main effects between the critical factors with minimum experimental runs.[20] Furthermore, the Box-Behnken design does not contain any vertices of the design space, which typically represent factor-level combinations that are either too expensive or impractical to test due to physical process limitations. Note that this is not the situation in this study. A potential implication is that estimations near the edges of the design space may not be accurate.[20] 2) As the Box-Behnken design is rotatable (or nearly rotatable), i.e., the variance of the predicted response

is reasonably stable and consistent, it provides good predictions in all directions.[21] More often than not, the location of the region (combination of processing parameters) in which the responses of interest is satisfactory, is unknown prior to running the response surface experiments. Since the objective of the factorial study is to identify a prospective HME design space, rotatability is an important criterion for the selection of a response surface design. 3) The Box-Behnken design is a second-order factorial design capable of describing systems that exhibit curvature, i.e., systems whereby main effects, as well as second-order interactions are equally important.[22] Three processing factors – temperature, residence time, and screw rotation speed – were studied at three levels along with one center point, resulting in a total of 13 extrusion experiments (Table 5-2). All statistical analyses were conducted using SAS 9.4 (SAS Institute Inc., Cary, NC).

5.3.2.2 Hot melt extrusion

Table 5-3 shows the formulation of GSF and IBU BDSDs. Based on preliminary experiments, the amount of PLX (processing aid) in each formulation was varied accordingly so that processing temperatures under 50°C can be attained. The weight ratio of API to OS-DLB was kept constant at 3:1. In a typical HME experiment, 4 g of API, OS-DLB, and PLX was first blended by gentle vortexing for approximately 1 min. The mixture was then fed into a Thermo Scientific HAAKE MiniLab micro compounder (Waltham, MA), equipped with dual conical corotating screws (screw diameter of 14 to 5 mm, 11 cm length), and with a valve for controlling the residence time of the sample through the extruder chamber. The feeding step into the extruder was completed within 3 min.

5.3.2.3 Quantification of drug association

The amount of API associated with OS-DLB in solution was quantified following a 3-step procedure. First, 500 µL of dimethyl sulfoxide was added to an equal volume of aqueous solution of API, DLB, and PLX and agitated at room temperature for 30 min, to extract the drug molecules from the colloidal DLB particles. Following the extraction of the API from the DLB, 500 µL of 20% (w/w) sodium chloride solution was added to the mixture and

agitated at room temperature for 30 min to precipitate the DLB nanoparticles. Finally, the mixture was centrifuged at 12,000 rpm for 20 min, and the amount of drug in the supernatant was assayed using HPLC.

5.3.2.4 Time-concentration profile

The dissolution study was performed by suspending a sample equivalent to 2.5 ± 0.2 mg of API into the barrel of a 30 mL syringe, filled with 28 mL of deionized water and fitted with a 0.45 μm surfactant-free cellulose acetate syringe filter. The syringe was placed on a rotating shaker set at 10 rpm at room temperature. A 2 mL aliquot was collected from the mixing solution at the first time point, and 1 mL aliquots were withdrawn at subsequent time points. The samples were treated and analyzed according to the extraction and HPLC quantification procedure described above.

5.3.2.5 X-ray diffraction

Powder X-ray diffraction was performed using a Rigaku SmartLab X-ray diffractometer (Tokyo, Japan). Measurements were taken using CuKα radiation at 40 kV and 44 mV over a 2θ angle range of 5°-40°, with a scan rate of 4°/min and a step size of 0.02°. The percent crystallinity of the API in the BDSD was estimated with respect to its corresponding physical mixture (PM) using PONKCS (partial or no known crystal structure), a Rietveld refinement method described by Scarlett and Madsen.[23] Data analysis was conducted using Panalytical X'Pert HighScore Plus 4 (Almelo, the Netherlands).[24] First, an *hkl* file that best fit the observed amorphous halo was generated for each, DLB and PLX, based on the diffraction pattern of the pure material. The diffraction pattern of the APIs was refined using the crystal structure information obtained from the Cambridge Structural Database. Subsequently, the peak files were incorporated into the quantification of the phases present in the PMs, where the pseudo-formula mass of DLB and PLX was scaled according to their known weight fractions. Finally, the values determined for the pseudo-formula mass were used in all subsequent analyses of corresponding BDSDs. The percent crystallinity of the

API in the BDSD is defined as the ratio of the API phase in the BDSD relative to that present in the PM.

5.4 Results and Discussion

5.4.1 HME design space for IBU BDSDs

Figure 5-3 shows the dissolution profile of IBU for the 13 BDSD batches produced. The variation among batches is larger at the beginning of the release. After 60 min, equilibrium was mostly achieved, and the difference between the batches is significantly reduced. Table 5-4 shows the estimated percent crystallinity of IBU in the BDSDs with respect to their corresponding physical mixture (PM). IBU, which has a weak crystal structure (Chapter 2), lost almost one-third of its crystallinity during the process. This is attributed to the crystal disruption effect exerted by PLX. The identification of subtle differences in both Figure 5-3 and Table 5-4, by means of direct comparison and analysis, is challenging and may not be fully informative. Multivariate data analysis was therefore conducted, to examine all the variables captured in the DOE study, as well as to explore the underlying mechanisms that affect the properties of the BDSDs, as discussed below.

The variable influence on projection (VIP) is a variable selection method for discriminating between important and unimportant predictors in a partial least squares (PLS) model. PLS is used to describe the relationship between two data matrices – predictor variables, **X**, and response variables, **Y** – by a linear multivariate model.[25] The VIP plot summarizes the relative contribution of each predictor in modeling both **X** and **Y**. In most cases, predictors with VIP value greater than 1 are considered influential variables.[26] Figure 5-4 shows the VIP plots for modeling the extrusion parameters, including the second-order interactions between the parameters (X-variables), as well as the dissolution profile and crystallinity of IBU (Y-variables). Third and higher order effects are generally assumed to be unimportant.[22] Even though PLS regression has the ability to analyze and model multiple Y-variables simultaneously[25], initial evaluation of all the response variables in a single model shows that the dissolution profile and crystallinity of IBU can be clustered into two

separate groups on the correlation loading plot (data not shown). Therefore, it is more appropriate in this case to model the dissolution profile and crystallinity of IBU separately. Figure 5-4a shows that processing temperature is the most influential predictor for describing the dissolution profile of IBU, with a high VIP of 2.0. In contrast, screw speed, as well as the second-order interactions involving screw speed, are important variables for modeling the crystallinity of IBU in the BDSDs (Figure 5-4b). The interaction between residence time and screw speed corresponds to the number of revolutions, which in turn is related to the amount of mixing / mechanical shear forces imparted onto the formulation during the extrusion process. Unlike the interaction between residence time and screw speed, the implication of the interaction between processing temperature and screw speed is less clear. A rationalization of this interaction is that while the processing (extruder barrel) temperature was set at a fixed temperature, the higher the screw speed, the greater the shear forces imparted onto the formulation, thus resulting in localized increase in product temperature. The melting temperature of PLX is approximately 57°C, therefore partial melting of PLX (or even IBU) is likely to have occurred as a result of localized overheating of the formulation. In Chapter 2, it has been demonstrated that PLX has the potential to disrupt the crystalline structure of IBU. Consequently, partial miscibility of IBU with PLX is likely to be induced. In both situations (i.e., second-order interactions involving screw speed), one would expect that the higher the screw speed, the greater the likelihood of disrupting the crystalline structure of the IBU, and therefore reduction of crystallinity of the drug in the BDSD.

Principal component analysis (PCA) is also multivariate projection method, concerned with explaining the variance-covariance structure of a data matrix, **Y**, through a few linear combinations of these variables.[27] The main objective of a PCA is to reveal relationships between observations and variables, and among variables themselves.[26] Figure 5-5a shows the relationship between the 13 batches based on the dissolution profile of IBU from the BDSDs. The first principal component explains the largest sample variance of 85%, followed by the second principal component of 12%. Collectively, the first two principal components explain about 97% of the total sample variance. The batches can be clustered into three evident groups, based on the temperature at which the batches were processed.

This result is in agreement with the VIP plot, where the processing temperature is an important predictor in modeling the dissolution profile of IBU. Figure 5-5b examines the relationship between the batches based on their X-ray diffraction pattern. The first two principal components explain about 57% and 38% of the total sample variance, respectively. Collectively, the first two principal components explain about 95% of the total sample variance. Unlike the PCA plot based on the dissolution profile of IBU (Figure 5-5a), no obvious clusters can be discerned, indicating that the diffraction pattern of the batches are very similar.

The primary concern of this study is to investigate the effects of HME as an enabling processing technology on the dissolution behavior and crystallinity of the drug. Three response variables (critical quality attributes) were selected for the DOE effects analysis: dissolution of IBU from the BDSDs at 1 and 120 min, and percent crystallinity of IBU in the BDSDs. The concentration of IBU at 1 min corresponds to the initial dissolution rate (*DR*) of IBU, which is related to the apparent solubility of the solute (S_{app}), as described by the Noyes-Whitney equation:

$$DR = \frac{dM}{dt} = kA\left(S_{app} - C\right) \qquad 5.1$$

where k is a constant that is related to the hydrodynamics of the dissolution medium, A is the surface area of the solute, and C is the concentration of the solute in the medium. Since $C = 0$ at time zero, the initial dissolution rate is directly proportional to the apparent solubility of the solute. The concentration of IBU at 120 min, where a plateau has been achieved, corresponds to the supersaturated concentration of the solute. An optimal BDSD is one that gives a fast initial dissolution with high and long-lasting supersaturation, while retaining a predominantly crystalline state of the API. The latter is a conflicting goal, since amorphization leads to the formation of metastable phases, thereby improves the initial dissolution rate and supersaturated concentration of the solute. However, this supersaturation may only last temporarily and will eventually revert to the equilibrium solubility of the most stable (crystalline) state. Clearly, there is a need to establish a HME design space that can address these conflicting goals, as described below.

The robustness of a model can be validated by a predicted vs. observed plot. A high R^2 value implies that the model is capable of explaining the variability of the data. However, it should be noted that this is merely a diagnostic tool, and not an end onto itself. Based on the VIP plot in Figure 5-4a, processing temperature is the most important factor in modeling the dissolution profile of IBU. The model comprising of processing temperature alone gives a high R^2 of 0.93 for the dissolution response at 1 min, but a rather low R^2 of 0.55 for the dissolution response at 120 min (data not shown). However, with the inclusion of residence time, screw speed, and the second-order interactions involving screw speed in the model, the R^2 for the dissolution responses at 1 and 120 min increases to 0.99 and 0.97, respectively, as shown in Figure 5-6a. The model is also adequate for modeling the crystallinity response, giving an R^2 of 0.99 (Figure 5-6b). The mean squared error (MSE) obtained for the dissolution responses at 1 and 120 min, and crystallinity are 3.34, 0.48 and 0.11, respectively.

Figure 5-7 is a prediction profiler and it shows the effects of the process parameters on the responses, while changing only one process parameter at a time. The prediction profiler is an exploratory analysis to assess the relative importance of the parameters in a way that is independent of the model. It is based on the response surface methodology and it can be viewed as a cross-section of the three-dimensional response surface plots. The prediction profiler shows that the responses depend more strongly on processing temperature than on residence time and screw speed. It is noteworthy that the top left plot on the prediction profiler suggests a strong dependence of the initial dissolution of IBU on processing temperature. The higher the processing temperature, the lower the initial dissolution of IBU. A similar but attenuated effect is observed for the dissolution at 120 min. At first glance, these results appear counterintuitive. One would expect that the higher the processing temperature, the greater the likelihood to disperse IBU at the molecular level, given its weak crystal structure and appreciable miscibility with PLX. Consequently, faster initial dissolution and higher supersaturation concentration would be reasonably expected. However, the predicted responses are attributable to the molecular interaction between PLX and OS-DLB. At processing temperatures close to the melting temperature of PLX, molten PLX forms a surface coating on OS-DLB, thereby reduces the hydrophobicity of

the non-polar microenvironment of OS-DLB when in solution, and consequently the solubility enhancement of IBU by OS-DLB. Previous studies have demonstrated the importance of polarity match between the solvating environment and the solute molecules, whereby maximum solubility enhancement is achieved when the hydrophobicity of the solute molecules closely matches the polarity of the solvating environment.[28, 29] Furthermore, the non-polar microenvironment of OS-DLB may become saturated with PLX, thus reducing the capacity of the microenvironment to accommodate IBU solute molecules. These actions would then retard the dissolution of IBU from the BDSDs.

In this study, the response surface methodology is used to establish a HME design space for processing BDSDs. Figure 5-8 shows the three-dimensional response surface plots for the dissolution and crystallinity responses, as a function of residence time and screw speed, while holding temperature constant at 30°C. The red regions represent the combination of processing parameters that will maximize the responses. The response surface plot for dissolution at 1 min (Figure 5-8a) shows that maximal initial dissolution of IBU can be achieved when the BDSD is processed at high screw speed (> 120 rpm) but low residence time (< 20 min), or low screw speed (< 80 rpm) but high residence time (> 15 min). This indicates that a moderate (neither insufficient nor excessive) amount of mixing is necessary to enhance the initial dissolution of IBU from the BDSD. Since OS-DLB is a biopolymer, excessive mixing or shear forces may damage its polymeric structure, thus reducing its efficiency as a carrier matrix. On the other hand, the response surface plot for dissolution at 120 min (Figure 5-8b) suggests that residence time is no longer an influential factor. High supersaturation concentration can be attained when the BDSD is processed at a relatively high screw speed. Again, this result indicates the necessity of an intimate mixture in enhancing the dissolution of IBU from the BDSD. Figure 5-8c shows the response surface plot for the crystallinity of IBU in the BDSD. It should be noted that while X-ray diffractometry is a widely used technique for assessing crystallinity, the major drawback of this analytical method is its low sensitivity. The detection limit for percent crystallinity typically ranges between 5 to 10%.[30-32] It is plausible that even though the calculated crystallinity of batches 3 and 10 are 66.5% and 70.6%, respectively, the degree of crystallinity between these batches are similar due to the detection limitation of X-ray

diffractometry. In consideration of this practical limitation, the color scale of the response surface plot for crystallinity has been manually adjusted to accommodate a range of 10% to reflect the variation (or lack thereof) in crystallinity between the batches. It is apparent that the crystallinity of IBU in the BDSD is not strongly influenced by residence time and screw speed. This is within expectation because at 30°C, the propensity of PLX to disrupt the crystal structure of the drug is minimal.

The final step is to find a set of processing conditions that optimizes all responses (dissolution at 1 and 120 min, and crystallinity) through the use of desirability functions, proposed by Derringer and Suich[33]. First, each response is transformed into a desirability function, d_i, where the scale varies between 0 (unacceptable response value) and 1 (desirable response value). Since the objective of the responses is a maximum value, the desirability function is defined as

$$d = \begin{cases} 0 & y < L \\ \left(\dfrac{y-L}{U-L}\right)^r & L \le y \le U \\ 1 & y > U \end{cases} \qquad 5.2$$

where L and U represents the lower and upper limits, respectively, and r is the weight. Assuming that the desirability function is linear, $r = 1$. The overall desirability, D, is the geometric mean of the individual desirability values

$$D = \left(d_1 \times d_2 \times \ldots \times d_m\right)^{1/m} \qquad 5.3$$

where m is the number of responses. The overall desirability will be zero if any of the individual responses is unacceptable. Figure 5-9 shows an overlay of the contour plots from Figure 5-8 and a proposed HME design space for producing IBU BDSD. The red region represents the combination of processing parameters that gives the highest overall desirability. Based on the proposed design space, fast initial dissolution, high supersaturation concentration, and maximum crystallinity can be attained when the BDSD is processed at 30°C, high screw speed (> 120 rpm) and moderate residence time (< 25 min).

5.4.2 HME design space for GSF BDSDs

Figure 5-10 shows the dissolution profile of GSF from the BDSDs. In comparison to the dissolution profiles of IBU in Figure 5-3, the variation between the batches and throughout the dissolution run is substantially greater. The release of GSF from batches 1-3 was markedly lower than the rest of the batches. The underlying reason for this anomalous dissolution behavior is not immediately evident. Table 5-5 shows the estimated percent crystallinity of GSF in the BDSDs with respect to their corresponding physical mixture (PM). GSF, which has a high crystal lattice energy (Chapter 2), preserved almost all of its original crystalline structure. Since the processing temperature at which the BDSDs were processed was varied between 30°C and 50°C, well below the melting temperature of GSF (217°C), the potential for PLX to disrupt the crystalline structure of the drug is low.

Figure 5-11 shows the VIP plots for modeling the extrusion parameters, including the second order interactions between the parameters, as well as the dissolution profile and crystallinity of GSF. The dissolution profile and crystallinity of GSF were modeled separately because the responses are on different scales. Figure 5-11a shows that residence time and second-order interactions involving residence time are important factors in modeling the dissolution behavior of GSF from the BDSDs. The interaction between processing temperature and residence time is somewhat similar to that between processing temperature and screw speed, as mentioned in the preceding section. HME is an energy-intensive mixing process, in which localized overheating of the formulation as a result of excessive shear heating may occur.[3] Therefore, one would expect that the longer the residence time, the greater the tendency to form “hot spots”. Figure 5-11b suggests that processing temperature is the most influential predictor for describing the crystallinity of GSF, with a high VIP of 1.5, followed by screw speed, with a VIP of 1.1.

Figure 5-12a shows the relationship among the 13 batches, based on the dissolution profile of GSF from the BDSDs. The first two principal components explain approximately 98% and 1% of the sample variance, respectively, and in total, they explain almost 99% of the total sample variance. There are at least three clusters on the PCA plot, and the most salient attribute differentiating the clusters is the screw speed at which the GSF BDSDs were

processed. This result, however, is in conflict with the VIP plot (Figure 5-11a), where screw speed is not one of the influential variables for describing the dissolution behavior of GSF from the BDSDs. This result thus reflects the presence of underlying interactions between the processing parameters. Figure 5-12b examines the relationship between the batches based on their X-ray diffraction pattern. The first two principal components explain approximately 86% of the total sample variance. Similar to Figure 5-5b, no obvious clusters can be observed, indicating that the diffraction patterns of the batches are very similar.

A model comprising processing temperature, residence time, screw speed, and the second-order interactions involving residence time, was used to describe the dissolution responses at both 1 and 120 min, as well as the crystallinity response. The model, validated by the respective predicted vs. observed plots, gives a high R^2 of > 0.99 for both dissolution responses, and 0.95 for the crystallinity response. The mean square error obtained for dissolution at 1 and 120 min, and crystallinity are 0.69, 3.14, and 0.20, respectively.

As shown in Figure 5-14, the prediction profiler visually confirms that the process variables have a stronger impact on the concentration of GSF at 1 and 120 min, than on the crystallinity of GSF. Interestingly, the prediction uncertainty (blue-shaded region) associated with the dissolution response at 120 min is considerably larger than that associated with the other two responses. This result suggests that most of the variability observed in the dissolution response at 120 min cannot be attributed to a single process variable, but rather the interaction between multiple process parameters.

Figure 5-15 shows the response surface plots for the dissolution and crystallinity responses, as a function of residence time and screw speed. The temperature is fixed at 40°C, because the dissolution responses appear to be maximized at this temperature, as shown on the prediction profile (Figure 5-14). The initial dissolution of GSF is insensitive to the changes in residence time, despite the relative importance shown in the VIP plot. This is so because the VIP plot evaluates the dissolution profiles in their entirety. At low screw speed (< 100 rpm), the release of GSF from BDSDs at 1 min is maximized. Likewise, the concentration of GSF at 120 min is relatively insensitive to the changes in residence time. However, it

appears that a moderate amount of mixing is required to achieve high supersaturation. Insufficient or excessive mixing reduces the efficiency of OS-DLB as a solubilizing carrier. As expected, the response surface plot for crystallinity (Figure 5-14) shows that the crystallinity of GSF in the BDSD is neither influenced by residence time nor screw speed.

Figure 5-16 overlays the contour plots from Figure 5-15 and a suggested HME design space for producing GSF BDSD. Unlike the HME design space for IBU BDSD, the design space for processing GSF shows that the quality attributes of GSF BDSD is relatively less sensitive to the processing variables. The mechanism of drug solubilization by OS-DLB is largely through the molecular association between the nonpolar solute molecules and the hydrophobic C_8 chains on the surface of OS-DLB. The hydrophobic microenvironment present in OS-DLB matches more closely to the hydrophobicity of IBU, relative to GSF, therefore the solubilizing effect of OS-DLB on IBU is greater than on GSF. Subsequently, changes in the polarity of the solvating environment of OS-DLB (e.g. PLX-mediated increase in hydrophilicity) has a greater impact on the solubilization capacity of OS-DLB for IBU than for GSF.

On the one hand, the response surface plots illustrate the importance of an intimate mixture in enhancing the efficiency of OS-DLB as a solubilizing carrier. On the other hand, intimate mixing promotes excessive molecular distribution of PLX, which in turn decreases the solubilization effect of OS-DLB on IBU. Therefore, the production of IBU BDSD involves a delicate balance of processing conditions. However, this is not the case for the production of GSF BDSD. In Chapter 3, it has been found that the presence of PLX accentuates the solubilizing effect of OS-DLB on GSF. This is primarily attributable to the improvement in the polarity match between the nonpolar microenvironment of OS-DLB and the drug molecule. In this case, as long as there is sufficient mixing to ensure a good distribution of PLX throughout the BDSD while maintaining the structural integrity of OS-DLB as a carrier matrix, enhanced dissolution of GSF from the BDSD will be achieved. In short, the dissolution enhancement of GSF based on the BDSD platform is primarily a reflection of the formulation rather than the extrusion process.

5.5 Conclusions

This study exemplifies the usefulness of a QbD / systematic approach in elucidating the interdependencies of the various complex formulation and processing factors that were previously unknown. Even though both IBU and GSF are poorly water-soluble drugs, the processing strategy to design a quality BDSD is rationally different in each case. IBU, whose solubility is primarily limited by its hydrophobic character, depends strongly upon the characteristics of OS-DLB as a solubilizing carrier. The processing of IBU BDSDs requires a delicate balance of processing variables to ensure intimate but not excessive mixing while maintaining the intrinsic properties of OS-DLB. GSF, which has a strong crystal lattice, is more sensitive to the formulation than to the processing conditions. Optimal GSF BDSD performance can be achieved through careful combination of additional functional excipients. As detailed in previous chapters, the processing aid was limited to PLX in this study for the sole reason that by itself, PLX does not act as solubilizer of the model APIs. Such restriction would not apply for QbD study of expanded scope, as would be the case in an industrial product development situation. However, the method and tools described in the development of the QbD study here are applicable to BSDS formulations in general, without limitation to any particular processing aid or excipient. This is advantageous because it allows greater flexibility for future process improvement as well as processing at multiple operational scales.

5.6 Acknowledgments

Financial support from the Dane O. Kildsig Center for Pharmaceutical Processing Research (CPPR), Purdue Research Foundation, and the National Science Foundation (NSF DMR 1310475) is gratefully acknowledged. We thank Prof. Yuan Yao's laboratory for providing the DLB material used in the study.

Table 5-1. List of currently marketed products utilizing HME technology.[1] Reproduced with permission from Springer Nature.

Trade Name	Product	Indication	Function of HME	Company
Lacrisert	Hydroxypropyl cellulose ophthalmic insert	Dry eye syndrome	Shaped system	Merck
Zoladex	Goserelin acetate injectable implant	Prostate cancer	Shaped system	AstraZeneca
Implanon	Etonogestrel implant	Contraceptive	Shaped system	Organon
Gris-PEG	Griseofulvin	Antifungal	Crystalline dispersion	Pedinol Pharmacal
NuvaRing	Etonogestrel, ethinyl estradiol depot system	Contraceptive	Shaped system	Merck
Norvir	Ritonavir	Antiviral (HIV)	Amorphous dispersion	Abbott Laboratorie
Kaletra	Ritonavir, lopinavir	Antiviral (HIV)	Amorphous dispersion	Abbott Laboratorie
Eucreas	Vildagliptin, metformin HCl	Diabetes	Melt granulation	Novartis
Zithromax	Azythromycin enteric-coated multiparticulates	Antibiotic	Taste masking	Pfizer
Orzurdex	Dexamethasone implantable device	Macular edema	Shaped system	Allergan
Fenoglide	Fenofibrate	Dyslipidemia	Amorphous dispersion	Life Cycle Pharma

Table 5-2. A three-factor three-level Box-Behnken design for evaluating the effects of processing temperature, residence time, and screw speed on the quality attributes of the BDSDs.

Run	Temperature (°C)	Time (min)	Speed (rpm)
1	50	30	90
2	30	30	90
3	50	10	90
4	30	10	90
5	50	20	135
6	30	20	135
7	50	20	45
8	30	20	45
9	40	30	135
10	40	10	135
11	40	30	45
12	40	10	45
13	40	20	90

Table 5-3. Composition of GSF and IBU BDSDs.

	Composition (% w/w)		
	API	OS-DLB	PLX
IBU	61.5	20.5	18.0
GSF	56.25	18.75	25.0

Table 5-4. Estimated percent crystallinity of IBU in the BDSDs relative to that in the PM.

Run	Crystallinity (%)
1	67.6
2	69.4
3	66.5
4	67.6
5	66.5
6	67.3
7	69.3
8	67.3
9	66.5
10	70.6
11	68.5
12	69.1
13	69.1

Table 5-5. Estimated percent crystallinity of GSF in the BDSDs relative to that in the PM.

Run	Crystallinity (%)
1	100
2	100
3	99.1
4	100
5	100
6	99.8
7	99.5
8	98.4
9	98.9
10	99.6
11	99.6
12	100
13	98.6

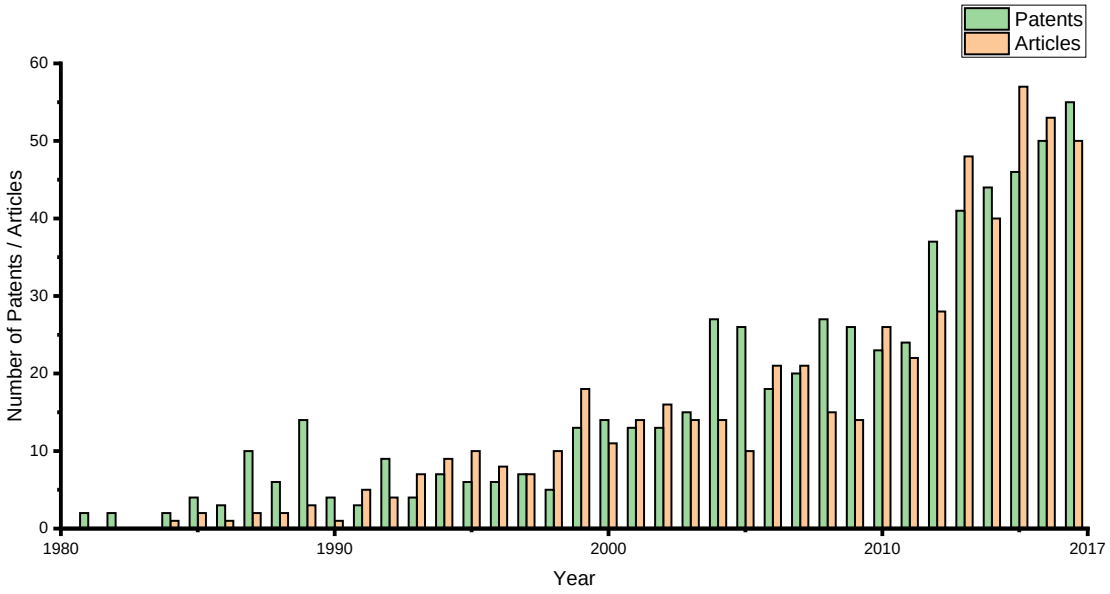

Figure 5-1. Number of patents issued and journal articles published for pharmaceutical applications of HME. *Web of Science*[*] was used to generate the citation counts.

[*] The following search query was used:
TS=((extru* AND extruder) AND (pharmaceutical OR drug))
Refined by: RESEARCH DOMAINS: (SCIENCE TECHNOLOGY) AND DOCUMENT TYPES: (ARTICLE OR PATENT)
Timespan: 1980-2017.
Search language=Auto

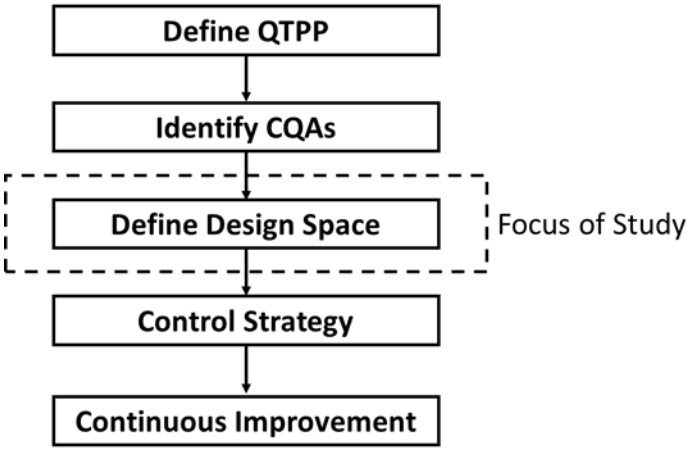

Figure 5-2. Key steps in a QbD approach to pharmaceutical product development.

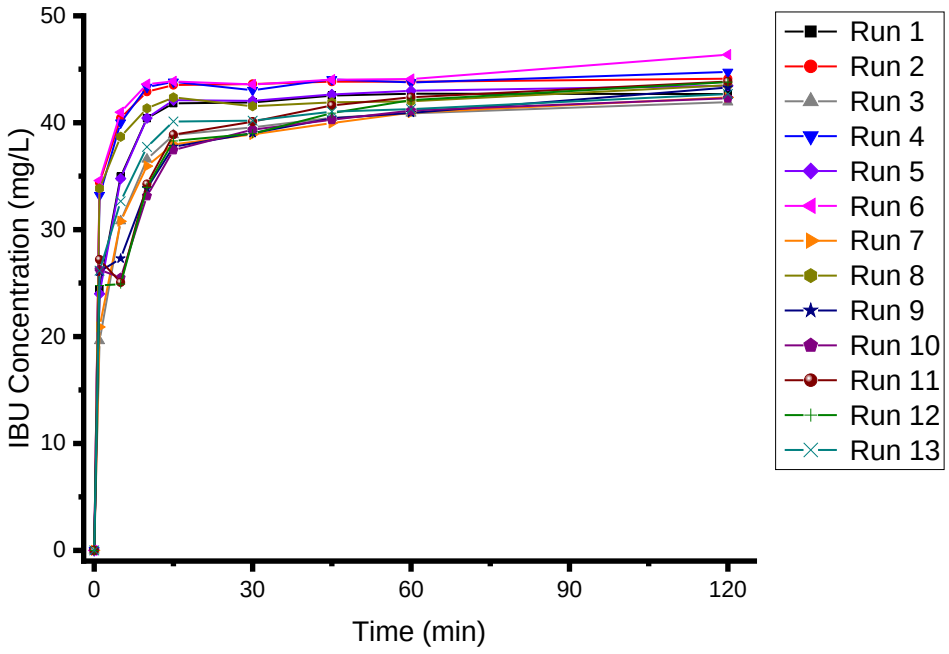

Figure 5-3. Time-concentration profiles of IBU from BDSDs.

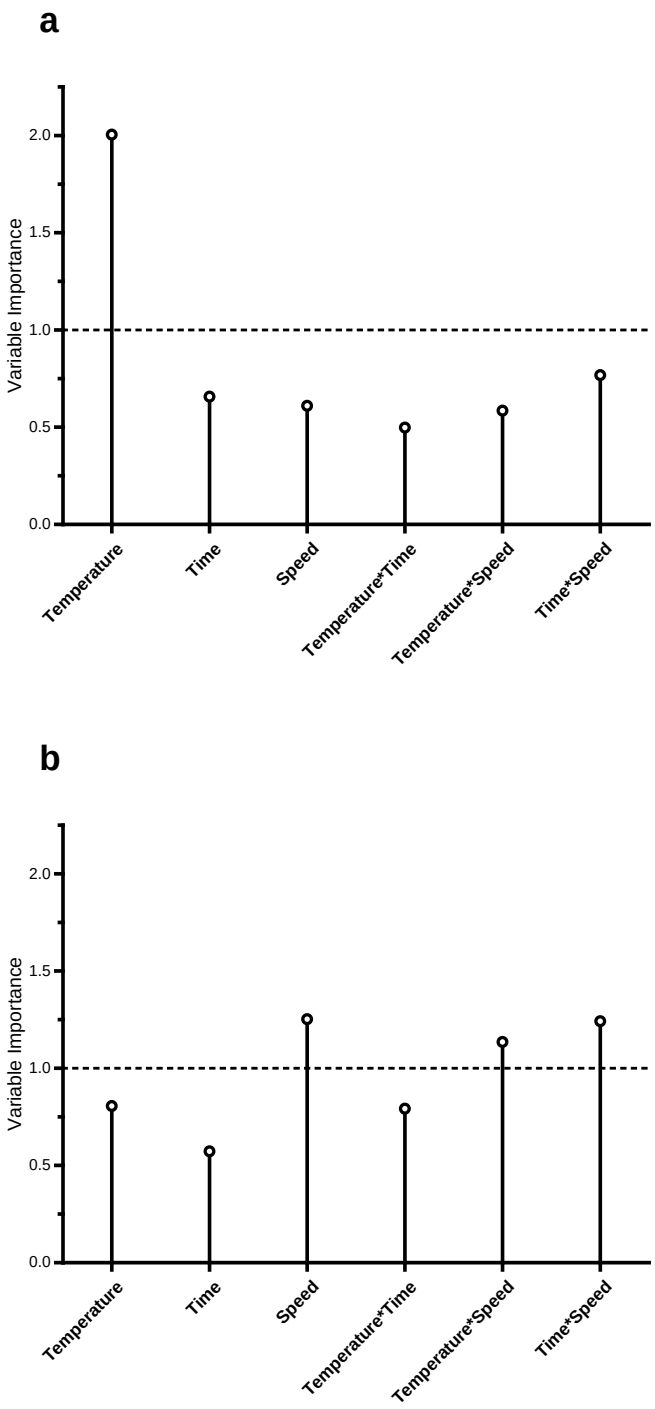

Figure 5-4. VIP plot for modeling (a) dissolution profile of IBU from and (b) crystallinity of IBU in BDSDs. Predictors with a VIP > 1 are considered influential variables in the model.[26]

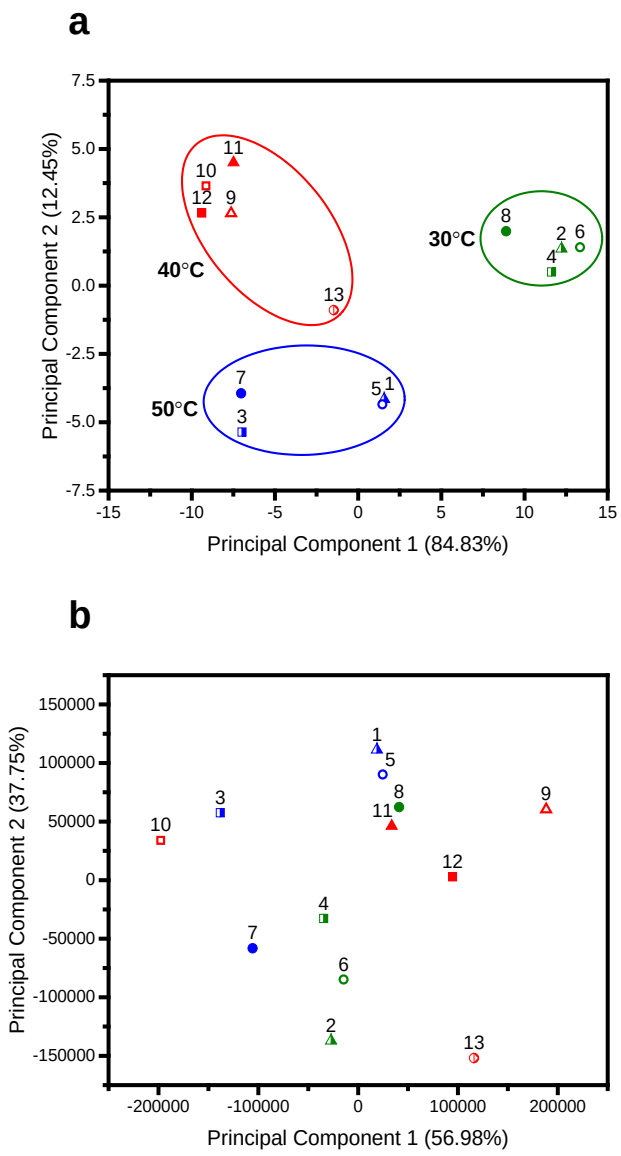

Figure 5-5. PCA scores plot of the first two principal components of the (a) dissolution profile and (b) X-ray diffraction pattern of 13 IBU BDSDs batches. Legend: Processing temperature: green – 30°C, red – 40°C, blue – 50°C. Residence time: square – 10 min, circle – 20 min, triangle – 30 min. Screw speed: full symbol – 45 rpm, half symbol – 90 rpm, open symbol – 135 rpm.

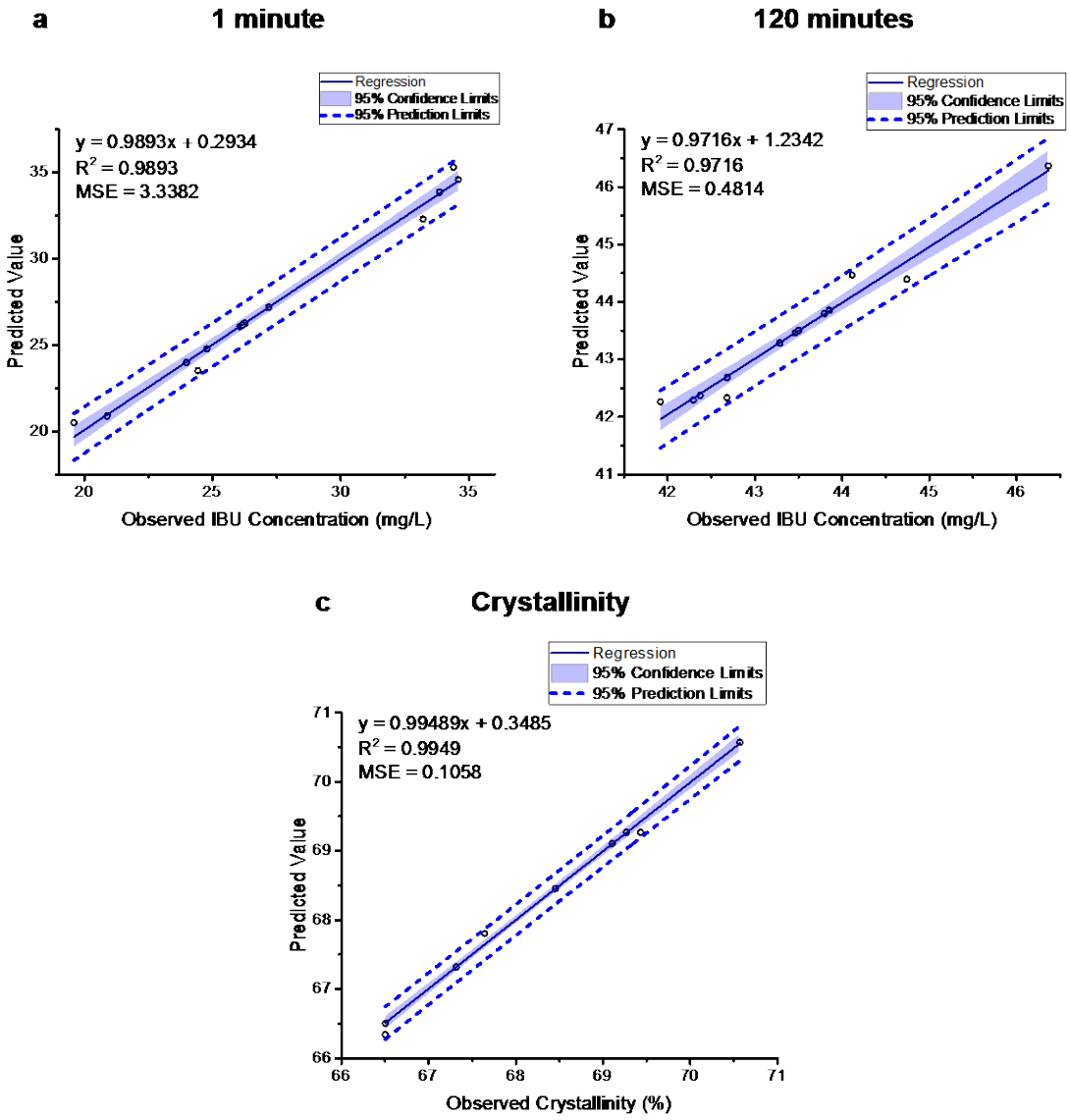

Figure 5-6. Predicted vs. observed plots for modeling dissolution of IBU from BDSDs at **(a)** 1 min, **(b)** 120 min, and **(c)** crystallinity of IBU in BDSDs. MSE: mean squared error.

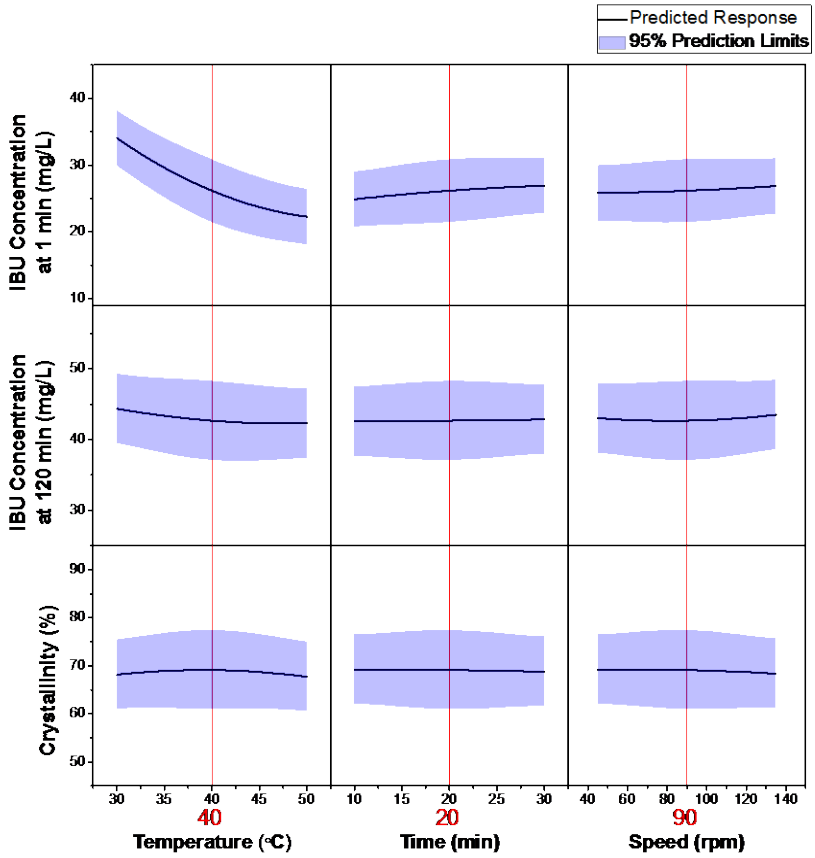

Figure 5-7. Prediction profiler for modeling the extrusion process. The outputs and 95% prediction intervals are shown for dissolution of IBU at 1 and 120 min, and crystallinity of IBU, as a function of processing temperature, residence time, and screw speed.

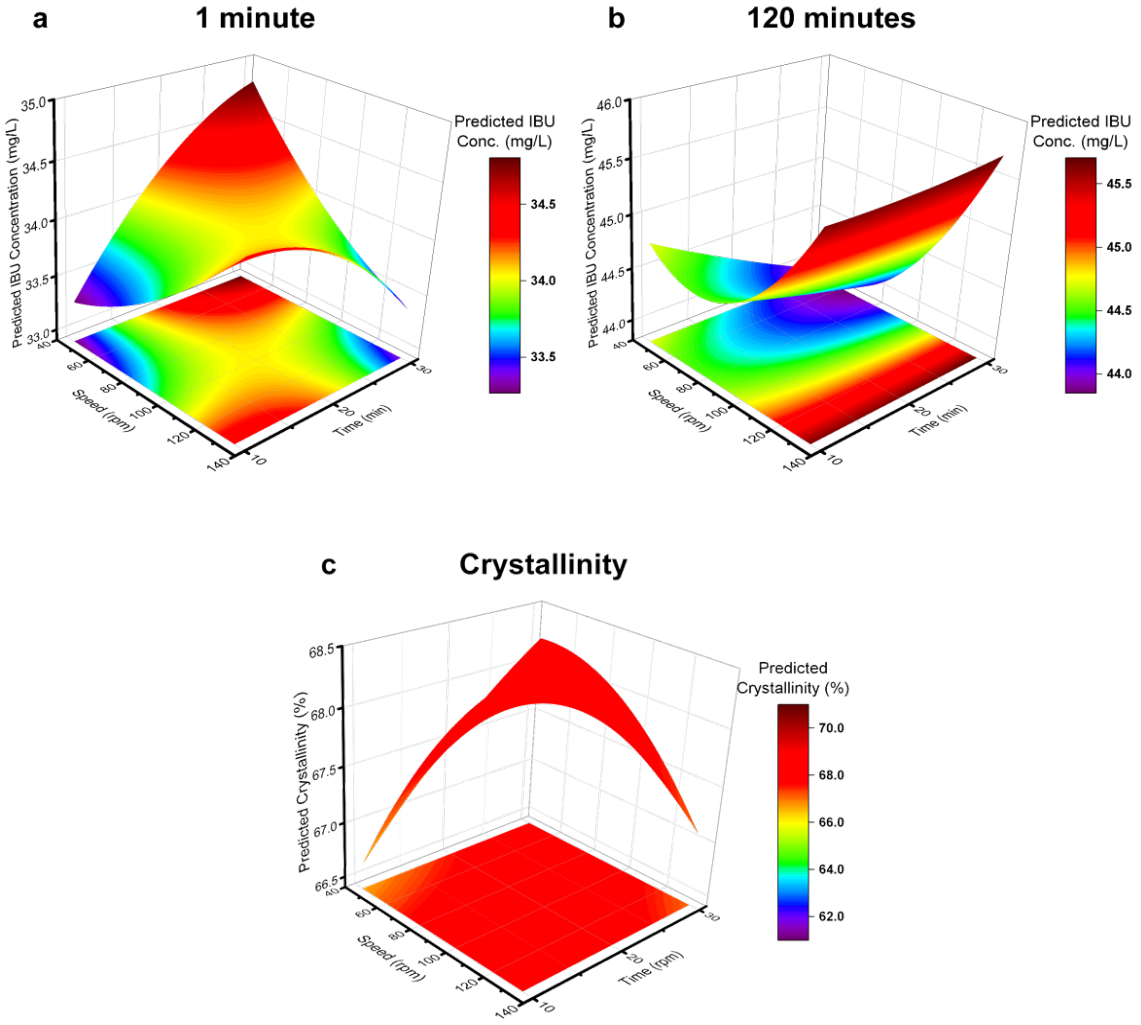

Figure 5-8. Response surface plots of dissolution of IBU from BDSDs at **(a)** 1 min, **(b)** 120 min, and **(c)** crystallinity of IBU in BDSDs. Temperature is fixed at 30°C.

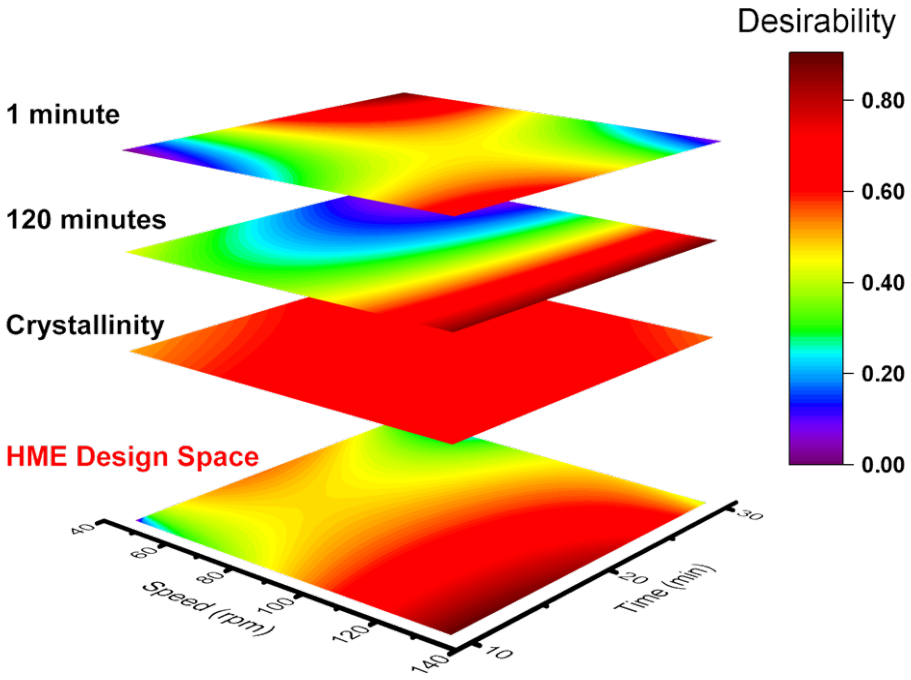

Figure 5-9. Contour plots from Figure 5-8 and a proposed HME design space for producing IBU BDSD. Temperature is fixed at 30°C.

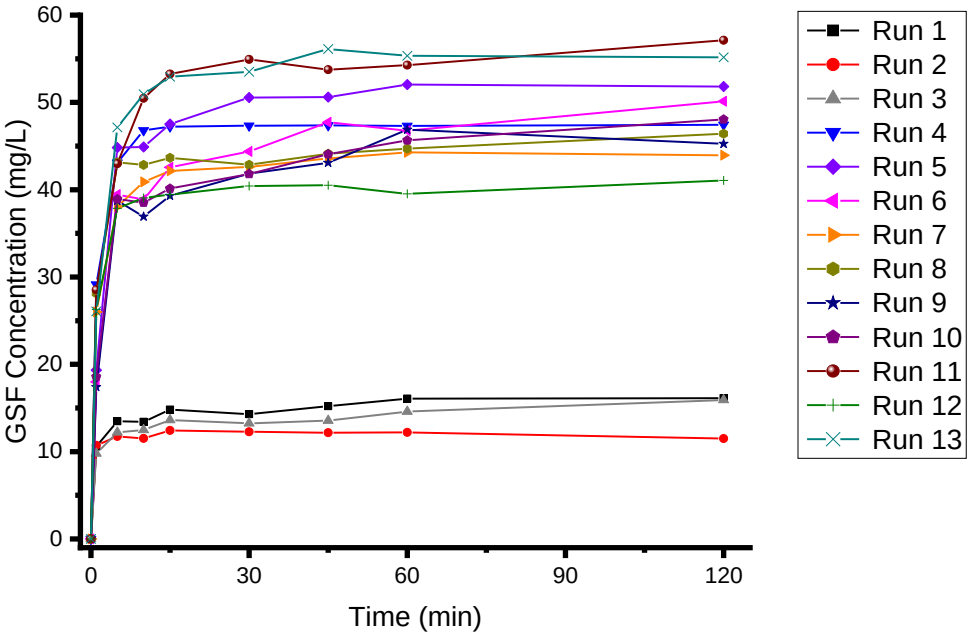

Figure 5-10. Time-concentration profiles of GSF from BDSDs

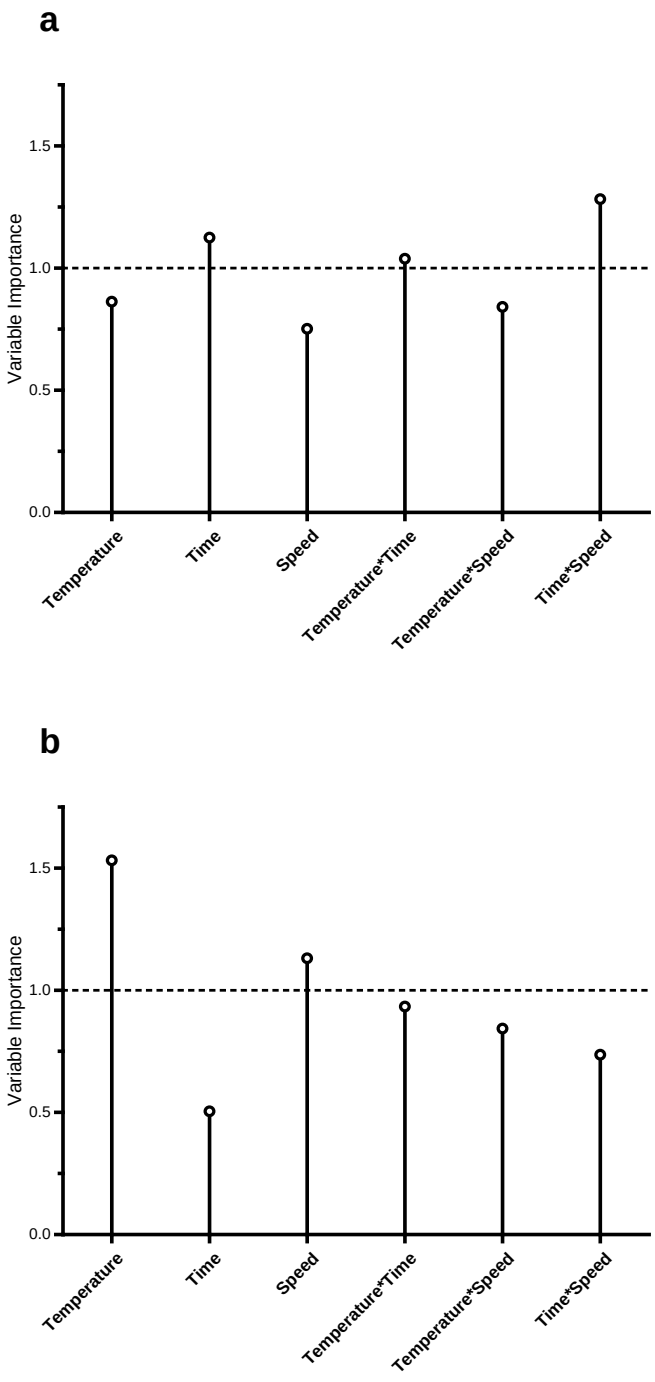

Figure 5-11. VIP plot for modeling (a) dissolution profile of GSF from and (b) crystallinity of GSF in BDSDs. Predictors with a VIP > 1 are considered influential variables in the model.[26]

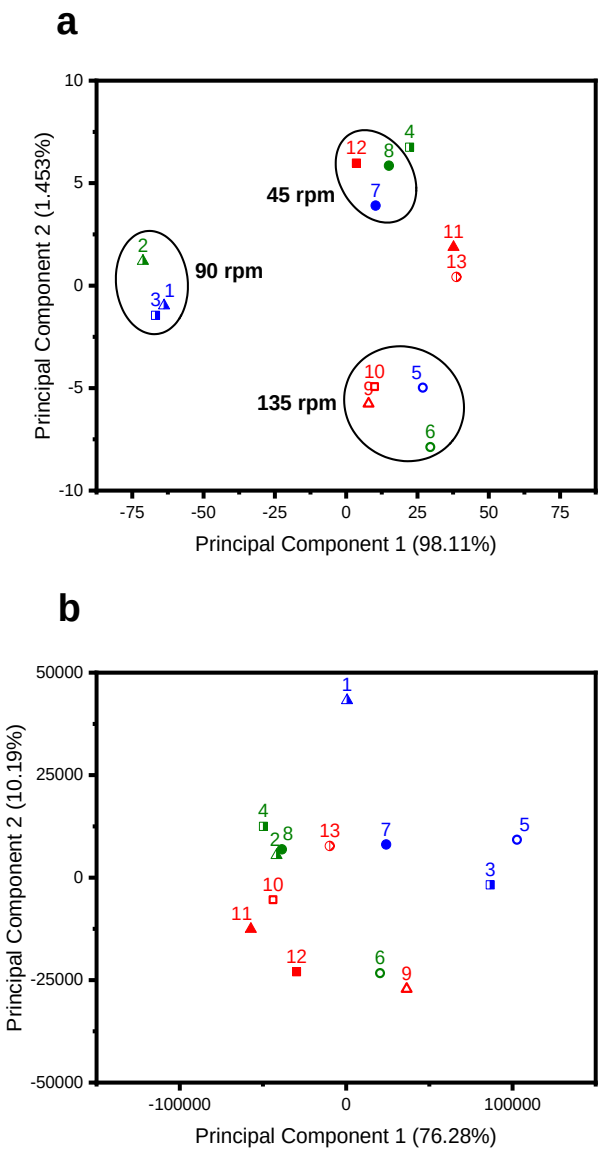

Figure 5-12. PCA scores plot of the first two principal components of the (a) dissolution profile and (b) X-ray diffraction pattern of 13 GSF BDSDs batches. Legend: Processing temperature: green – 30°C, red – 40°C, blue – 50°C. Residence time: square – 10 min, circle – 20 min, triangle – 30 min. Screw speed: full symbol – 45 rpm, half symbol – 90 rpm, open symbol – 135 rpm.

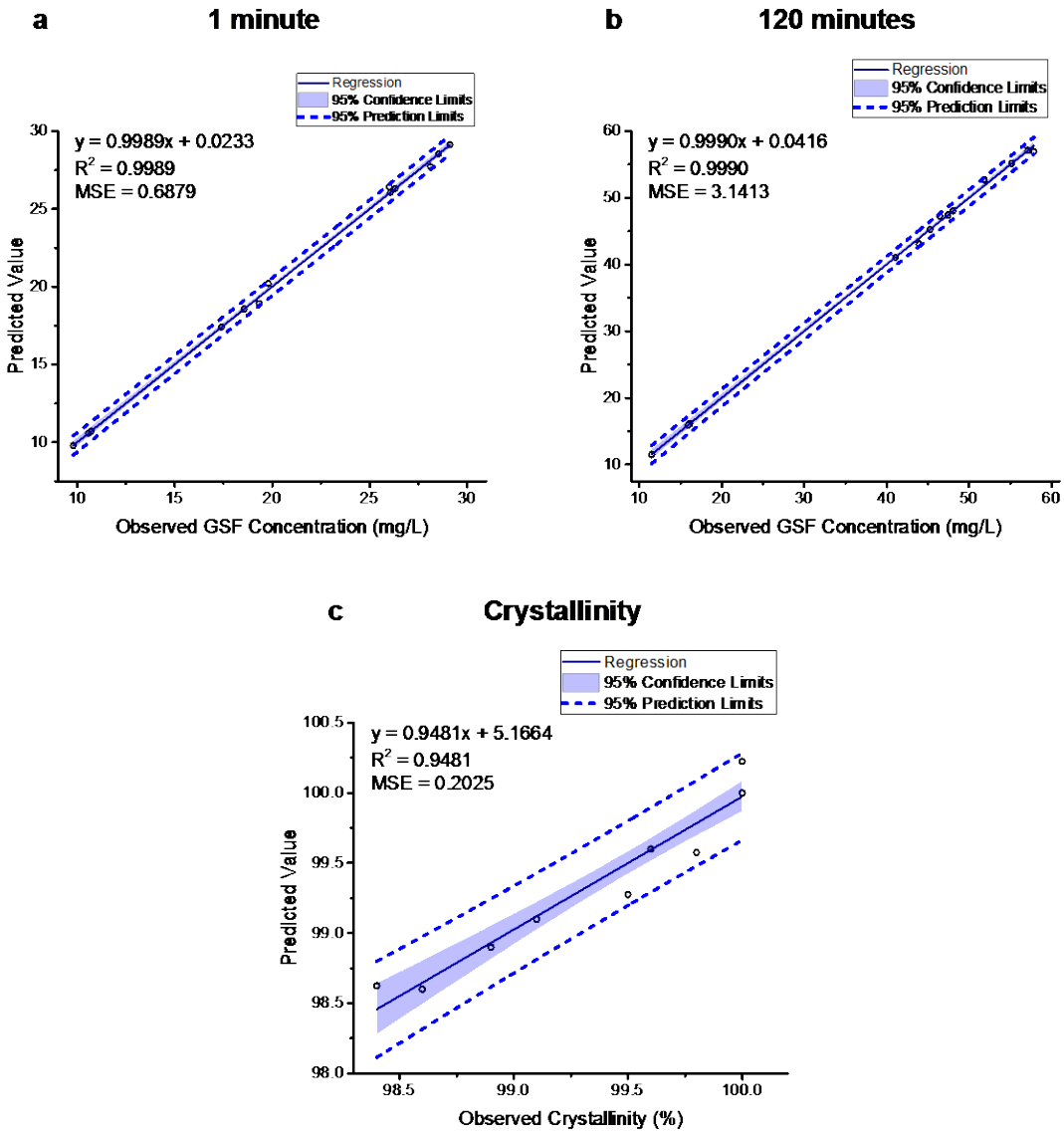

Figure 5-13. Predicted vs. observed plots for modeling dissolution of GSF from BDSDs at **(a)** 1 min, **(b)** 120 min, and **(c)** crystallinity of GSF in BDSDs.

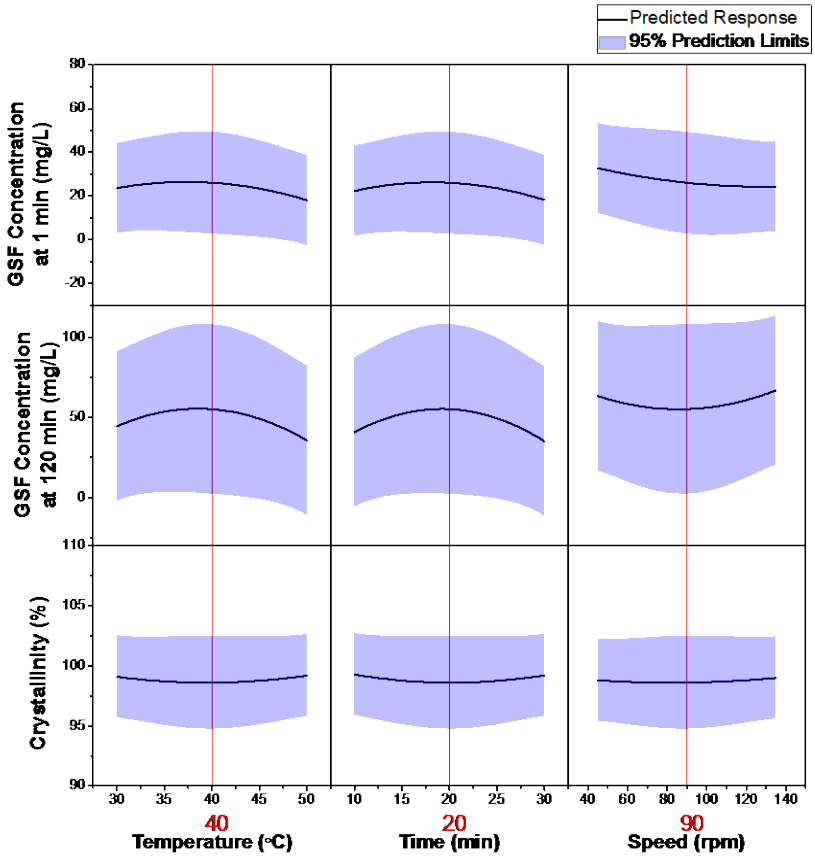

Figure 5-14. Prediction profiler for modeling the extrusion process. The outputs and 95% prediction intervals are shown for dissolution of GSF at 1 and 120 min, and crystallinity of GSF, as a function of processing temperature, residence time, and screw speed.

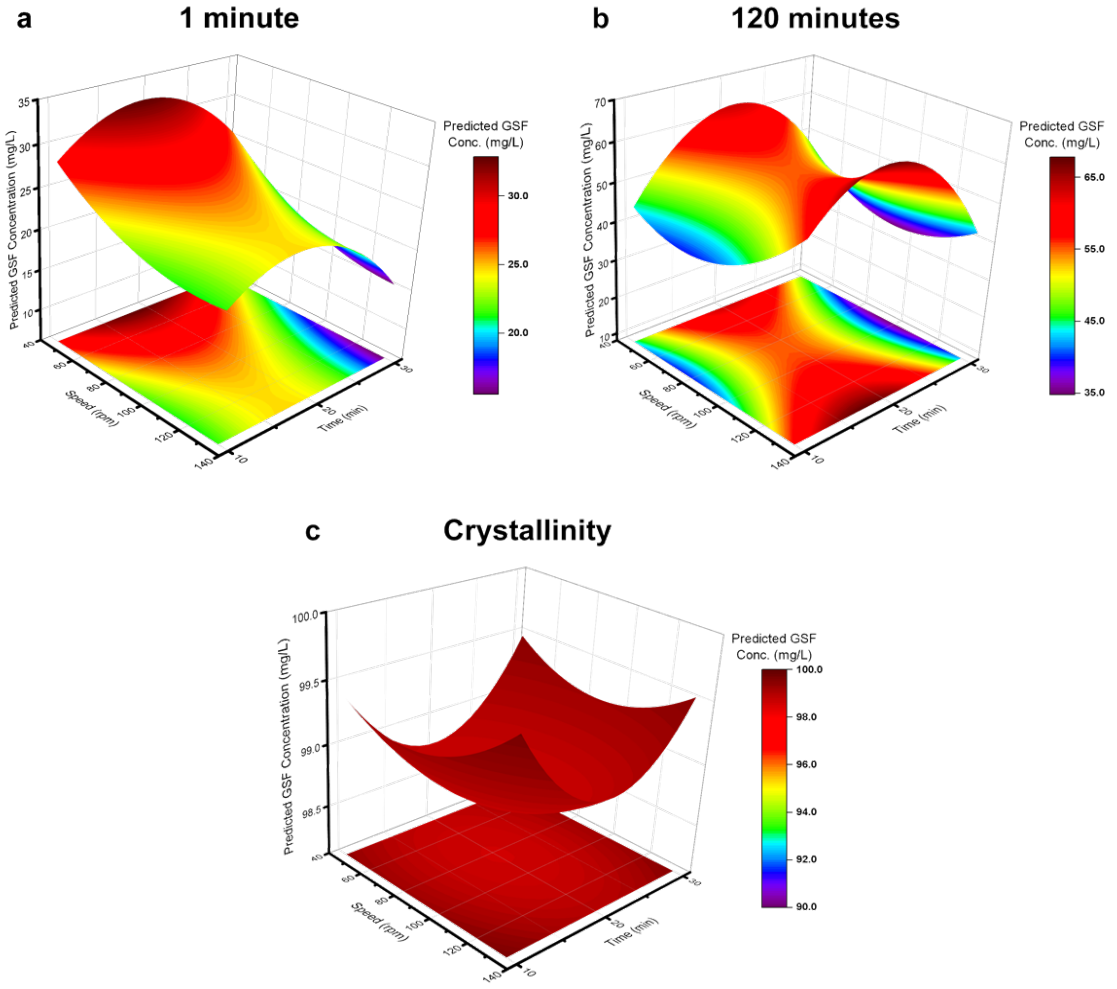

Figure 5-15. Response surface plots of dissolution of GSF from BDSDs at **(a)** 1 min, **(b)** 120 min, and **(c)** crystallinity of GSF in BDSDs. Temperature is fixed at 40°C.

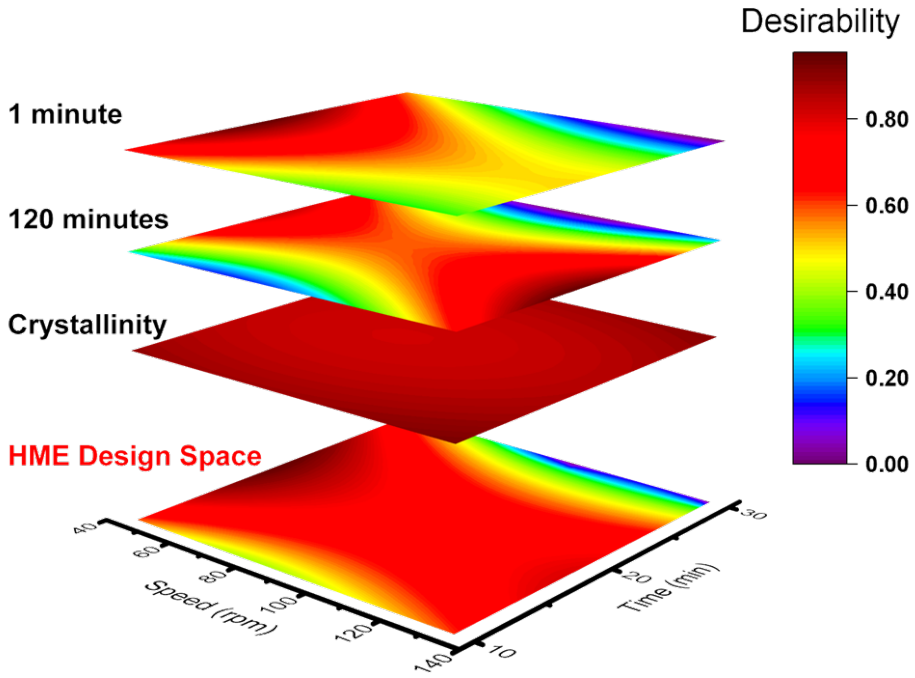

Figure 5-16. Contour plots from Figure 5-15 and a proposed HME design space for producing GSF BDSD. Temperature is fixed at 40°C.

5.7 References

1. S. Shah and M. A. Repka. Melt extrusion in drug delivery: Three decades of progress. In M. A. Repka, N. Langley, and J. DiNunzio (eds), *Melt extrusion: Materials, technology and drug product design* (M. A. Repka, N. Langley, and J. DiNunzio, eds), Springer New York, New York, NY, 2013, pp. 3-46.
2. J.-M. Bouvier and O. H. Campanella. *Extrusion processing technology: Food and non-food biomaterials*, John Wiley & Sons, 2014.
3. I. Ghebre-Sellassie. *Pharmaceutical extrusion technology*, M. Dekker, New York, 2003.
4. D. Daurio, K. Nagapudi, and F. Alvarez-Núñez. Manufacture of pharmaceutically relevant materials by mechanochemistry using twin screw extrusion. In A. M. Repka, N. Langley, and J. DiNunzio (eds), *Melt extrusion: Materials, technology and drug product design* (A. M. Repka, N. Langley, and J. DiNunzio, eds), Springer New York, New York, NY, 2013, pp. 223-242.
5. A. N. Ghebremeskel, C. Vemavarapu, and M. Lodaya. 2006. Use of surfactants as plasticizers in preparing solid dispersions of poorly soluble api: Stability testing of selected solid dispersions. *Pharmaceutical Research* **23**: 1928-1936.
6. A. L. Sarode, H. Sandhu, N. Shah, W. Malick, and H. Zia. 2013. Hot melt extrusion (hme) for amorphous solid dispersions: Predictive tools for processing and impact of drug–polymer interactions on supersaturation. *European Journal of Pharmaceutical Sciences* **48**: 371-384.
7. J.-Y. Lee, W.-S. Kang, J. Piao, I.-S. Yoon, D.-D. Kim, and H.-J. Cho. 2015. Soluplus(®)/tpgs-based solid dispersions prepared by hot-melt extrusion equipped with twin-screw systems for enhancing oral bioavailability of valsartan. *Drug Design, Development and Therapy* **9**: 2745-2756.
8. A. T. M. Serajuddin. 1999. Solid dispersion of poorly water-soluble drugs: Early promises, subsequent problems, and recent breakthroughs. *Journal of Pharmaceutical Sciences* **88**: 1058-1066.
9. M. Thommes, D. R. Ely, M. T. Carvajal, and R. Pinal. 2011. Improvement of the dissolution rate of poorly soluble drugs by solid crystal suspensions. *Molecular Pharmaceutics* **8**: 727-735.
10. K. Boksa, A. Otte, and R. Pinal. 2014. Matrix-assisted cocrystallization (mac) simultaneous production and formulation of pharmaceutical cocrystals by hot-melt extrusion. *Journal of Pharmaceutical Sciences* **103**: 2904-2910.
11. D. Daurio, C. Medina, R. Saw, K. Nagapudi, and F. Alvarez-Núñez. 2011. Application of twin screw extrusion in the manufacture of cocrystals, part i: Four case studies. *Pharmaceutics* **3**: 582.
12. S. Li, T. Yu, Y. Tian, C. P. McCoy, D. S. Jones, and G. P. Andrews. 2016. Mechanochemical synthesis of pharmaceutical cocrystal suspensions via hot melt extrusion: Feasibility studies and physicochemical characterization. *Molecular Pharmaceutics* **13**: 3054-3068.
13. ICH Q8(R2) harmonized tripartite guideline on pharmaceutical development, 2008.
14. ICH Q10 harmonized tripartite guideline on pharmaceutical quality system, 2008.

15. J. Thiry, P. Lebrun, C. Vinassa, M. Adam, L. Netchacovitch, E. Ziemons, P. Hubert, F. Krier, and B. Evrard. 2016. Continuous production of itraconazole-based solid dispersions by hot melt extrusion: Preformulation, optimization and design space determination. *International Journal of Pharmaceutics* **515**: 114-124.
16. H. G. Claycamp, R. Kona, R. Fahmy, and S. W. Hoag. 2016. Quality-by-design ii: Application of quantitative risk analysis to the formulation of ciprofloxacin tablets. *AAPS PharmSciTech* **17**: 233-244.
17. A. Eitzlmayr, G. Koscher, G. Reynolds, Z. Huang, J. Booth, P. Shering, and J. Khinast. 2014. Mechanistic modeling of modular co-rotating twin-screw extruders. *International Journal of Pharmaceutics* **474**: 157-176.
18. A. Eitzlmayr, J. Khinast, G. Hörl, G. Koscher, G. Reynolds, Z. Huang, J. Booth, and P. Shering. 2013. Experimental characterization and modeling of twin-screw extruder elements for pharmaceutical hot melt extrusion. *AIChE Journal* **59**: 4440-4450.
19. S. L. Scheffler, L. Huang, L. Bi, and Y. Yao. 2010. In vitro digestibility and emulsification properties of phytoglycogen octenyl succinate. *Journal of Agricultural and Food Chemistry* **58**: 5140-5146.
20. M. Cavazzuti. Design of experiments, *Optimization methods: From theory to design scientific and technological aspects in mechanics*, Springer Berlin Heidelberg, Berlin, Heidelberg, 2013, pp. 13-42.
21. D. C. Montgomery. *Design and analysis of experiments*, John wiley & sons, 2017.
22. M. H. Kutner. *Applied linear statistical models*, McGraw-Hill Irwin, 2005.
23. N. V. Y. Scarlett and I. C. Madsen. 2006. Quantification of phases with partial or no known crystal structures. *Powder diffraction* **21**: 278-284.
24. T. Degen, M. Sadki, E. Bron, U. König, and G. Nénert. 2014. The highscore suite. *Powder Diffraction* **29**: S13-S18.
25. S. Wold, M. Sjöström, and L. Eriksson. 2001. Pls-regression: A basic tool of chemometrics. *Chemometrics and Intelligent Laboratory Systems* **58**: 109-130.
26. L. Eriksson, T. Byrne, E. Johansson, J. Trygg, and C. Vikström. *Multi-and megavariate data analysis basic principles and applications*, Umetrics Academy, 2013.
27. R. A. Johnson. *Applied multivariate statistical analysis*, Englewood Cliffs, N.J. : Prentice-Hall, Englewood Cliffs, N.J., 1988.
28. J. T. Rubino. Cosolvents and cosolvency, *Encyclopedia of pharmaceutical technology*, Vol. 3, Marcel Dekker, New York, NY, 1988, pp. 375-398.
29. Y. Miyako, H. Tai, K. Ikeda, R. Kume, and R. Pinal. 2008. Solubility screening on a series of structurally related compounds: Cosolvent-induced changes on the activity coefficient of hydrophobic solutes. *Drug Development and Industrial Pharmacy* **34**: 499-505.
30. J. A. Newman, P. D. Schmitt, S. J. Toth, F. Deng, S. Zhang, and G. J. Simpson. 2015. Parts per million powder x-ray diffraction. *Analytical chemistry* **87**: 10950-10955.
31. C. Nunes, A. Mahendrasingam, and R. Suryanarayanan. 2005. Quantification of crystallinity in substantially amorphous materials by synchrotron x-ray powder diffractometry. *Pharmaceutical Research* **22**: 1942-1953.

32. A. Saleki-Gerhardt, C. Ahlneck, and G. Zografi. 1994. Assessment of disorder in crystalline solids. *International Journal of Pharmaceutics* **101**: 237-247.
33. G. Derringer and R. Suich. 1980. Simultaneous optimization of several response variables. *Journal of Quality Technology* **12**: 214-219.

CHAPTER 6. FUTURE DIRECTION AND CONCLUDING REMARKS

In the preceding chapters, it has been demonstrated that the use of an octenylsuccinate (OS)-modified dendrimer-like biopolymer (DLB) as a solubilizing carrier, enabled by hot melt extrusion (HME), can enhance the apparent solubility and dissolution rate of poorly water-soluble drugs, while retaining a predominantly crystalline state of the drug. This non-amorphous, biodendrimeric solid dispersion (BDSD) platform is expected to have applications with a large number of poorly soluble drugs, offering a new, complementary approach to existing processing and drug solubilization methods. The primary objective of this chapter is to describe some of the future studies that would help provide an improved understanding of the underlying solubilization mechanisms of OS-DLB and the BDSD platform. Formulation strategies that would enhance the solubilization of poorly soluble drugs by DLB will be proposed. In addition, the potential applications of DLB, the BDSD platform, and HME will be discussed in the context of formulating poorly soluble drugs.

6.1 Future Studies

6.1.1 Development of DLB

The importance of polarity match between the hydrophobic solute and the nonpolar microenvironment of OS-DLB has been demonstrated in Chapters 3 and 4. It was found that the more hydrophobic the solute, the greater the solubilizing effect of OS-DLB. The polarity of a solute can be modified by means of chemical modification. However, this is often accompanied by a concomitant change in the physicochemical properties and/or therapeutic effects of the drug. Alternatively, the polarity of the microenvironment of DLB can be modified in the same manner surfactants and complexing ligands are typically modified to enhance their solubilization capacity for nonpolar solutes. In the present research, the OS moiety comprising of an 8-carbon chain was used to create a nonpolar microenvironment encompassing the naturally hydrophilic DLB. The polarity of the microenvironment can be altered by changing the length of the aliphatic hydrocarbon

chain. As a rule-of-thumb, the longer the aliphatic hydrocarbon chain, the lower the polarity of the microenvironment. The volume of the nonpolar region encompassing DLB and consequently its solubilization capacity toward highly hydrophobic drugs, are also expected to increase as the length of the hydrocarbon chain increases. However, the use of long alkyl chains risks reducing the aqueous solubility of DLB. Elworthy and Patel[1] have shown that the solubilization ability of surfactants with alkyl chains more than 16 carbons decreased due to their lower solubility in water. Several studies[2, 3] have demonstrated that the polarity of the hydrocarbon chain can be increased by incorporating a double bond, an ether group, a hydroxy group, or a carbonyl group into the hydrocarbon chain of a surfactant. One important consideration is that the OS chemistry has been designated as generally recognized as safe (GRAS) by the FDA. Therefore, while modifications to the aliphatic chain may have improved physicochemical properties, they will come with a heavy cost in terms of regulatory approval for use as part of a pharmaceutical excipient. In Chapter 3, it was shown that even though PLX is not a solubilizer of the model drugs used, it can actually modify the microenvironment created by the OS groups, with measurable effects on the solubilizing ability of OS-DLB. Based on the two above considerations, a more sensible approach would be to explore already approved excipients, other than PLX, as modifiers of the OS microenvironment, in order to further understand and explore the solubilizing ability of OS-DLB. Jansook and Loftsson[4] have shown that common pharmaceutical excipients, such as edetate disodium, benzalkonium chloride, and hydroxypropylmethylcellulose, can influence the affinity of cyclodextrins for various poorly water-soluble drugs by modifying the polarity of cyclodextrin cavity. This demonstrates that common pharmaceutical excipients can also have significant effect on the polarity of the microenvironment of cyclodextrin, and consequently its solubilization power for poorly soluble drugs.

The degree of solubility enhancement of the hydrophobic solute by OS-DLB depends on the extent of deviation from ideal mixing. Unlike cosolvents whose polarity can be quantified easily in terms of surface tension, solubility parameter, dielectric constant and octanol-water partition coefficient, the quantification of the polarity of the microenvironment encompassing DLB is less straightforward. The hydrophobicity of the

solutes can be easily determined from their thermal properties and through solubility measurements. In order to establish the closest matches between the solute and the microenvironment of DLB, i.e. maximum solubilization effect of DLB, a solubility screening study involving a group of DLB with different chemical surface modifications and a multitude of poorly soluble model compounds covering a range of hydrophobicity can be conducted. A separate solubility screening study that includes common pharmaceutical excipients, such as salts, preservatives, hydrophilic polymers, etc., can also be performed to fully understand the influence of these excipients on the solubilization of drugs by DLB. From a "developability" point of view, such solubilization screening studies will facilitate future drug development efforts. Formulation scientists are able to establish early in the process the best-suited chemical functionalization of DLB for a new chemical entity of known hydrophobicity.

On a related note, OS-modified starches have been widely used as food additives for more than half a century.[5] The synthesis and chemical functionalization procedures, structural characterization methods, and physicochemical properties of OS-modified starches are well-studied and well-established. OS-modified starches are potential alternatives to surfactants; not only do they display excellent surface-active properties, they also lack the bitter taste characteristic of many common oral surfactants.[6] The question arises as to whether commercially available OS-modified starches are capable of achieving a similar solubilizing effect as those displayed by OS-DLB. The short answer is no. Phase solubility measurements of ibuprofen with two commercially available OS-modified starches – Cleargum® CO 01 (Roquette, France) and Capsul® (Ingredion, Westchester, IL) – were conducted according to methods described in Chapters 2 and 3. The average particle size of Cleargum and Capsul are 38.7 ± 0.9 μm and 14.9 ± 0.6 μm, respectively. The results in Figure 6-1 show that the solubilizing effect of these commercial starches is almost negligible. There are two possibilities. First, the colloidal particles of these starches are likely to be separated from the aqueous solution when filtered through a 0.45 μm membrane. Consequently, the solubilizing effect of these commercial starches, even if substantial, would not be measurable. In comparison, the colloidal dispersions of OS-DLB, whose average particle size is 63.5 ± 0.7 nm, behave like "solutions", hence the colloidal particles

can filter through the membrane filters. In turn, the solubilizing effect of OS-DLB is quantifiable. Second, the degree of OS substitution of commercially available starches is likely insufficient to generate a substantial solubilization effect on poorly soluble drugs. In the United States, the maximum allowable OS treatment on starch utilized as food additive is 3%, which in theory, is equivalent to a degree of substitution of 0.02.[7] This suggests that commercial OS-modified starches for food applications are still too hydrophilic in nature despite the OS modification. In comparison, the degree of OS substitution in OS-DLB is approximately 0.51,[8] giving it a substantially more (favorable) hydrophobic character. Nevertheless, in view of the existing technical and economic advantages (relative to OS-DLB), commercial OS-modified starches still hold considerable potential for further study and development as a solubilizing agents.

6.1.2 Development of BDSD

It has been demonstrated in Chapters 2 and 5 that HME-processed BDSDs are capable of producing high and long-lasting supersaturation, in relation to their corresponding physical mixtures. There is no doubt that the solubilizing effect of OS-DLB is a solution-phase phenomenon. However, it is also evident that the HME process has a pronounced effect on the dissolution profiles of BDSDs. Therefore, knowledge of the interaction between the components in BDSDs (i.e., drug, OS-DLB and processing aid) during the dissolution process may be an essential piece of information for elucidating the impact of the HME process. This can be achieved through measuring the energetics associated with the dissolution of BDSDs and their corresponding physical mixtures by solution calorimetry. Solution calorimetry is often viewed as a method of choice for elucidating liquid-liquid and solid-liquid interactions.[9, 10] The working hypothesis is that differences in (a) physical arrangements of the components, (b) energy states of the components, (c) interactions between the components themselves, and (d) interactions between the components and water will manifest themselves in the heats of solution. In a study by Craig and Newton[11], solid dispersions of nortriptyline hydrochloride were prepared either by flash-cooling in liquid nitrogen or by slow-cooling at 5°C/h. In both processes, the original crystalline phase of the drug was maintained. Unlike differential scanning calorimetry, solution calorimetry

was capable of discriminating between the solid dispersions prepared by different processes.

In the present research, the BDSDs were prepared at processing temperatures well below the melting temperature of the APIs. Consequently, the original crystalline phase of the API in the BDSD was mostly preserved during the extrusion process. Therefore, by virtue of being non-amorphous, BDSDs are thermodynamically stable. On the other hand, the DLB material – phytoglycogen – used in the present research is a naturally occurring, dendrimeric-like polysaccharide that has a strong tendency to incorporate water molecules into its highly-branched network. Nickels et al.[12] found that phytoglycogen nanoparticles are highly hydrated and that each phytoglycogen nanoparticle contains between 250% and 285% of its weight in water. The high water retention capacity of phytoglycogen could potentially compromise the quality of BDSD, specifically, in terms of reproducibility. Clearly, the long-term physical and chemical stability of BDSDs is a knowledge gap that should be addressed in future studies.

6.2 Applications

6.2.1 Potential applications of DLB

DLB has several unique and advantageous properties, such as high water retention, low viscosity, and exceptional stability in water[12], which makes this biopolymer a promising excipient in semisolid dosage forms, such as creams, ointments, and gels. DLB can function as (a) a drug carrier as demonstrated in the present research, (b) an emulsifier when the DLB material is derivatized with nonpolar moieties such as octenylsuccinate, and (c) an absorbent given its high absorbency of water.

DLB is also a promising solubilizing agent and drug carrier, worth exploring for injectable formulations. Conventional strategies for solubilizing poorly soluble drugs intended for parenteral use include pH adjustment, cosolvency, micellization and complexation. While these strategies have been proven effective, they are not without limitations. For example,

formulations should ideally be developed as close as possible to the physiological pH (~ 7.4) to avoid discomfort and irritation at the injection site. Cosolvents are typically used in high concentrations as solubilizing agents, hence they may pose undesirable or even adverse pharmacological effects. Surfactants, especially ionic surfactants can cause hemolysis of red blood cells and the destruction of T lymphocyte cells.[13] Similarly, parenteral administration of cyclodextrins can cause hemolysis of red blood cells and cell alteration. In comparison, DLB is non-toxic (edible) and biocompatible. Furthermore, it possesses many geometric characteristics favorable to nanotherapeutic applications, such as nano-sized (30-100 nm), roughly spherical, and monodisperse.[14] The nanosize of DLB can potentially promote passive tumor targeting due to enhanced permeability and retention (EPR) effect of the tumor vasculature.[15] However, a major disadvantage of using DLB as a drug carrier is that it is a natural material and this may lead to inconsistent final product attributes.

6.2.2 Potential applications of BDSD

In the present research, poloxamer was incorporated into the BDSD formulation to enable the processability under extrusion. The choice of processing aid was limited to one that does not act as a solubilizer, in order to minimize any confounding effect on the solubilizing properties of DLB. Poloxamer was selected precisely because it was found to have no appreciable solubilizing effect on any of the model drugs evaluated in the present research. However, the role of the processing aid / polymer matrix can be expanded to impart additional functionality into BDSD, such as taste masking, moisture barrier protection, abuse resistance and tailored drug release kinetics. The ability to precisely control the drug release kinetics of BDSDs through the selection of polymer matrix is perhaps most pertinent to the present research. In the current BDSD formulation, an initial burst release of the poorly soluble drug was observed. The incorporation of a polymer matrix suitable for sustained release would allow the formulation to slowly release drug particles and DLB, which then undergo rapid dissolution once water comes into contact. Polyethylene oxide (PEO), by virtue of its thermoplastic characteristics, is a potential polymer matrix for such application. Despite its high molecular weight, PEO has a melting temperature around

65°C. This is advantageous because HME processing can be conducted at relatively low temperatures. High molecular weight PEO can be used to achieve sustained release of the drug and DLB nanoparticles, while low molecular weight PEO can be incorporated into the formulation as a plasticizer for the higher molecular weight PEO.[16] From a practical point of view, the use of low molecular weight PEO as a plasticizer for higher molecular weight PEO is advantageous because it minimizes potential excipient-excipient or even drug-excipient compatibility issues.

6.2.3 Potential applications of HME

HME has been demonstrated as a feasible route for screening and manufacturing of pharmaceutical relevant materials, such as cocrystals[17] and salts[18], by means of mechanochemistry. HME provides highly efficient and intensive mixing of solids, which in turn leads to intimate surface contact and packing between components, thereby facilitating compound formation with little or no solvent being required. By exploiting this unique and advantageous feature of HME, it is possible that DLBs with different surface polarity can be generated easily in relation to chemical functionalization. It has been demonstrated in Chapter 5 that HME was capable of increasing the polarity of the microenvironment of OS-DLB by means of dispersing poloxamer throughout the extrudate, and that the extent of increase was influenced by the processing parameters. Taking this notion one step further, HME is well suited for customizing the polarity of existing polymers according to one's needs without laborious chemical reactions. Unlike conventional polymer processing which involves the melting and mixing of polymeric mixtures to form structurally different polymers or polymer blends, the HME approach does not involve the disruption or destruction of the parent polymer. On the one hand, the intrinsic (and desirable) properties of the parent polymer are maintained and, on the other hand, the polarity of the polymer can be tailored to match the hydrophobicity of the solute. While covalent functionalization is the most reliable approach in ensuring permanent modification of the polymer, it is not always feasible due to the absence of specific functional groups in the polymer. Conversely, the modification of the surface properties of a polymer simply through intimate contact between the polymer and functional moieties of

interest eliminates the need for chemical recognition and specificity between the components. This approach is expected to be applicable to a wide range of formulations of poorly water-soluble drugs.

A key aspect of HME is that the product can be easily configured into different shapes and sizes depending on the desired final application. HME has long been the process of choice for preparing thermoplastic medical devices and implants, however, the use of HME to manufacture shaped oral dosage forms is relatively new. A potential application of HME in this arena is the multiparticulate drug delivery system. The extrudate can be shaped into multiple, small discrete units, such as pellets, beads, and granules, which can be administered by themselves (e.g. “sprinkles”) or further processed to produce other solid dosage forms (e.g. capsules). Multiparticulate drug delivery systems offer the advantage of ease of administration to pediatric and geriatric patients with dysphagia, for example. Furthermore, multiparticulate systems lend themselves to dosing flexibility, a cornerstone of patient-centric medications. Combination therapies comprising two or more drugs, can also be easily prepared from multiparticulate systems. Moreover, they are suitable for the simultaneous delivery of incompatible drugs, and for administering drugs at different release rates.

6.3 Concluding Remarks

The present research tackles an old problem that will persist for years to come. The use of OS-DLB as a solubilizing carrier, enabled by HME, offers a viable, complementary approach for enhancing the apparent solubility and dissolution rate of poorly water-soluble drugs, while retaining a predominantly crystalline state of the API. It is evident that DLB has wide applicability in pharmaceutical formulation development. From solid to liquid dosage forms, DLB offers formulation scientists a novel and inexpensive solution for solubilizing poorly soluble drugs. Additionally, HME represents a promising processing technology for preparing enabled formulations. In addition to amorphous solid dispersions, it is apparent that HME offers a broad range of (still unexplored) pharmaceutical application capabilities. As more research is devoted to understanding the underlying

solubilization mechanisms of DLB and HME-enabled formulations, the efficiency and effectiveness of DLB as a solubilizing agent and HME as an enabling technology will continue to improve.

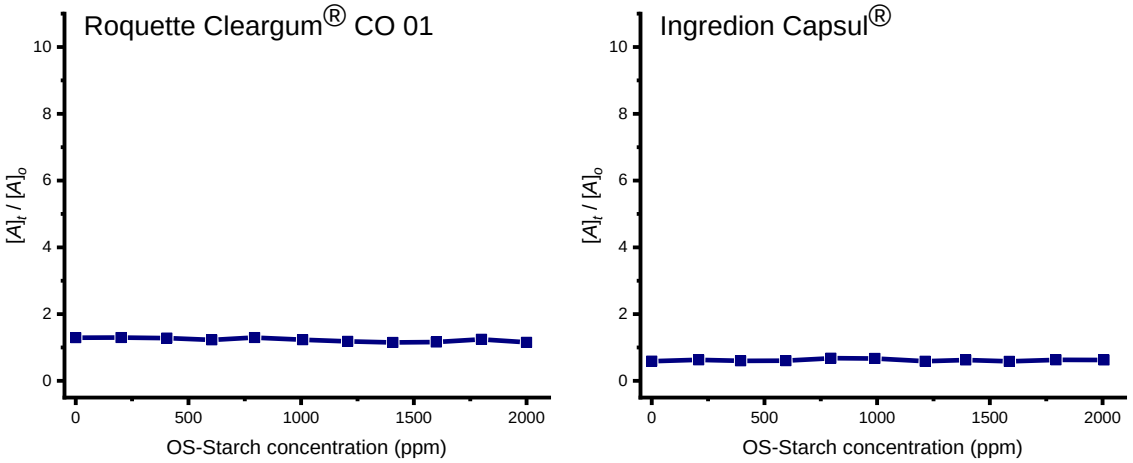

Figure 6-1. Solubility enhancement of ibuprofen in aqueous solutions of commercially available OS-modified starches at 25°C ± 0.5°C. S and S_o represent the equilibrium solubility of ibuprofen in the presence of starch in solution and the solubility in plain water, respectively.

6.4 References

1. P. H. Elworthy and M. S. Patel. 1982. Demonstration of maximum solubilization in a polyoxyethylene alkyl ether series of non-ionic surfactants. *Journal of Pharmacy and Pharmacology* **34**: 543-546.
2. D. Attwood, P. H. Elworthy, and M. J. Lawrence. 1989. Effect of structural variations of non-ionic surfactants on micellar properties and solubilization: Surfactants with semi-polar hydrophobes. *Journal of Pharmacy and Pharmacology* **41**: 585-589.
3. M. J. Lawrence, P. H. Elworthy, and D. Attwood. 1985. The effect of modification on solubilisation and micellar properties of a non-ionic surfactant. *Journal of Pharmacy and Pharmacology* **37**: 2P-2P.
4. P. Jansook and T. Loftsson. 2009. Cds as solubilizers: Effects of excipients and competing drugs. *International Journal of Pharmaceutics* **379**: 32-40.
5. M. C. Sweedman, M. J. Tizzotti, C. Schäfer, and R. G. Gilbert. 2013. Structure and physicochemical properties of octenyl succinic anhydride modified starches: A review. *Carbohydrate Polymers* **92**: 905-920.
6. M. Kuentz, P. Egloff, and D. Röthlisberger. 2006. A technical feasibility study of surfactant-free drug suspensions using octenyl succinate-modified starches. *European Journal of Pharmaceutics and Biopharmaceutics* **63**: 37-43.
7. J. Z. Li. Chapter 18 - the use of starch-based materials for microencapsulation, *Microencapsulation in the food industry*, Academic Press, San Diego, 2014, pp. 195-210.
8. Y. Xie and Y. Yao. 2018. Octenylsuccinate hydroxypropyl phytoglycogen, a dendrimer-like biopolymer, solubilizes poorly water-soluble active pharmaceutical ingredients. *Carbohydrate Polymers* **180**: 29-37.
9. S. E. Hogan and G. Buckton. 2000. The quantification of small degrees of disorder in lactose using solution calorimetry. *International Journal of Pharmaceutics* **207**: 57-64.
10. D. Gao and J. H. Rytting. 1997. Use of solution calorimetry to determine the extent of crystallinity of drugs and excipients. *International Journal of Pharmaceutics* **151**: 183-192.
11. D. Q. M. Craig and J. M. Newton. 1991. Characterisation of polyethylene glycol solid dispersions using differential scanning calorimetry and solution calorimetry. *International Journal of Pharmaceutics* **76**: 17-24.
12. J. D. Nickels, J. Atkinson, E. Papp-Szabo, C. Stanley, S. O. Diallo, S. Perticaroli, B. Baylis, P. Mahon, G. Ehlers, J. Katsaras, and J. R. Dutcher. 2016. Structure and hydration of highly-branched, monodisperse phytoglycogen nanoparticles. *Biomacromolecules* **17**: 735-743.
13. S. H. Yalkowsky. *Solubility and solubilization in aqueous media*, American Chemical Society, 1999.
14. J.-L. Putaux, A. Buléon, R. Borsali, and H. Chanzy. 1999. Ultrastructural aspects of phytoglycogen from cryo-transmission electron microscopy and quasi-elastic light scattering data. *International Journal of Biological Macromolecules* **26**: 145-150.
15. S. Mizrahy and D. Peer. 2012. Polysaccharides as building blocks for nanotherapeutics. *Chemical Society Reviews* **41**: 2623-2640.

16. M. M. Crowley, F. Zhang, J. J. Koleng, and J. W. McGinity. 2002. Stability of polyethylene oxide in matrix tablets prepared by hot-melt extrusion. *Biomaterials* **23**: 4241-4248.
17. D. Daurio, C. Medina, R. Saw, K. Nagapudi, and F. Alvarez-Núñez. 2011. Application of twin screw extrusion in the manufacture of cocrystals, part i: Four case studies. *Pharmaceutics* **3**: 582.
18. D. Daurio, K. Nagapudi, and F. Alvarez-Núñez. Manufacture of pharmaceutically relevant materials by mechanochemistry using twin screw extrusion. In A. M. Repka, N. Langley, and J. DiNunzio (eds), *Melt extrusion: Materials, technology and drug product design* (A. M. Repka, N. Langley, and J. DiNunzio, eds), Springer New York, New York, NY, 2013, pp. 223-242.

APPENDIX A. SOLUBILITY MODELS

SOLUTION BEHAVIOR OF IBU AND LOR

The parallel solution phase equilibrium in a mixture containing either IBU or LOR, OS-DLB, and PLX can be represented as follows:

$$A + D \underset{\longleftarrow}{\overset{K_p}{\rightleftharpoons}} \langle AD \rangle \qquad \text{Equilibrium 1}$$

where A and D represent API and OS-DLB, respectively, and $\langle AD \rangle$ represents the nanocomplex of API and OS-DLB. K_p represents the partition equilibrium constant,

$$K_p = \frac{[A]_{\langle AD \rangle}}{[A]} \qquad \text{Equation 1}$$

where $[A]$ and $[A]_{\langle AD \rangle}$ are the concentrations of the molecularly free drug in solution and the concentration of the drug in the $\langle AD \rangle$ phase, respectively. In a saturated solution, $[A]$ is equivalent to its intrinsic solubility, $[A]_o$. Alternatively, K_p can be expressed as

$$K_p = \frac{\left[\langle AD \rangle\right]}{[A]_o [D]} \qquad \text{Equation 2}$$

where $[D]$ and $\left[\langle AD \rangle\right]$ denote the concentrations of OS-DLB and the nanocomplex of API and OS-DLB, respectively. From Equation 2,

$$\left[\langle AD \rangle\right] = K_p [A]_o [D] \qquad \text{Equation 3}$$

The total concentration of API in solution, $[A]_t$, is given by

$$[A]_t = [A]_o + \left[\langle AD \rangle\right] \qquad \text{Equation 4}$$

Substituting Equation 3 in the preceding euqation gives the general equation for solubilization by OS-DLB:

$$[A]_t = [A]_o + K_p [A]_o [D] \qquad \text{Equation 5}$$

Alternatively,

$$\frac{[A]_t}{[A]_o} = 1 + K_p [D] \qquad \text{Equation 6}$$

SOLUTION BEHAVIOR OF PHT AND GSF

In addition to the solution phase equilibrium (Equilibrium 1), an additional secondary equilibrium involving the formation of insoluble nanocomplexes of API and OS-DLB is present:

$$A + \langle AD \rangle \rightleftharpoons^{K_{sp}} \langle AD \rangle_s \qquad \text{Equilibrium 2}$$

where $\langle AD \rangle_s$ denotes the solid (insoluble) nanocomplex and K_{sp} represents the solubility product of the equilibrium. Accordingly,

$$K_{sp} = [A]_o [D]_{\max} \qquad \text{Equation 7}$$

where $[D]_{\max}$ denotes the limiting concentration of OS-DLB at which the $\langle AD \rangle$ nanocomplex precipitates. From Equation 7,

$$[D]_{\max} = \frac{K_{sp}}{[A]_o} \qquad \text{Equation 8}$$

Substituting Equation 8 in Equation 3 gives

$$\left[\langle AD \rangle\right]_{\max} = K_p K_{sp} \qquad \text{Equation 9}$$

where $\left[\langle AD \rangle\right]_{\max}$ is the solubility limit of the nanocomplex. Substituting Equation 9 in Equation 4 give the total concentration of API in solution, $[A]_t$, above the solubility product of $\langle AD \rangle$ nanocomplex:

$$[A]_t = [A]_o + K_p K_{sp} \qquad \text{Equation 10}$$

Accordingly, the solubility enhancement of PHT and GSF by OS-DLB is described as follows:

$$\frac{[A]_t}{[A]_o} = \begin{cases} 1 + K_p [D] & [A][D] < K_{sp} \\ 1 + \dfrac{K_p K_{sp}}{[A]_o} & [A][D] \geq K_{sp} \end{cases} \qquad \text{Equation 11}$$

SOLUTION BEHAVIOR OF GSF IN THE PRESENCE OF OS-DLB AND PLX

Analogous to Equilibrium 1, the solution phase equilibrium in a mixture containing GSF, OS-DLB and PLX can be represented as follows:

$$A + D \underset{\longleftarrow}{\overset{K_p^{'}}{\rightleftharpoons}} \langle AD \rangle \qquad \text{Equilibrium 3}$$

where $K_P^{'}$ represents the equilibrium constant for the nanocomplex formation, under the influence of a cosolvency-like solubilization effect. Accordingly,

$$K_p^{'} = 10^{\sigma[D]} K_p \qquad \text{Equation 12}$$

where σ is the solubilization power of PLX over the inherent solubilization power of OS-DLB. The equilibrium constant, $K_P^{'}$, reflects an enhancement in the partition-association of the hydrophobic solute molecules and the microenvironment created by the combined effect of OS-DLB and PLX. Substituting Equation 12 in Equation 3 gives

$$\left[\langle AD \rangle\right] = 10^{\sigma[D]} K_p [A]_o [D] \qquad \text{Equation 13}$$

Similarly, an additional secondary equilibrium involving the formation of insoluble nanocomplexes can be represented by:

$$A + \langle AD \rangle \underset{\longleftarrow}{\overset{K_{sp}}{\rightleftharpoons}} \langle AD \rangle_s \qquad \text{Equilibrium 4}$$

Accordingly, at concentrations above the solubility maximum of the $\langle AD \rangle$ nanocomplex, the concentration of the soluble nanocomplex is given by

$$\left[\langle AD \rangle\right]_{\max} = 10^{\sigma[D]_{\max}} K_p K_{sp} \qquad \text{Equation 14}$$

Therefore, the solubility enhancement of GSF by OS-DLB and PLX is described as follows:

$$\frac{[A]_t}{[A]_o} = \begin{cases} 1 + 10^{\sigma[D]} K_p [D] & [A][D] < K_{sp} \\ 1 + \dfrac{10^{\sigma[D]_{\max}} K_p K_{sp}}{[A]_o} & [A][D] \geq K_{sp} \end{cases} \qquad \text{Equation 15}$$

APPENDIX B. ITC MODELS

In a typical ITC system, the total heat of the system Q is given by

$$Q = Q^{syr} + Q^{cell}$$

where the superscripts *syr* and *cell* refer to the syringe and reaction cell of the isothermal titration calorimeter, respectively. The mass balance between the syringe and the cell yields

$$\Delta V\left(A_W^{syr} + A_{\langle AD\rangle}^{syr}\right) = V_o \Delta A_t^{cell}$$

$$\Delta V D_t^{syr} = V_o \Delta D_t^{cell}$$

where ΔV and V_o denote the volume of injection and cell volume, respectively, A and D denote the concentration of API and OS-DLB, respectively, the subscripts W and $\langle AD\rangle$ denote the different environments (W: water, $\langle AD\rangle$: API-DLB nanocomplex), and the subscript t denotes the total concentration of the component. The mass balance inside the cell is

$$A_t^{cell} = A_W^{cell} + A_{\langle AD\rangle}^{cell}$$

For simplicity, A_t^{cell}, A_W^{cell}, $A_{\langle AD\rangle}^{cell}$, and D_t^{cell} will be denoted as A_t, A_W, $A_{\langle AD\rangle}$, and D_t, respectively. Subsequently,

$$\frac{\partial A_t}{\partial A_t} = \frac{\partial A_W}{\partial A_t} + \frac{\partial A_{\langle AD\rangle}}{\partial A_t} \Rightarrow \frac{\partial A_W}{\partial A_t} = 1 - \frac{\partial A_{\langle AD\rangle}}{\partial A_t}$$

$$\frac{\partial A_t}{\partial D_t} = \frac{\partial A_W}{\partial D_t} + \frac{\partial A_{\langle AD\rangle}}{\partial D_t} \Rightarrow \frac{\partial A_W}{\partial D_t} = -\frac{\partial A_{\langle AD\rangle}}{\partial D_t}$$

The enthalpy variation of the syringe contents upon an injection is

$$Q^{syr} = -\Delta V\left(A_W^{syr} h_W^A + A_{\langle AD\rangle}^{syr} h_{\langle AD\rangle}^A + D_t^{syr} h^D\right)$$

where h denotes the partial molar enthalpy of the component, and the superscripts denote the component where A and D refer to API and OS-DLB, respectively.

The enthalpy variation of the cell contents upon an injection is

$$
\begin{aligned}
&Q^{cell} \\
&= V_o \left[\left(\frac{\partial A_W}{\partial A_t} \Delta A_t + \frac{\partial A_W}{\partial D_t} \Delta D_t \right) h_W^A + \left(\frac{\partial A_{\langle AD \rangle}}{\partial A_t} \Delta A_t + \frac{\partial A_{\langle AD \rangle}}{\partial D_t} \Delta D_t \right) h_{\langle AD \rangle}^A + \left(\frac{\partial D_t}{\partial A_t} \Delta A_t + \frac{\partial D_t}{\partial D_t} \Delta D_t \right) h^D \right] \\
&= V_o \left[\Delta A_t h_W^A - \frac{\partial A_{\langle AD \rangle}}{\partial A_t} \Delta A_t h_W^A - \frac{\partial A_{\langle AD \rangle}}{\partial D_t} \Delta D_t h_W^A + \frac{\partial A_{\langle AD \rangle}}{\partial A_t} \Delta A_t h_{\langle AD \rangle}^A + \frac{\partial A_{\langle AD \rangle}}{\partial D_t} \Delta D_t h_{\langle AD \rangle}^A + \Delta D_t h^D \right] \\
&= V_o \left[\Delta A_t h_W^A + \Delta D_t h^D + \frac{\partial A_{\langle AD \rangle}}{\partial A_t} \Delta A_t \left(h_{\langle AD \rangle}^A - h_W^A \right) + \frac{\partial A_{\langle AD \rangle}}{\partial D_t} \Delta D_t \left(h_{\langle AD \rangle}^A - h_W^A \right) \right] \\
&= V_o \left[\Delta A_t h_W^A + \Delta D_t h^D + \left(\frac{\partial A_{\langle AD \rangle}}{\partial A_t} \Delta A_t + \frac{\partial A_{\langle AD \rangle}}{\partial D_t} \Delta D_t \right) \left(h_{\langle AD \rangle}^A - h_W^A \right) \right]
\end{aligned}
$$

The total change in the enthalpy content of the system upon an injection is

$$
\begin{aligned}
&Q \\
&= Q^{syr} + Q^{cell} \\
&= -\Delta V \left(A_W^{syr} h_W^A + A_{\langle AD \rangle}^{syr} h_{\langle AD \rangle}^A + D_t^{syr} h^D \right) \\
&\quad + V_o \left[\Delta A_t h_W^A + \Delta D_t h^D + \left(\frac{\partial A_{\langle AD \rangle}}{\partial A_t} \Delta A_t + \frac{\partial A_{\langle AD \rangle}}{\partial D_t} \Delta D_t \right) \left(h_{\langle AD \rangle}^A - h_W^A \right) \right] \\
&= -\Delta V A_W^{syr} h_W^A - \Delta V A_{\langle AD \rangle}^{syr} h_{\langle AD \rangle}^A - \Delta V D_t^{syr} h^D + \Delta V A_W^{syr} h_W^A + \Delta V A_{\langle AD \rangle}^{syr} h_W^A + \Delta V D_t^{syr} h^D \\
&\quad + V_o \left(\frac{\partial A_{\langle AD \rangle}}{\partial A_t} \Delta A_t + \frac{\partial A_{\langle AD \rangle}}{\partial D_t} \Delta D_t \right) \left(h_{\langle AD \rangle}^A - h_W^A \right) \\
&= -\Delta V A_{\langle AD \rangle}^{syr} \left(h_{\langle AD \rangle}^A - h_W^A \right) + V_o \left(\frac{\partial A_{\langle AD \rangle}}{\partial A_t} \Delta A_t + \frac{\partial A_{\langle AD \rangle}}{\partial D_t} \Delta D_t \right) \left(h_{\langle AD \rangle}^A - h_W^A \right)
\end{aligned}
$$

The partition-association equilibrium constant K_P is defined as

$$K_p = \frac{A_{\langle AD \rangle}}{A_W D_t}$$

which upon rearrangement becomes

$$A_{\langle AD \rangle} = K_p A_W D_t = K_p \left(A_t - A_{\langle AD \rangle} \right) D_t = K_p A_t D_t - K_p A_{\langle AD \rangle} D_t$$

$$A_{\langle AD \rangle} \left(1 + K_p D_t \right) = K_p A_t D_t$$

$$A_{\langle AD \rangle} = \frac{K_p A_t D_t}{1 + K_p D_t}$$

Subsequently,

$$\frac{\partial A_{\langle AD\rangle}}{\partial A_t} = \frac{K_p D_t}{1+K_p D_t}$$

$$\frac{\partial A_{\langle AD\rangle}}{\partial D_t} = \frac{K_p A_t}{1+K_p D_t} - \frac{K_p\left(K_p A_t D_t\right)}{\left(1+K_p D_t\right)^2} = \frac{K_p A_t}{1+K_p D_t}\left(1-\frac{K_p D_t}{1+K_p D_t}\right)$$

Let $M = \frac{K_p D_t}{1+K_p D_t}$ and $N = \frac{K_p A_t}{1+K_p D_t}$,

$$\frac{\partial A_{\langle AD\rangle}}{\partial A_t} = M$$

$$\frac{\partial A_{\langle AD\rangle}}{\partial D_t} = N\left(1-M\right)$$

Therefore, the amount of heat released or absorbed upon an injection is

$$Q = -\Delta V A^{syr}_{\langle AD\rangle}\left(h^A_{\langle AD\rangle} - h^A_W\right) + V_o\left[M\Delta A_t + N\left(1-M\right)\Delta D_t\right]\left(h^A_{\langle AD\rangle} - h^A_W\right)$$

where $\Delta h^A_{W\to\langle AD\rangle} = h^A_{\langle AD\rangle} - h^A_W$ represents the enthalpy of transfer of API solute from water to OS-DLB to form nanocomplex.

In a translocation model, it is assumed that a fraction of the API solutes is entrapped in the OS-DLB dendrimeric structure and therefore, have to be excluded from consideration in the fit procedures. Subsequently,

$$Q = -\Delta V\left(\alpha A^{syr}_{\langle AD\rangle}\right)\left(h^A_{\langle AD\rangle} - h^A_W\right) + V_o\left[M\Delta A_t + N\left(1-M\right)\Delta D_t\right]\left(h^A_{\langle AD\rangle} - h^A_W\right)$$

where α is the fraction of API solutes that is not entrapped in the OS-DLB dendrimeric structure, i.e. available for redistribution between water and OS-DLB after each injection.

IBU-DLB-PLX → H_2O (Stoichiometric interaction of PLX)

Assuming that the interaction between IBU, OS-DLB and PLX is stoichiometric, the equilibrium in a mixture containing IBU, OS-DLB and PLX can be represented as follows:

$$A + D + P \underset{}{\overset{K}{\rightleftharpoons}} \langle ADP \rangle$$

where A, D and P represent the concentration of API, OS-DLB and PLX, respectively, $\langle ADP \rangle$ represents the concentration of the nanocomplex of API, OS-DLB and PLX, and K represents the partition-association constant. Note that this model is ruled out due to the poor fit of the data.

The heat of the system Q is given by

$$Q = Q^{syr} + Q^{cell}$$

where the superscripts *syr* and *cell* refer to the syringe and reaction cell of the isothermal titration calorimeter, respectively. The mass balance between the syringe and the cell yields

$$\Delta V \left(A_W^{syr} + A_{\langle ADP \rangle}^{syr} \right) = V_o \Delta A_t^{cell}$$

$$\Delta V D_t^{syr} = V_o \Delta D_t^{cell}$$

$$\Delta V P_t^{syr} = V_o \Delta P_t^{cell}$$

where ΔV and V_o denote the volume of injection and cell volume, respectively, the subscripts W and $\langle ADP \rangle$ denote the different environments (W: water, $\langle ADP \rangle$: API-DLB-PLX nanocomplex), and the subscript t denotes the total concentration of the component. The mass balance inside the cell is

$$A_t^{cell} = A_W^{cell} + A_{\langle ADP \rangle}^{cell}$$

For simplicity, A_t^{cell}, A_W^{cell}, $A_{\langle ADP \rangle}^{cell}$, D_t^{cell}, and P_t^{cell} will be denoted as A_t, A_W, $A_{\langle ADP \rangle}$, D_t, and P_t respectively. Subsequently,

$$\frac{\partial A_t}{\partial A_t} = \frac{\partial A_W}{\partial A_t} + \frac{\partial A_{\langle ADP \rangle}}{\partial A_t} \Rightarrow \frac{\partial A_W}{\partial A_t} = 1 - \frac{\partial A_{\langle ADP \rangle}}{\partial A_t}$$

$$\frac{\partial A_t}{\partial D_t} = \frac{\partial A_W}{\partial D_t} + \frac{\partial A_{\langle ADP \rangle}}{\partial D_t} \Rightarrow \frac{\partial A_W}{\partial D_t} = -\frac{\partial A_{\langle ADP \rangle}}{\partial D_t}$$

$$\frac{\partial A_t}{\partial P_t} = \frac{\partial A_W}{\partial P_t} + \frac{\partial A_{\langle ADP \rangle}}{\partial P_t} \Rightarrow \frac{\partial A_W}{\partial P_t} = -\frac{\partial A_{\langle ADP \rangle}}{\partial P_t}$$

The enthalpy variation of the syringe contents upon an injection is

$$Q^{syr} = -\Delta V \left(A_W^{syr} h_W^A + A_{\langle ADP \rangle}^{syr} h_{\langle ADP \rangle}^A + D_t^{syr} h^D + P_t^{syr} h^P \right)$$

where *h* denotes the partial molar enthalpy of the component, and the superscripts denote the component where *A*, *D* and *P* refer to API, OS-DLB and PLX, respectively.

The enthalpy variation of the cell contents upon an injection is

$$\begin{aligned}
&Q^{cell} \\
&= V_o \left[\left(\frac{\partial A_W}{\partial A_t} \Delta A_t + \frac{\partial A_W}{\partial D_t} \Delta D_t + \frac{\partial A_W}{\partial P_t} \Delta P_t \right) h_W^A + \left(\frac{\partial A_{\langle ADP \rangle}}{\partial A_t} \Delta A_t + \frac{\partial A_{\langle ADP \rangle}}{\partial D_t} \Delta D_t + \frac{\partial A_{\langle ADP \rangle}}{\partial P_t} \Delta P_t \right) h_{\langle ADP \rangle}^A \right. \\
&\quad \left. + \left(\frac{\partial D_t}{\partial A_t} \Delta A_t + \frac{\partial D_t}{\partial D_t} \Delta D_t + \frac{\partial D_t}{\partial P_t} \Delta P_t \right) h^D + \left(\frac{\partial P_t}{\partial A_t} \Delta A_t + \frac{\partial P_t}{\partial D_t} \Delta D_t + \frac{\partial P_t}{\partial P_t} \Delta P_t \right) h^P \right] \\
&= V_o \left[\Delta A_t h_W^A + \Delta D_t h^D + \Delta P_t h^D - \frac{\partial A_{\langle ADP \rangle}}{\partial A_t} \Delta A_t h_W^A - \frac{\partial A_{\langle ADP \rangle}}{\partial D_t} \Delta D_t h_W^A - \frac{\partial A_{\langle ADP \rangle}}{\partial P_t} \Delta P_t h_W^A \right. \\
&\quad \left. + \frac{\partial A_{\langle ADP \rangle}}{\partial A_t} \Delta A_t h_{\langle ADP \rangle}^A + \frac{\partial A_{\langle ADP \rangle}}{\partial D_t} \Delta D_t h_{\langle ADP \rangle}^A + \frac{\partial A_{\langle ADP \rangle}}{\partial P_t} \Delta P_t h_{\langle ADP \rangle}^A \right] \\
&= V_o \left[\Delta A_t h_W^A + \Delta D_t h^D + \Delta P_t h^D + \frac{\partial A_{\langle ADP \rangle}}{\partial A_t} \Delta A_t \left(h_{\langle ADP \rangle}^A - h_W^A \right) + \frac{\partial A_{\langle ADP \rangle}}{\partial D_t} \Delta D_t \left(h_{\langle ADP \rangle}^A - h_W^A \right) \right. \\
&\quad \left. + \frac{\partial A_{\langle ADP \rangle}}{\partial P_t} \Delta P_t \left(h_{\langle ADP \rangle}^A - h_W^A \right) \right] \\
&= V_o \left[\Delta A_t h_W^A + \Delta D_t h^D + \Delta P_t h^D + \left(\frac{\partial A_{\langle ADP \rangle}}{\partial A_t} \Delta A_t + \frac{\partial A_{\langle ADP \rangle}}{\partial D_t} \Delta D_t + \frac{\partial A_{\langle ADP \rangle}}{\partial P_t} \Delta P_t \right) \left(h_{\langle ADP \rangle}^A - h_W^A \right) \right]
\end{aligned}$$

The total change in the enthalpy content of the system upon an injection is

$$
\begin{aligned}
&Q \\
&= Q^{syr} + Q^{cell} \\
&= -\Delta V\left(A_W^{syr}h_W^A + A_{\langle ADP\rangle}^{syr}h_{\langle ADP\rangle}^A + D_t^{syr}h^D + P_t^{syr}h^P\right) \\
&+V_o\left[\Delta A_t h_W^A + \Delta D_t h^D + \Delta P_t h^D + \left(\frac{\partial A_{\langle ADP\rangle}}{\partial A_t}\Delta A_t + \frac{\partial A_{\langle ADP\rangle}}{\partial D_t}\Delta D_t + \frac{\partial A_{\langle ADP\rangle}}{\partial P_t}\Delta P_t\right)\left(h_{\langle ADP\rangle}^A - h_W^A\right)\right] \\
&= -\Delta VA_W^{syr}h_W^A - \Delta VA_{\langle ADP\rangle}^{syr}h_{\langle ADP\rangle}^A - \Delta VD_t^{syr}h^D - \Delta VP_t^{syr}h^P \\
&+\Delta VA_W^{syr}h_W^A + \Delta VA_{\langle ADP\rangle}^{syr}h_W^A + \Delta VD_t^{syr}h^D + \Delta VP_t^{syr}h^P \\
&V_o\left(\frac{\partial A_{\langle ADP\rangle}}{\partial A_t}\Delta A_t + \frac{\partial A_{\langle ADP\rangle}}{\partial D_t}\Delta D_t + \frac{\partial A_{\langle ADP\rangle}}{\partial P_t}\Delta P_t\right)\left(h_{\langle ADP\rangle}^A - h_W^A\right) \\
&= -\Delta VA_{\langle ADP\rangle}^{syr}\left(h_{\langle ADP\rangle}^A - h_W^A\right) + V_o\left(\frac{\partial A_{\langle ADP\rangle}}{\partial A_t}\Delta A_t + \frac{\partial A_{\langle ADP\rangle}}{\partial D_t}\Delta D_t + \frac{\partial A_{\langle ADP\rangle}}{\partial P_t}\Delta P_t\right)\left(h_{\langle ADP\rangle}^A - h_W^A\right)
\end{aligned}
$$

The partition-association equilibrium constant K is defined as

$$K = \frac{A_{\langle ADP\rangle}}{A_W D_t P_t}$$

which upon rearrangement becomes

$$A_{\langle ADP\rangle} = KA_W D_t P_t = K\left(A_t - A_{\langle ADP\rangle}\right)D_t P_t = KA_t D_t P_t - KA_{\langle ADP\rangle}D_t P_t$$

$$A_{\langle ADP\rangle} = \frac{KA_t D_t P_t}{1 + KD_t P_t}$$

Subsequently,

$$\frac{\partial A_{\langle ADP\rangle}}{\partial A_t} = \frac{KD_t P_t}{1 + KD_t P_t}$$

$$\frac{\partial A_{\langle ADP\rangle}}{\partial D_t} = \frac{KA_t P_t}{1 + KD_t P_t} - \frac{KP_t\left(KA_t D_t P_t\right)}{\left(1 + KD_t P_t\right)^2} = \frac{KA_t P_t}{1 + KD_t P_t}\left(1 - \frac{KD_t P_t}{1 + KD_t P_t}\right)$$

$$\frac{\partial A_{\langle ADP\rangle}}{\partial P_t} = \frac{KA_t D_t}{1 + KD_t P_t} - \frac{KD_t\left(KA_t D_t P_t\right)}{\left(1 + KD_t P_t\right)^2} = \frac{KA_t D_t}{1 + KD_t P_t}\left(1 - \frac{KD_t P_t}{1 + KD_t P_t}\right)$$

Let $M = \frac{KD_t P_t}{1 + KD_t P_t}$, $N = \frac{KA_t P_t}{1 + KD_t P_t}$, and $R = \frac{KA_t D_t}{1 + KD_t P_t}$,

Therefore, the amount of heat released or absorbed upon an injection is

$$Q = -\Delta V A^{syr}_{\langle ADP \rangle} \left(h^{A}_{\langle ADP \rangle} - h^{A}_{W} \right) + V_o \left[M \Delta A_t + N \left(1 - M \right) \Delta D_t + R \left(1 - M \right) \Delta P_t \right] \left(h^{A}_{\langle ADP \rangle} - h^{A}_{W} \right)$$

and $\Delta h^{A}_{W \to \langle ADP \rangle} = h^{A}_{\langle ADP \rangle} - h^{A}_{W}$ represents the enthalpy of transfer of API solute from water to OS-DLB to form nanocomplex.

In a translocation model, it is assumed that a fraction of the API solutes is entrapped in the OS-DLB dendrimeric structure and therefore, have to be excluded from consideration in the fit procedures. Subsequently,

$$Q = -\Delta V \left(\alpha A^{syr}_{\langle ADP \rangle} \right) \left(h^{A}_{\langle ADP \rangle} - h^{A}_{W} \right) + V_o \left[M \Delta A_t + N \left(1 - M \right) \Delta D_t + R \left(1 - M \right) \Delta P_t \right] \left(h^{A}_{\langle ADP \rangle} - h^{A}_{W} \right)$$

where α is the fraction of API solutes that is not entrapped in the OS-DLB dendrimeric structure, i.e. available for redistribution between water and OS-DLB after each injection,

APPENDIX C. SAS PROGRAM

```
data IBUDOE;
infile 'H:\Research\IBU DOE\IBU DOE (BBD).csv' dlm=',';
input ID $ Temp Time Speed T1 T5 T10 T15 T30 T45 T60 T120
Crys XRD1-XRD2251;
run;
proc print data=IBUDOE;
run;

proc pls data=IBUDOE method=pls plots=all details;
model T1 T5 T10 T15 T30 T45 T60 T120 = Temp Time Speed
Temp*Time Temp*Speed Time*Speed;
ods output VariableImportancePlot=VIP;
run;
proc print data=VIP;
run;

proc pls data=IBUDOE method=pls plots=all details;
model Crys = Temp Time Speed Temp*Time Temp*Speed Time*Speed;
ods output VariableImportancePlot=VIP;
run;
proc print data=VIP;
run;

proc princomp data=IBUDOE cov plots=all n=2 out=out;
var T1 T5 T10 T15 T30 T45 T60 T120;
run;
proc print data=out;
run;

proc princomp data=IBUDOE cov plots=all n=2 out=out;
var XRD1-XRD2251;
run;
proc print data=out;
run;

proc glm data=IBUDOE plots=all plot=diagnostics(label);
class Temp Time Speed;
model T1 T120 Crys = Temp Time Speed Temp*Speed Time*Speed;
output out=out p=p_T1 p_T120 p_Crys;
run;
proc print data=out;
run;
```

```
proc rsreg data=IBUDOE plots=surface(3d at (Temp=30) unpack)
out=out;
model T1 T120 Crys = Temp Time Speed/nocode press lackfit
predict residual l95 u95 l95m u95m d;
proc print data=out;
run;

data temperature;
do;
do Temp = 30 to 50 by 0.5;
Time = 20;
Speed = 90;
T1 = . ;
T120= . ;
Crys = . ;
output;
end;
end;
run;
data temperature;
set IBUDOE temperature;
run;
proc rsreg data=temperature out=predict_temp;
model T1 T120 Crys = Temp Time Speed/l95 u95 l95m u95m;
proc sort data=predict_temp;
by _TYPE_;
proc print data=predict_temp;
run;

data time;
do;
do Time = 10 to 30 by 0.5;
Temp = 40;
Speed = 90;
T1 = . ;
T120 = . ;
Crys = . ;
output;
end;
end;
run;
data time;
set IBUDOE time;
run;
proc rsreg data=time out=predict_time;
model T1 T120 Crys = Temp Time Speed/l95 u95 l95m u95m;
proc sort data=predict_time;
```

```
by _TYPE_;
proc print data=predict_time;
run;

data speed;
do;
do Speed = 45 to 135 by 1;
Temp = 40;
Time = 20;
T1 = . ;
T120 = . ;
Crys = .;
output;
end;
end;
run;
data speed;
set IBUDOE speed;
run;
proc rsreg data=speed out=predict_speed;
model T1 T120 Crys = Temp Time Speed/l95 u95 l95m u95m;
proc sort data=predict_speed;
by _TYPE_;
proc print data=predict_speed;
run;
```